Adjacent Box Beam Connections: Performance and Optimization

U.S. Department of Transportation
Federal Highway Administration

FOREWORD

With the ever-increasing congestion and deterioration of the Nation's highway system, there is a need to develop highly durable and rapidly constructed infrastructure systems. Durable bridge structures that require less intrusive maintenance and exhibit longer life spans, thus maximizing the use of the facilities, are highly desirable. Expediting bridge construction can minimize traffic flow disruptions. The precast prestressed concrete box beam bridge is one type of bridge system that can be constructed in an accelerated process with wide applications in short- and medium-span bridges in the United States.

The study presented herein was completed as part of the Federal Highway Administration's Structural Concrete Research Program. It investigated the connection design details for this type of bridge, including novel connection details whose performance surpasses common practice. The findings provide an innovative solution that could advance the state of the practice in bridge construction. An executive summary of the information contained in this report has been published as a TechBrief titled *Adjacent Box Beam Connections: Performance and Optimization*.[1] This report will be of interest to engineers, academics, researchers, and industry partners who are involved the design, fabrication, construction, or maintenance of short- and medium-span bridges.

Cheryl Allen Richter, Ph.D., P.E.
Director, Office of Infrastructure
Research and Development

TECHNICAL REPORT DOCUMENTATION PAGE

1. Report No. FHWA-HRT-17-093	2. Government Accession No.	3. Recipient's Catalog No.	
4. Title and Subtitle Adjacent Box Beam Connections: Performance and Optimization		5. Report Date February 2018	
		6. Performing Organization Code:	
7. Author(s) Jiqiu Yuan, Benjamin A. Graybeal, and Kevin Zmetra		8. Performing Organization Report No.	
9. Performing Organization Name and Address Office of Infrastructure Research & Development Federal Highway Administration 6300 Georgetown Pike McLean, VA 22101-2296		10. Work Unit No.	
		11. Contract or Grant No. DTFH61-10-D-00017	
12. Sponsoring Agency Name and Address Office of Infrastructure Research & Development Federal Highway Administration 6300 Georgetown Pike McLean, VA 22101-2296		13. Type of Report and Period Covered Final Report; March 2013–September 2016	
		14. Sponsoring Agency Code HRDI-40	
15. Supplementary Notes This report was developed by research staff at the Turner-Fairbank Highway Research Center. Jiqiu Yuan and Kevin Zmetra are contract researchers who support the Federal Highway Administration's (FHWA) structural concrete research efforts, and Ben Graybeal of FHWA manages the FHWA Structural Concrete Research Program and leads the Bridge Engineering Research team.			

16. Abstract

Precast prestressed concrete adjacent box beam bridges are widely utilized for short- and medium-span bridges throughout North America. However, a recurring issue with this bridge type is the deterioration of the shear key connection, resulting in substandard performance of the overall bridge system. This research investigated partial- and full-depth connection designs utilizing conventional non-shrink grout and ultra-high performance concrete (UHPC) by conducting full-scale structural testing. Quantitative measures to evaluate the connection performance that may assist in examining similar types of bridges are suggested in this study. A model to calculate the shear force in the connection is proposed, and both the shear and tensile stresses at the connection are analyzed. The findings can be used to assist in the design of connections for this bridge type. The performance of conventionally grouted and UHPC connections are presented and compared. It was found that the adjacent box beam bridges with UHPC connections can be a resilient bridge superstructure system, providing an innovative solution that can advance the state of the practice in bridge construction. This report corresponds to the accompanying TechBrief, *Adjacent Box Beam Connections: Performance and Optimization*.[1]

17. Key Words Box beam bridge, Connection, Shear key design, Transverse post-tension, Transverse shear, Transverse tension, Ultra-high performance concrete, UHPC		18. Distribution Statement No restrictions. This document is available to the public through the National Technical Information Service, Springfield, VA 22161. http://www.ntis.gov		
19. Security Classif. (of this report) Unclassified		20. Security Classif. (of this page) Unclassified	21. No. of Pages 129	22. Price N/A

Form DOT F 1700.7 (8-72)   Reproduction of completed page authorized.

SI* (MODERN METRIC) CONVERSION FACTORS

APPROXIMATE CONVERSIONS TO SI UNITS

Symbol	When You Know	Multiply By	To Find	Symbol
LENGTH				
in	inches	25.4	millimeters	mm
ft	feet	0.305	meters	m
yd	yards	0.914	meters	m
mi	miles	1.61	kilometers	km
AREA				
in^2	square inches	645.2	square millimeters	mm^2
ft^2	square feet	0.093	square meters	m^2
yd^2	square yard	0.836	square meters	m^2
ac	acres	0.405	hectares	ha
mi^2	square miles	2.59	square kilometers	km^2
VOLUME				
fl oz	fluid ounces	29.57	milliliters	mL
gal	gallons	3.785	liters	L
ft^3	cubic feet	0.028	cubic meters	m^3
yd^3	cubic yards	0.765	cubic meters	m^3
NOTE: volumes greater than 1000 L shall be shown in m^3				
MASS				
oz	ounces	28.35	grams	g
lb	pounds	0.454	kilograms	kg
T	short tons (2000 lb)	0.907	megagrams (or "metric ton")	Mg (or "t")
TEMPERATURE (exact degrees)				
^oF	Fahrenheit	5 (F-32)/9 or (F-32)/1.8	Celsius	^oC
ILLUMINATION				
fc	foot-candles	10.76	lux	lx
fl	foot-Lamberts	3.426	candela/m^2	cd/m^2
FORCE and PRESSURE or STRESS				
lbf	poundforce	4.45	newtons	N
lbf/in^2	poundforce per square inch	6.89	kilopascals	kPa

APPROXIMATE CONVERSIONS FROM SI UNITS

Symbol	When You Know	Multiply By	To Find	Symbol
LENGTH				
mm	millimeters	0.039	inches	in
m	meters	3.28	feet	ft
m	meters	1.09	yards	yd
km	kilometers	0.621	miles	mi
AREA				
mm^2	square millimeters	0.0016	square inches	in^2
m^2	square meters	10.764	square feet	ft^2
m^2	square meters	1.195	square yards	yd^2
ha	hectares	2.47	acres	ac
km^2	square kilometers	0.386	square miles	mi^2
VOLUME				
mL	milliliters	0.034	fluid ounces	fl oz
L	liters	0.264	gallons	gal
m^3	cubic meters	35.314	cubic feet	ft^3
m^3	cubic meters	1.307	cubic yards	yd^3
MASS				
g	grams	0.035	ounces	oz
kg	kilograms	2.202	pounds	lb
Mg (or "t")	megagrams (or "metric ton")	1.103	short tons (2000 lb)	T
TEMPERATURE (exact degrees)				
^oC	Celsius	1.8C+32	Fahrenheit	^oF
ILLUMINATION				
lx	lux	0.0929	foot-candles	fc
cd/m^2	candela/m^2	0.2919	foot-Lamberts	fl
FORCE and PRESSURE or STRESS				
N	newtons	0.225	poundforce	lbf
kPa	kilopascals	0.145	poundforce per square inch	lbf/in^2

*SI is the symbol for the International System of Units. Appropriate rounding should be made to comply with Section 4 of ASTM E380.
(Revised March 2003)

TABLE OF CONTENTS

LIST OF FIGURES

LIST OF TABLES

LIST OF ABBREVIATIONS AND SYMBOLS

Abbreviations

AASHTO   American Association of State Highway and Transportation Officials

EA   exposed aggregate

FHWA   Federal Highway Administration

LRFD   Load and Resistance Factor Design

LVDT   linear variable differential transformer

PT   post-tensioning

SB   sandblasted

UHPC   ultra-high performance concrete

Symbols

b distance from each end support to each loading point

EI beam stiffness

EI_{eff} effective beam stiffness

$EI_{eff,\delta}$ effective beam stiffness based on deflection measurements

$EI_{eff,\varepsilon}$ effective beam stiffness based on strain measurements

f'_c compressive strength of concrete

l span length

M moment at the mid-span

$M_{equivalent}$ equivalent moment transferred through the connection

M_{max} maximum moment transferred through the connection

P load at each load point

v'_{max} maximum distributed shear force

V_y transverse shear distribution

V'_y triangular shear distribution

y distance from where the tensile strain is measured to the neutral axis of the cross section

δ deflection at the mid-span

δ_A deflection of beam A at the mid-span

δ_{AE} deflection from the loaded beam on the exterior linear variable differential transformer

δ_{AI} deflection from the loaded beam on the interior linear variable differential transformer

δ_B	deflection of beam B at the mid-span
δ_{BE}	deflection from the unloaded beam on the exterior linear variable differential transformer
δ_{BI}	deflection from the unloaded beam on the interior linear variable differential transformer
$\delta_{calculated}$	calculated deflection of the beam
$\delta_{measured}$	measured deflection in beam B when beam A is loaded at the maximum load and beam B is loaded at the minimum level
Δ_δ	differential deflection
ε	longitudinal tensile strain at the mid-span
ε'	additional strain in beam B due to the equivalent moment
ε_{5kip}	strain in beam B when both beams are loaded at 5 kip (22 kN)
ε_A	longitudinal tensile strain in beam A
ε_B	longitudinal tensile strain in beam B
$\varepsilon_{calculated}$	calculated strain
$\varepsilon_{measured}$	measured strain in beam B when beam A is loaded at the maximum load and beam B is loaded at the minimum load

CHAPTER 1. INTRODUCTION

BACKGROUND

Precast prestressed concrete adjacent box beams are widely used throughout the United States. Box beams are normally fabricated by a precast concrete producer in a controlled environment, enabling production of durable structural elements. They are then transported and assembled on the job site using field-cast shear key connections, transverse ties, and potentially a structural overlay to form a complete bridge system. This type of bridge superstructure is considered to have a lower erection cost and be easier to construct compared to other systems. One of the recurring issues for this bridge system is degradation of the shear key connections, which can compromise both the strength and serviceability of the bridge. When the ability for shear key connections to transfer loads to adjacent beams is affected by degradation, the live load may remain concentrated in the few beams under the wheels. This can potentially lead to damage caused by exceeding the designed allowable load of those beams. Beams do not deflect uniformly under live loads when the shear keys have failed. Excessive differential deflection (Δ_δ) between adjacent beams may lead to widening of existing cracks in the shear keys as well as reflective cracking in the overlay if one is present. These cracks can allow chloride-laden water to infiltrate the structure and result in corrosion of the tie bars, prestressing strands, and embedded steel reinforcement. Decades of experience have demonstrated that the field-cast shear key connections are a weak link in the box beam system that can lead to substandard performance of the overall bridge system.[12–4]

Most shear key connections are designed using regional standard details that are of uncertain origin with neither information on the magnitude of forces transferred through the shear key nor the ability of a given detail to resist these loads.[2] Neither the American Association of State Highway and Transportation Officials' (AASHTO) *Standard Specifications for Highway Bridges*, the *AASHTO Load and Resistance Factor Design (LRFD) Bridge Design Specifications*, nor the *AASHTO LRFD Bridge Construction Specifications* provides specific guidance for the design or construction of the connection between adjacent box beams.[5–7] The AASHTO *Standard Specifications for Highway Bridges* states that "the interaction between the beams is developed by continuous longitudinal shear keys used in combination with transverse tie assemblies which may, or may not, be prestressed"(p. 34).[5] The shear key design details and the calculation of the transverse forces are not provided. In the *AASHTO LRFD Bridge Design Specifications*, a minimum of 0.25 ksi (1.7 MPa) transverse prestress is suggested, but no further guidance on the connection geometry or prestressing forces is provided.[6] The *Precast Prestressed Concrete Bridge Design Manual* presents an empirical design based on the State of Oregon's experience and suggests a design procedure based on research conducted by El-Remaily et al. and Hanna et al.[3,8,9]

This procedure assumes that post-tensioning (PT) transverse diaphragms are the primary mechanism for the distribution of wheel loads across the bridge; longitudinal shear keys are not required for the structural performance of the bridge. In the design, the required transverse PT force at diaphragms is calculated so that diaphragm concrete stresses due to the combination of wheel loads and PT forces are maintained within allowable limits. The limit for compression is $0.6f'_c$, where f'_c is the specified compressive strength of the concrete. No tension is permitted.

This design methodology was initially developed based on practices in Japan, where cast-in-place concrete is placed in relatively wide and deep connections at diaphragms in conjunction with high levels of PT.[8] The Canadian Bridge Design Code assumes that the load is transferred from one beam to another primarily through transverse shear; transverse rigidity is neglected.[10] Figure 5.7.1.8 in the Canadian Bridge Design Code provides charts to determine the shear force, and a reinforced concrete structural slab is required to provide the shear transfer between beams.[10]

Shear key connection deterioration can be caused by many factors, such as shrinkage during curing of the grouting material, the live load being transferred through the shear key to/from adjacent beams, thermal effects, misalignment, and general poor construction practices. Prior research on shear key connections has investigated the possibility of using a variety of grout materials (e.g., magnesium ammonium phosphate grout and epoxy grout) and shear key designs (e.g., partial- and full-depth shear keys) as well as improving the mechanical behavior of the connection (e.g., providing increased transverse PT).[11–13]

This research compared and evaluated four connection designs. Two of the connection details are currently considered to be operating in good practice by utilizing high-strength, non-shrink grout in combination with transverse PT. The other two details utilize ultra-high performance concrete (UHPC). Full-scale tests were conducted to investigate the factors affecting shear key performance, including simulated traffic loads, thermal loads, and the magnitude of transverse PT forces.

OBJECTIVE

This research evaluated and compared the performance of four connection designs. Based on the results, quantitative measures to assist bridge owners in evaluating existing shear key performance are suggested. Three critical design parameters were investigated: (1) the magnitude of the transverse PT force, (2) the transverse shear strength of the shear key, and (3) the condition of the interface between the connection material and box beam concrete. Design suggestions are provided for each of these parameters that can be used to assist bridge owners in the use of this economical bridge system.

REPORT ORGANIZATION

This research investigated different connection designs for precast prestressed box beam bridges. The results of full-scale testing of four connection details are included in this report, which is divided into six chapters and an appendix. Chapter 1 provides an introduction and the objective of the research. The experimental test setup is presented in chapter 2. Chapter 3 presents the analytical models and assumptions used to compare the specimens. Chapter 4 includes the results from the thermal and cyclic loading. Discussion of the effects of different design parameters are presented in chapter 5. Chapter 6 delivers the summary and conclusions of this research. Finally, the appendix provides drawings associated with the fabrication of the box beams.

A TechBrief was published that provides an executive summary of the information contained in this report.[1] Additionally, a peer-reviewed journal paper by Yuan and Graybeal also presents the results of this study.[14]

CHAPTER 2. EXPERIMENTAL INVESTIGATION

INTRODUCTION

Four connection design details were investigated with full-scale testing in this study using AASHTO type BII-36 box beams. These beams have a cross section of 36 inches (914 mm) wide, 33 inches (838 mm) deep, and 50 ft (15.2 m) long. Each test consisted of two box beams connected using one of the four connections being investigated. This chapter introduces the connection designs, construction materials, and construction procedures. It then presents the setup of the thermal loading and cyclic structural loading tests, including the loading protocols and instrumentation used.

SHEAR KEY AND BOX BEAM DESIGN DETAILS

Four connection designs were evaluated in this study. The first two used conventional high-strength non-shrink grout. One had a partial-depth connection, and the other had a full-depth connection, as shown in figure 1 and figure 2, respectively. It should be noted that, in accordance with common practice, the designs with conventional grout utilized transverse PT. Photographs of the partial-depth conventional grout shear key prior to casting and the means of applying the transverse PT force are presented in figure 3 and figure 4, respectively.
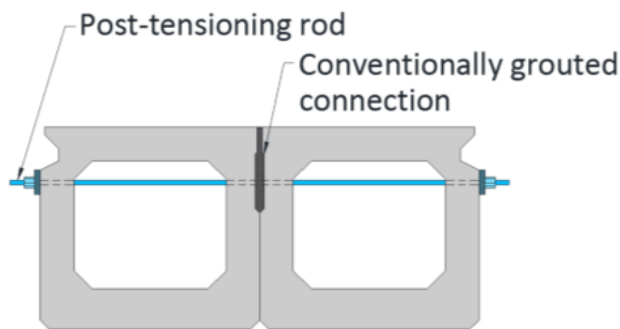
Source: FHWA.

Figure 1. Illustration. Partial-depth conventional grout connection.
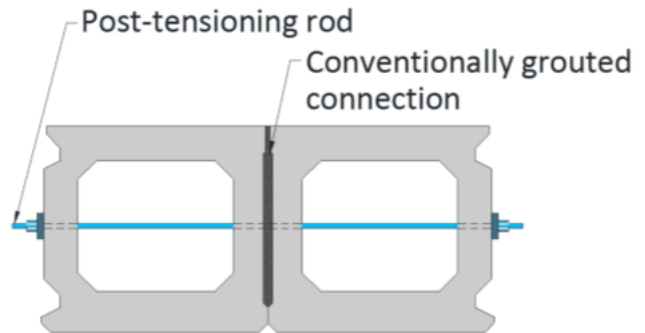
Source: FHWA.

Figure 2. Illustration. Full-depth conventional grout connection.

Figure 3. Photo. Alignment of the partial-depth conventional grout connection.

Figure 4. Photo. Transverse PT bars after installation.

The other two connections investigated were new design details that take advantage of the enhanced mechanical and durability properties of UHPC. The UHPC connections used the same two basic details: one had a partial-depth connection, and the other had a full-depth connection, as shown in figure 5 and figure 6, respectively.
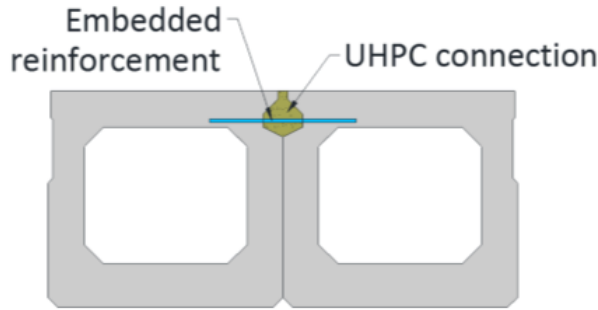
Source: FHWA.

Figure 5. Illustration. Partial-depth UHPC connection.
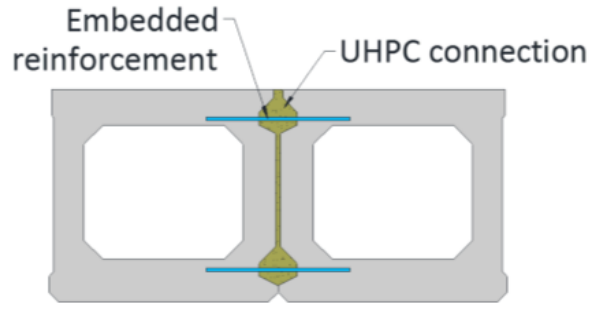
Source: FHWA.

Figure 6. Illustration. Full-depth UHPC connection.

The connection designs included two different surface finishes. The conventionally grouted connection used a sandblasted (SB) surface finish (see figure 7), while the UHPC connection used an exposed aggregate (EA) surface finish (see figure 8). The EA surface finish was created by applying a gelatinous set retarder to the formwork. This delayed the hydration reaction in the concrete, and the unhydrated paste was washed off with water after the formwork was removed. The EA surface preparation has been suggested for field applications of UHPC.[15–17]
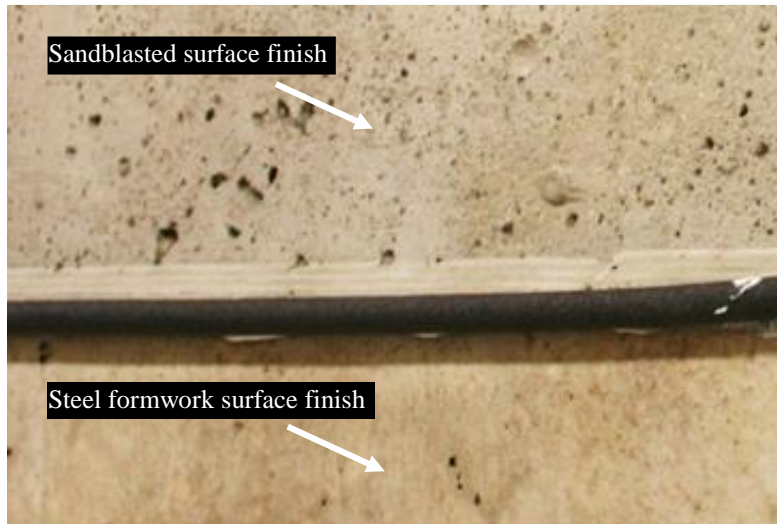
Source: FHWA.

Figure 7. Photo. SB surface finish utilized in the conventionally grouted connection.

Source: FHWA.

Figure 8. Photo. EA surface finish utilized in the UHPC connection.

The design of the UHPC connection included protruding reinforcing steel from each of the precast box beams. These rebars formed a non-contact lap splice when filled with UHPC. With UHPC, a reduced embedment length for deformed reinforcements allowed for simplified design and construction of connection details. An embedment length of 5.5 inches for a No. 4 bar (140 mm for an M13 bar) in the UHPC connections was used in this study and has been demonstrated to be sufficient to develop the yield strength of the steel bar.[18,19] Transverse PT was only applied to the UHPC beams during the casting of the connection to ensure stability of the system during construction. The partial-depth UHPC connection can be seen during and after alignment, as shown in figure 9 and figure 10, respectively.
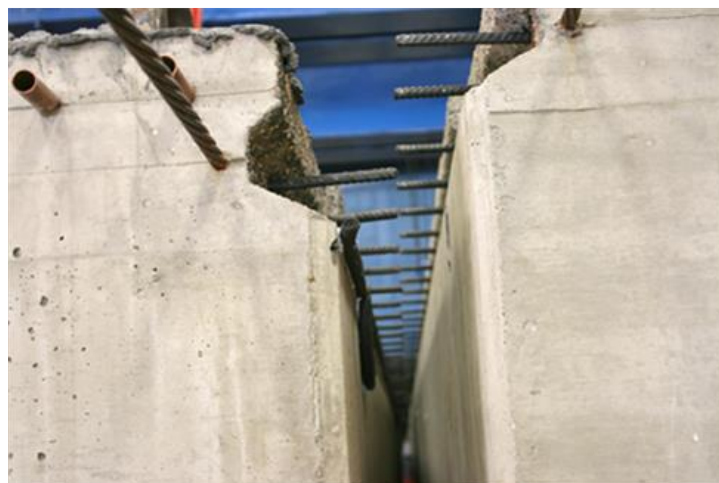
Source: FHWA.

Figure 9. Photo. Alignment of the partial-depth UHPC connection.
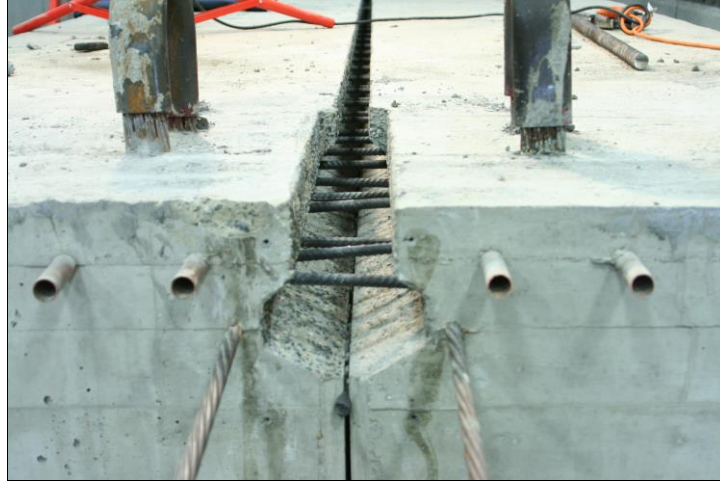
Source: FHWA.

Figure 10. Photo. Partial-depth UHPC connection after alignment.

The concepts for the partial- and full-depth connections are presented in figure 11 and figure 12, respectively. The box beam designs and connection detail dimensions are presented in figure 113 through figure 116 in the appendix. Each box beam has two connection details, one on each side. Figure 13 and figure 14 show the same box beams aligned for the conventional grout and the UHPC connections, respectively. With this design, each beam could be tested with both a conventional grout and a UHPC connection. The conventionally grouted connection was tested first, and the two beams were then separated and arranged to test the UHPC connection.
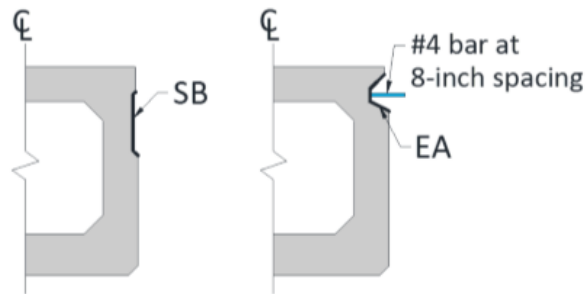
Source: FHWA.   Source: FHWA.

A. Conventional.   B. UHPC.

1 inch = 25.4 mm.

Figure 11. Illustrations. Partial-depth connection details for the conventional and UHPC connections.
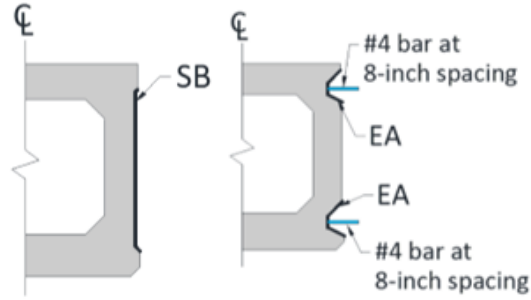
Source: FHWA.   Source: FHWA.

A. Conventional.   B. UHPC.

1 inch = 25.4 mm.

Figure 12. Illustrations. Full-depth connection details for the conventional and UHPC connections.

Source: FHWA.

Figure 13. Photo. Partial-depth beams aligned for connection with the conventional grout shear key connection.
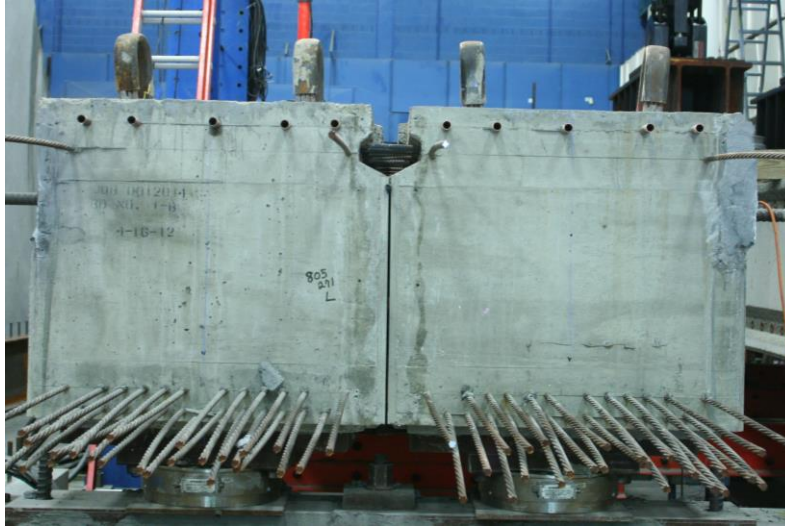
Source: FHWA.

Figure 14. Photo. Partial-depth beams aligned for connection with the UHPC shear key connection.

SHEAR KEY MATERIALS

Two field-cast cementitious materials were used in the connection details. One was a conventional non-shrink grout, and the other was UHPC.

Conventional Non-Shrink Grout

The conventional grout material used in this study was a portland cement-based, prepackaged, non-shrink grout. A water-to-solids ratio of 0.17 was used, and the grout reached an average compressive strength of between 7,800 and 8,120 psi (54 and 56 MPa) at the time of testing. Further assessment of the properties of this grout can be found elsewhere.[20,21] A summary of the properties of the grout is available in table 1. More details about the non-shrink grout and the UHPC can be found in research by Graybeal et al. (See references 16–18 and 20–24.)

Table 1. Typical material properties of the utilized conventional non-shrink grout.

Material Characteristic	Average Result
Water-to-solids ratio[a]	0.17
Average compressive strength[a] (ksi)	8.000
Flow after 25 drops[a] (inches)	9.125–10.0
Solid specific gravity[b]	2.93
Final time of set[b] (h)	6.8
Air content[b]	5.1
Unit weight[b] (lb/ft^3)	129

1 ksi = 6.89 MPa.
1 inch = 25.4 mm.
1 lb/ft^3 = 16 kg/m^3.
[a]Values recorded in this study.
[b]Values reported by De la Varga and Graybeal.[20]

9

UHPC

Advances in the science of concrete materials have led to the development of a new class of advanced cementitious materials, namely UHPC. These concretes tend to contain high amounts of cementitious materials and a very low water-to-cementitious materials ratio as well as exhibit high compressive and tensile strengths. Discrete steel fiber reinforcement is included in UHPC and allows the concrete to sustain a tensile load after the cracking of the cementitious matrix. UHPC has been defined as follows:

> UHPC is a cementitious composite material composed of an optimized gradation of granular constituents, a water-to-cementitious materials ratio less than 0.25, and a high percentage of discontinuous internal fiber reinforcement. The mechanical properties of UHPC include compressive strength greater than 21.7 ksi (150 MPa) and sustained post-cracking tensile strength greater than 0.72 ksi (5 MPa). UHPC has a discontinuous pore structure that reduces liquid ingress, significantly enhancing durability compared to conventional concrete. (p. 1)[22]

Typical field-cast UHPC material properties are presented in table 2, which represent average values for a number of test parameters relevant to the use of UHPC as obtained from independent testing of a commercially available product.[23] This research, which was published in 2006 by the Federal Highway Administration (FHWA), investigated a number of material properties of a UHPC.[23] It also analyzed both mechanical- and durability-based behaviors of UHPC to assess its potential for use in future highway and bridge construction projects.

Table 2. Typical field-cast UHPC material properties.

Material Characteristic	Average Result
Density (lb/ft^3)	155
Compressive strength (ksi) with 28-d strength (ASTM C39)[24]	18.3
Modulus of elasticity (ksi) at 28 d (ASTM C469)[25]	6,200
Split cylinder cracking strength (ksi) (ASTM C496)[26]	1.3
Prism flexure cracking strength (ksi) with 12-inch span (ASTM C1018)[27]	1.3
Mortar briquette cracking strength (ksi) (AASHTO T132)[28]	0.9
Direct tension cracking strength (i.e., axial tensile load) (ksi)	0.8–1.0
Prism toughness index I$_{30}$ (dimensionless) with 12-inch span (ASTM C1018)[27]	48
Long-term creep coefficient with 11.2-ksi load (ASTM C512)[29]	0.78
Long-term shrinkage with initial reading after set (microstrain (με)) (ASTM C157)[30]	555
Total shrinkage with embedded vibrating wire gauge (με)	790
Coefficient of thermal expansion (inch/inch/°F) (AASHTO TP60)[31]	8.2×10^{-6}
Chloride ion penetrability with 28-d test (coulombs) (ASTM C1202)[32]	360
Chloride ion permeability with 0.5-inch depth (lb/yd^3) (AASHTO T259)[33]	<0.10
Scaling resistance (ASTM C672)[34]	No scaling
Abrasion resistance with double weight ground surface (oz) (ASTM C944)[35]	0.026
Freeze–thaw resistance using method A for 600 cycles (percent) (ASTM C666)[36]	112
Alkali-silica reaction with 28-d test (ASTM C1260)[37]	Innocuous

1 lb/ft^3 = 16 kg/m^3.
1 ksi = 6.89 MPa.
1 inch = 25.4 mm.
1 inch/inch/°F = 1.8 mm/mm/°C.
1 lb/yd^3 = 0.593 kg/m^3.
1 oz = 28.35 g.

The UHPC used for this research was a proprietary product produced by a major materials supplier. The UHPC formulation contained a premix powder, water, a modified phosphonate plasticizer, a modified polycarboxylate high-range water-reducing admixture, a non-chloride accelerator, and non-deformed, cylindrical, high-tensile strength steel fibers. The steel fibers had a diameter of 0.008 inch (0.2 mm), a length of 0.5 inch (12.7 mm), tensile strength greater than 290 ksi (2,000 MPa), and a thin brass coating that provided lubrication during the drawing process and provided corrosion resistance. The proportions used in this mix are shown in table 3. The UHPC used for this study had an average compressive strength of 26 ksi (179 MPa) at the time of testing.

Table 3. UHPC mix design.

Material	Amount (lb/yd^3)
Premix powder	3,700
Water	219
Modified phosphonate plasticizer	30
Modified polycarboxylate high-range water reducer	20
Non-chloride accelerator	39
Steel fibers (2 percent by volume)	263

1 lb/yd^3 = 0.593 kg/m^3.

SHEAR KEY CONSTRUCTION

The primary objective of this research was to evaluate the connection performance under thermal and cyclically structural loading. To ensure that the connection material was not biased toward poor performance from early age degradation, such as shrinkage or debonding prior to structural loading, the following standard procedures were adopted:

- The connection interfaces were pre-wet with a wand sprayer 1 h before casting and again 10 min before casting (see figure 15). This minimized the water lost by the grout due to water absorption by the dry surface of the box beam.

- A wrench-tight force of approximately 10 kip (44 kN) was applied to each of the transverse PT bars while the connection was cast. The transverse force was removed 4 d after the connection was cast.

- Wet burlap was placed on top of the conventional grout after casting the connection (see figure 16). The burlap was placed after the construction process was complete (i.e., approximately 2 h) and was kept wet for 7 d.

- Two layers of plastic sheets were placed on top of the UHPC connection within 10 min of casting (see figure 17). The plastic sheets were kept in position for 7 d.

Figure 15. Photo. Pre-wetting the shear key prior to casting the grout.

Figure 16. Photo. Wet burlap curing for the conventionally grouted connection.

Figure 17. Photo. Plastic cover curing for the UHPC connection.

After the connection was cured, the top surface of the connection was ground to achieve a smooth surface. This served to assist in examining the shear key and in identifying interface cracking. An example of the ground connection surface is presented in figure 18.
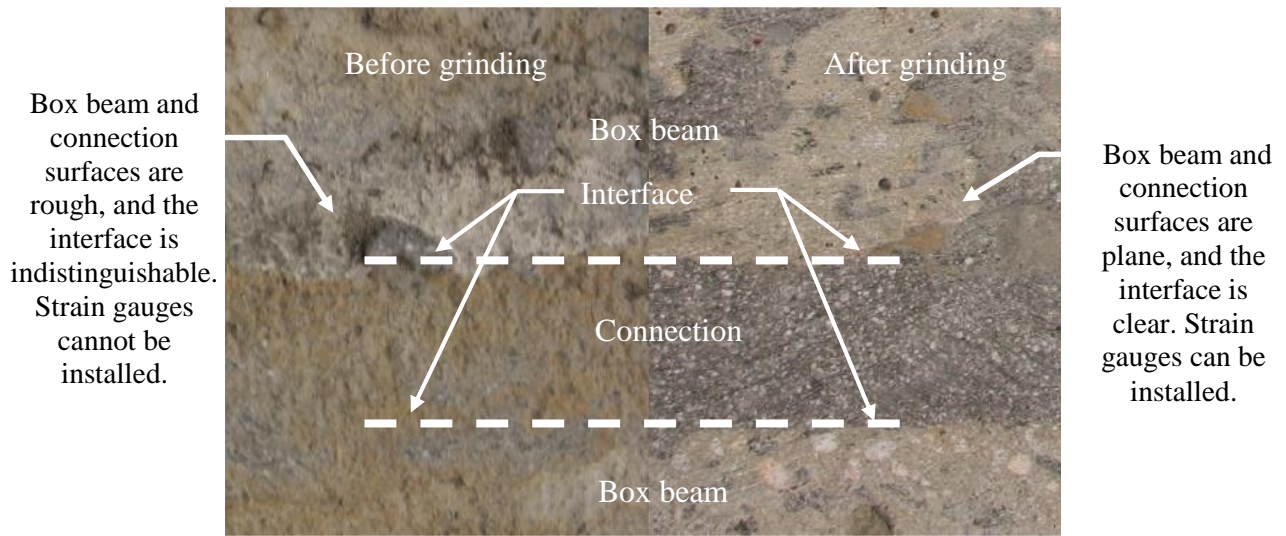
Source: FHWA.

Figure 18. Photo. Comparison of the connection surface and interface between the box beams before and after grinding.

THERMAL LOADING TEST SETUP

Thermal loading was simulated by pumping steam through copper tubes cast in the top flange of the box beams to create a temperature gradient through the depth of the beams. The copper tube arrangement is illustrated in figure 19 and can be seen in the box beam before the concrete was cast in figure 20.
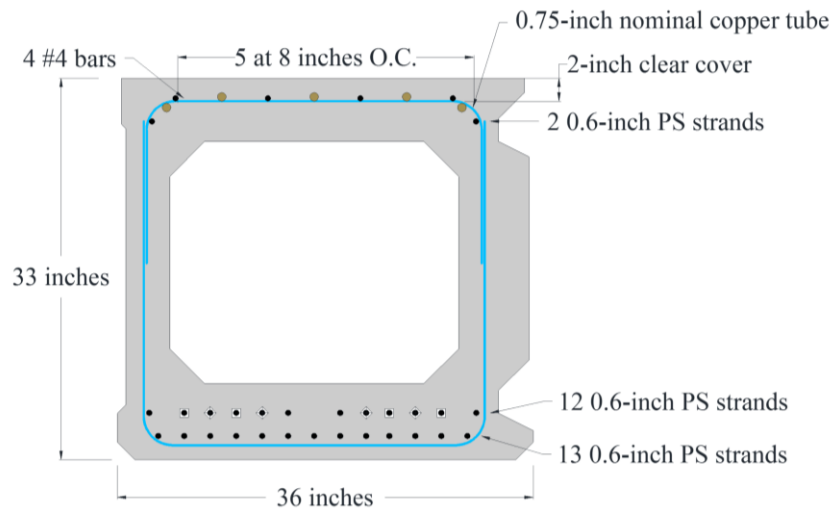
Source: FHWA.
1 inch = 25.4 mm.
PS = prestressing.
O.C. = on the center.

Figure 19. Illustration. Copper tube arrangement within the top flange of the beams.

Figure 20. Photo. Copper tubes in the box beam prior to casting.

The beams were kept inside the laboratory with a room temperature of 70 °F (21 °C). The rate of thermal heating was approximately 18 °F/h (10 °C/h). The steam was cut off when the temperature gradient between the flanges was approximately 50 °F (28 °C). A total of 10 cycles were performed on each connection configuration. Temperatures were recorded using thermocouples embedded within the beams.

CYCLIC STRUCTURAL LOADING TEST SETUP

Two box beams were connected, and four-point bending loads were applied. Three boundary configurations were used: one configuration with both beams simply supported, a second condition with limited end transverse rotation of both beams, and a third with the same limited end rotation plus an additional restraint on one beam's mid-span deflections. The latter two conditions provided more stiffness to the system.

Transverse PT

Transverse PT was used with the conventionally grouted connections. The transverse PT force varied from 0 to 100 kip (0 to 445 kN) at each transverse PT location. These applied PT levels ranged from 8 to 0 kip/ft (0 to 117 kN/m) (i.e., high to low). The transverse PT force was monitored using the load cells (see figure 21). The PT was applied through the internal diaphragms of the girders. No transverse PT was applied for the UHPC connections.

Figure 21. Photo. Transverse PT monitored with a load cell.

Transverse PT is widely used in precast prestressed box beam bridge systems. Annamalai and Brown conducted experimental studies to investigate the effect of transverse PT on the behavior of small assemblies.[38] They concluded that transverse PT exhibited a high degree of monolithic behavior and significantly improved the shear strength of grouted shear key connections. However, according to Russell, more than 80 percent of designers surveyed as part of a study did not complete any design calculations to determine the level of transverse PT force needed.[1] When box girder bridges were examined in the field by Huckelbridge et al., they concluded that transverse PT was ineffective at resisting $\varDelta_\delta$ after the connection partially fractured, despite observing a satisfactory load distribution among beams.[4]

Simply Supported Load and Reaction Arrangement

The loading setup on the two connected box beams is illustrated in figure 22. The box beams were simply supported at each end, providing a span length of 48 ft (14.6 m). Each individual beam was loaded with a spreader beam attached to an actuator. The loading points were 3 ft (0.9 m) on either side of the mid-span. The load was intentionally placed 6 inches (15 cm) off the centerline of the box beam to create a more severe tension force at the connection interface. A photograph showing the laboratory setup is presented in figure 23.

A. Side view.

B. End view.

Figure 22. Illustrations. Loading setup for the simply supported configuration.

Figure 23. Photo. Cyclic structural loading test setup.

Modified Reactions to Increase System Restraint

The simply supported two-beam system is more flexible than a multi-beam bridge. In a multi-beam bridge, adjacent members are forced to deflect simultaneously when load is applied to a single beam as vertical shear force is transferred through the connections. When the deflection of an adjacent member is restrained by other beams in the bridge, a higher shear force at the connection can be expected compared to the case with two members.

With this consideration, two strategies were used to provide additional stiffness in the two-beam system tested in this study. The first required clamping the beam ends to restrain end transverse rotation. The second employed end clamping in tandem with providing in-span support under one beam at the in-span diaphragms. These are referred to as "partially stiffened" and "fully stiffened" boundary conditions, respectively, while the simply supported condition is referred to as "unstiffened." The clamp-down force at each end was applied with two double C channels with a total clamp-down force of 100 kip (445 kN). For the support at the in-span diaphragms, the inside edge of the beam sat on a 6- by 24- by 2-inch (15- by 61- by 5-cm) neoprene pad, while the outside edge of the beam was tied down with a 35-kip (156-MPa) force to reduce the torsional rotation of the cross section when the beam was loaded. The setup is illustrated in figure 24 and pictured in figure 25 and figure 26.
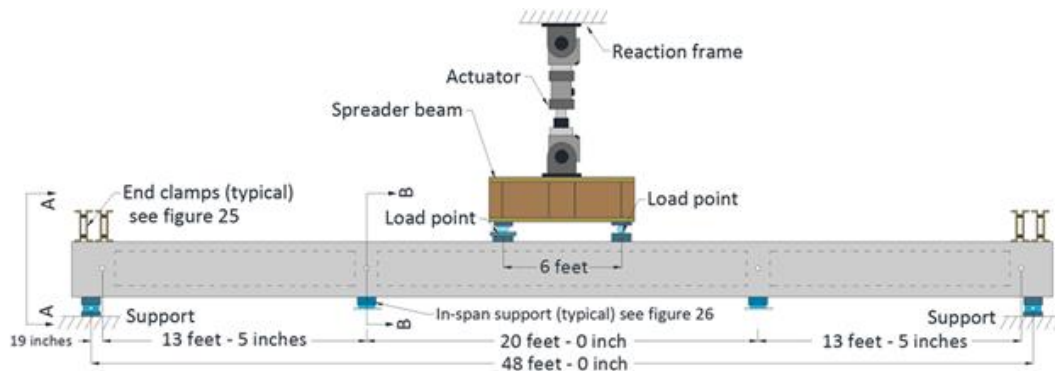
Source: FHWA.
1 ft = 0.305 m.
1 inch = 24.5 mm.

A. Side view.
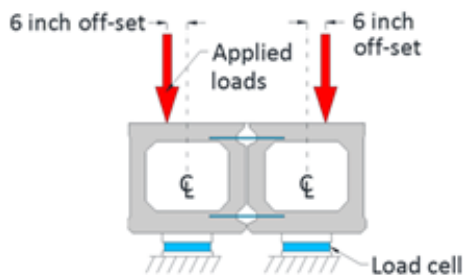
Source: FHWA.
1 inch = 24.5 mm.

B. Section A-A.
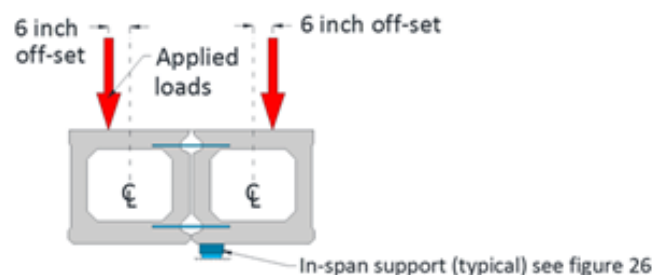
Source: FHWA.
1 inch = 24.5 mm.

C. Section B-B.

Figure 24. Illustrations. Boundary conditions intended to increase structural stiffness.

Source: FHWA.

Figure 25. Photo. Clamping at the beam ends to restrain the transverse rotation.
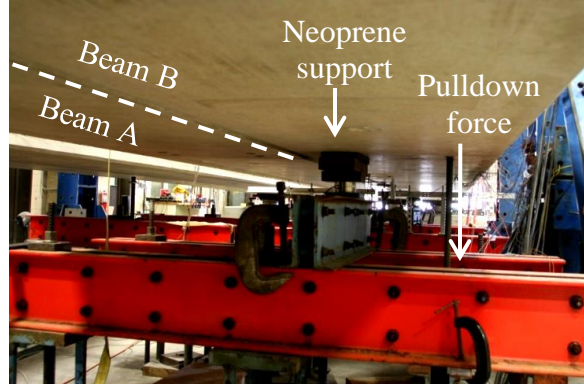
Source: FHWA.

Figure 26. Photo. Additional support provided at in-span diaphragms.

Loading Protocol

The basic cyclic loading protocol included load application to the two beams through a 2-Hz sinusoidal wave ranging from the minimum to the maximum load. A 180-degree phase angle between the actuators on each beam was included to generate load transfer through the connection. Load data from load cells on the actuators in one of the tests is shown in figure 27. A minimum load of 5 kip (34.5 kN) was employed to avoid actuator lift off and potential actuator movement relative to the beams.
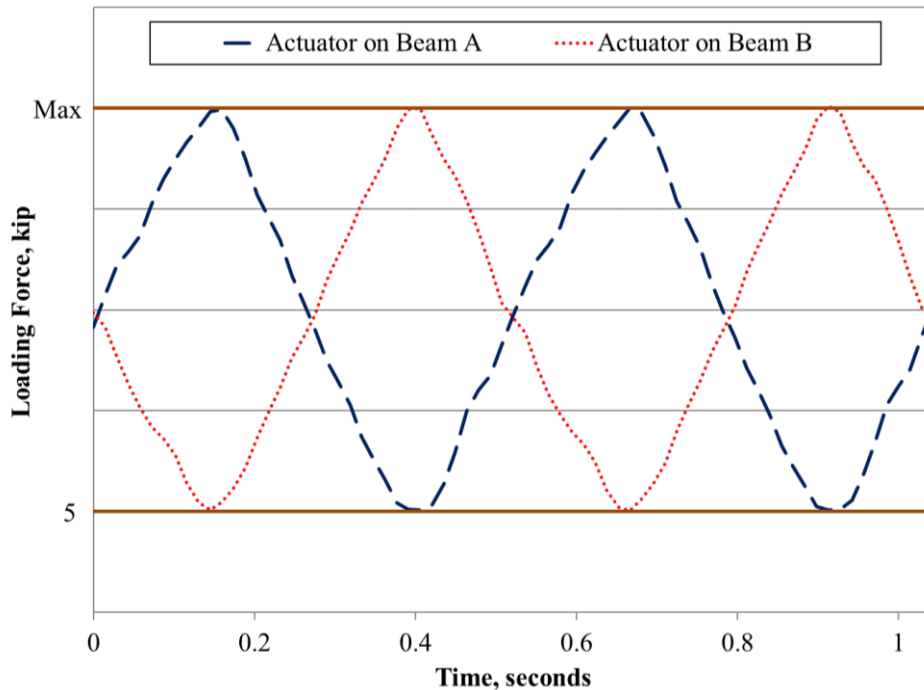
Source: FHWA.
1 kip = 4.448 kN.

Figure 27. Graph. Example of force read by the actuator load cells in the simply supported and partially stiffened beam setups.

When the partially stiffened configuration was used, the beams were loaded following the same loading protocol as the unstiffened configuration. For the fully stiffened configuration, the cyclic load was applied to the unrestrained beam, while the load on the restrained beam was held constant at 5 kip (22 kN). Some load data from load cells on the actuators in one of the tests are shown in figure 28. Minor fluctuations in beam B can be seen, which were caused by the loading on beam A.
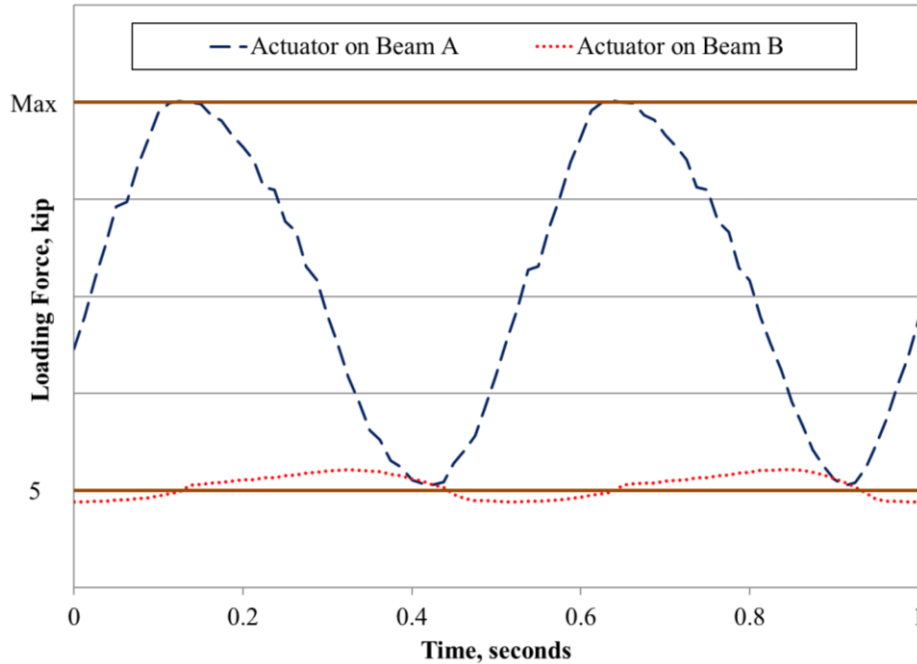
Source: FHWA.
1 kip = 4.448 kN.

Figure 28. Graph. Example of force read by the actuator load cells for beams with the fully stiffened boundary condition.

An analysis of a representative adjacent box beam bridge indicated that an 18-kip (80-kN) loading amplitude was approximately the force effect on a single beam induced by a fatigue truck in the *AASHTO LRFD Bridge Design Specifications*.[6] Based on this information, loading ranges of 18, 36, 54, 72, and 90 kip (80, 160, 240, 320, and 400 kN) were applied in the study. The loading summaries for the cyclic loading scenarios are presented in table 4 through table 7. They include the boundary conditions, loading ranges, PT levels, and number of cycles performed for each of the four test specimens.

Table 4. Summary of structural loading scenarios for the partial-depth conventional shear key connections.

Connection Condition	Boundary	Load Range (kip)	PT (kip/ft)	Cycles* (×10⁶)
Uncracked	Unstiffened	18, 36, 54, and 72	8.0	0.50
Uncracked	Unstiffened	90	8.0	1.00
Uncracked	Unstiffened	54, 72, and 90	6.0	0.50
Uncracked	Unstiffened	54 and 72	4.0	0.15
Uncracked	Unstiffened	90	4.0	0.50
Uncracked	Unstiffened	54 and 72	2.0	0.15
Uncracked	Unstiffened	90	2.0	0.50
Uncracked	Unstiffened	54 and 72	0.8	0.15
Uncracked	Unstiffened	90	0.8	0.50
Uncracked	Partially stiffened	54 and 72	2.0	0.15
Uncracked	Partially stiffened	90	2.0	0.50
Uncracked	Partially stiffened	54 and 72	0.8	0.15
Uncracked	Partially stiffened	90	0.8	0.50
Uncracked	Fully stiffened	54 and 72	2.0	0.15
Uncracked	Fully stiffened	90	2.0	0.50
Uncracked	Fully stiffened	54 and 72	0.8	0.02
Uncracked	Fully stiffened	90	0.8	0.55
Uncracked	Fully stiffened	54 and 72	0.0	0.03
Uncracked	Fully stiffened	90	0.0	0.30
Partially cracked	Fully stiffened	54 and 72	8.0	0.01
Partially cracked	Fully stiffened	90	8.0	0.15
Partially cracked	Fully stiffened	54 and 72	4.0	0.01
Partially cracked	Fully stiffened	90	4.0	0.30
Partially cracked	Fully stiffened	54 and 72	0.8	0.01
Partially cracked	Fully stiffened	90	0.8	0.15
Partially cracked	Fully stiffened	54 and 72	0.0	0.01
Partially cracked	Fully stiffened	90	0.0	0.15
Fully cracked	Fully stiffened	18, 36, 54, 72, and 90	8.0	0.01
Fully cracked	Fully stiffened	18, 36, 54, 72, and 90	4.0	0.01
Fully cracked	Fully stiffened	18, 36, 54, 72, and 90	0.8	0.01
Fully cracked	Fully stiffened	18, 36, 54, 72, and 90	0.0	0.01

1 kip = 4.448 kN.
1 kip/ft = 14.59 kN/m.
*Number of cycles listed is for each individual loading range, not the total for all loading ranges listed.

Table 5. Summary of structural loading scenarios for the full-depth conventional shear key connections.

Connection Condition	Boundary	Load Range (kip)	PT (kip/ft)	Cycles* ($\times 10^6$)
Partially cracked	Unstiffened	54 and 72	8.0	0.15
Partially cracked	Unstiffened	90	8.0	0.30
Partially cracked	Unstiffened	54 and 72	4.0	0.15
Partially cracked	Unstiffened	90	4.0	0.30
Partially cracked	Unstiffened	54 and 72	0.8	0.15
Partially cracked	Unstiffened	90	0.8	0.30
Partially cracked	Unstiffened	54 and 72	0.0	0.15
Partially cracked	Unstiffened	90	0.0	0.15
Fully cracked	Unstiffened	90	0.0	0.15

1 kip = 4.448 kN.
1 kip/ft = 14.59 kN/m.
*Number of cycles listed is for each individual loading range, not the total for all loading ranges listed.

Table 6. Summary of structural loading scenarios for the partial-depth UHPC shear key connections.

Connection Condition	Boundary	Load Range (kip)	PT (kip/ft)	Cycles* ($\times 10^6$)
Uncracked	Partially stiffened	54 and 72	0	0.15
Uncracked	Partially stiffened	54 and 72	0	0.15
Uncracked	Fully stiffened	54 and 72	0	0.15
Uncracked	Fully stiffened	90	0	0.65

1 kip = 4.448 kN.
1 kip/ft = 14.59 kN/m.
*Number of cycles listed is for each individual loading range, not the total for all loading ranges listed.

Table 7. Summary of structural loading scenarios for the full-depth UHPC shear key connections.

Connection Condition	Boundary	Load Range (kip)	PT (kip/ft)	Cycles* ($\times 10^6$)
Uncracked	Unstiffened	54, 72, and 90	0	0.050
Uncracked	Partially stiffened	54, 72, and 90	0	0.150
Uncracked	Fully stiffened	54 and 72	0	0.200
Uncracked	Fully stiffened	90	0	0.515

1 kip = 4.448 kN.
1 kip/ft = 14.59 kN/m.
*Number of cycles listed is for each individual loading range, not the total for all loading ranges listed.

Instrumentation

The beams were loaded with a computer-controlled servo-hydraulic loading system, and the structural response of each specimen was captured through the use of electronic instrumentation. The test utilized thermocouples, load cells, linear variable differential transformers (LVDTs), and strain gauges to record critical data on the structural performance. A high-speed data acquisition system was used for the capture of data from the instruments during both the thermal and cyclic loading.

Each beam was equipped with seven embedded thermocouples. There was one placed in the bottom flange at the mid-span, while the other six were distributed along the top flange. Of these six, three were placed around the mid-span (i.e., one at the mid-span and two 6 ft (1.83 m) longitudinally on each side of the mid-span). Two thermocouples were positioned to monitor incoming and outgoing steam temperatures at one beam end. The final thermocouple was at the opposite beam end.

The load was monitored by six load cells placed under the end supports of each beam, as shown in figure 29. The west end of the beams utilized a single load cell under each beam, while the east end had two load cells under each beam. Load cells inside each actuator captured the force imparted to the structure through the actuators. A load cell was also used to monitor the PT force in each PT bar.

Source: FHWA.

Figure 29. Photo. Load cell under the beam at the west support.

The vertical displacements of the beams were recorded by four LVDTs placed under the beam at the mid-span 2 inches (51 mm) away from each edge of each beam. Figure 30 shows the installation of these vertical transformers. Six transverse LVDTs measured separation of the connection between the beams. Three transverse LVDTs spanned the connection at the top of the beam, and three spanned the connection at the bottom of the beam. They were placed at the mid-span and 6 ft (1.83 m) longitudinally from the mid-span in each direction. The transverse bottom LVDT at the mid-span is visible in figure 30. Figure 31 shows a typical transverse LVDT spanning the top of the connection.

Source: FHWA.

Figure 30. Photo. Five LVDTs (four vertical and one transverse) at the mid-span used to measure vertical deflection of the beams and the transverse connection opening.

Source: FHWA.

Figure 31. Photo. Transverse LVDT and strain gauge on the top surface spanning the connection.

Electrical resistance strain gauges were used to capture longitudinal and transverse strain in the concrete. Each beam had six embedded strain gauges placed on sister rebar. The sister rebar was then coupled with the reinforcing steel of the beams. Figure 32 shows one of the longitudinal strain gauges at the mid-span in the bottom flange of one of the beams coupled with the top layer of prestressing strands. Transverse embedded strain gauges were placed at four locations: in the top and bottom flanges at the mid-span and in the top flange 6 ft (1.83 m) longitudinally on each side of the mid-span. Longitudinal strain gauges were placed in both the top and bottom flanges and at the mid-span. All embedded strain gauges were placed along the centerline of the beams. Some of the embedded strain gauges were not used in some of the tests. Table 8 shows what gauges were included in which tests.
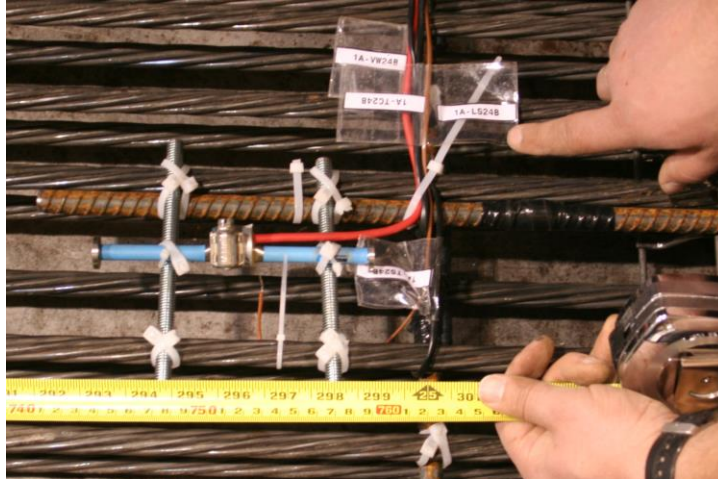
Figure 32. Photo. Longitudinal strain gauge and thermocouple located at the mid-span in the bottom flange of one of the beams.

Table 8. Strain gauges used in the test setups.

Setup	Embedded Transverse Gauges	Embedded Longitudinal Gauges	External Longitudinal Gauges	Transverse Grout Gauges	Transverse Near Connection	Transverse Top Beam
Partial-depth grout	Three on top (middle, east, and west) and one on the bottom	One on the top and one on the bottom	Not used	Not used	Not used	Not used
Partial-depth grout (fully stiffened)	Three on top (middle, east, and west) and one on the bottom	One on the top and one on the bottom	Two on each beam near the edge of the beams	One at the mid-span, one 6 ft east, one 6 ft west, and four PT	Not used	Not used
Full-depth grout	Three on top (middle, east, and west) and one on the bottom	One on the top and one on the bottom	Two on each beam near the edge of the beams	One at the mid-span, one 6 ft east, one 6 ft west, and four PT	Not used	Not used
Partial-depth UHPC	Three on top (middle, east, and west) and one on the bottom	One on the top and one on the bottom	Two on each beam near the edge of the beams	One at the mid-span, one 6 ft east, one 6 ft west, and four PT	Not used	Not used
Full-depth UHPC	One on the top of each beam (east gauges only were used in the north beam and middle gauges only were used in the south beam)	Bottom only	Two on each beam near the edge of the beams	One at the mid-span, one 6 ft east, and one 6 ft west	Two at the mid-span, two 6 ft east, and two 6 ft west each location one on each beam	Three at the mid-span and four 6 ft east (center of each beam and the outside edge*)

1 ft = 0.305 m.
*The southern mid-span gauge did not capture any data.

Surface strain gauges were installed after the beams were connected. Seven transverse surface strain gauges were installed along the length of the connection to measure PT confinement strain and the development of tensile strain during the tests. Gauges were located at the mid-span 6 ft (1.83 m) from the mid-span in each direction and at PT locations. Additional transverse gauges were located on the top of the girder at the mid-span and 6 ft on each side of the mid-span. Three gauges were placed on each beam at the centerline and 6 inches (152 mm) from each edge. The location 6 ft (1.83 m) east of the mid-span had all six gauges. At the mid-span, the southern-most gauge was missing. The location 6 ft (1.83 m) west only had the two gauges nearest the connection. Four longitudinal surface strain gauges were placed on the bottom flange at the mid-span 6 inches (152 mm) from each edge. It should be noted that the surface strain gauges were not used on every specimen. Table 8 shows what gauges were included in which tests. The arrangement of all of the instrumentation is shown in figure 33.
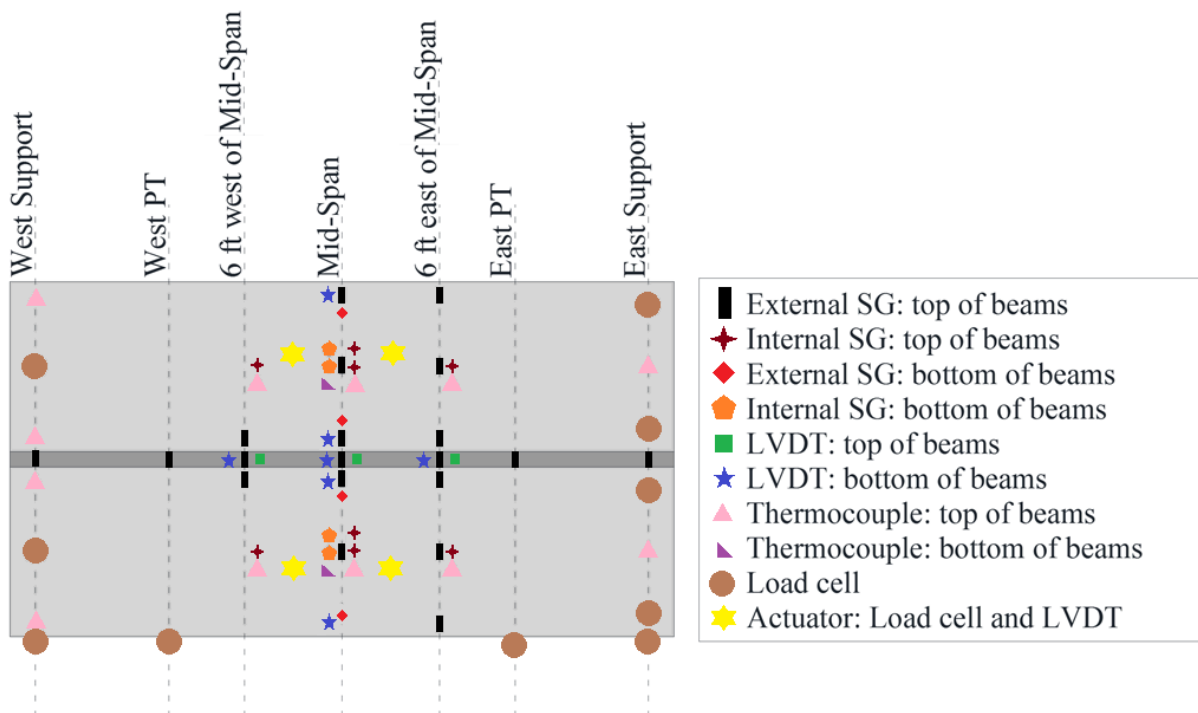
Source: FHWA.
1 ft = 0.305 m.
SG = strain gauge.

Figure 33. Illustration. Plan view of instrumentation installed on the test specimens.

CHAPTER 3. ANALYTICAL MODELING OF STRUCTURAL BEHAVIOR

Before discussing the connection performance under cyclic structural loading, the parameters used in the analysis and evaluation of the section must first be introduced.

PROPORTION OF MOMENT

The full-scale testing conducted in this research was intended to simulate the stress conditions within the connections in a real bridge. When wheel loads are applied to a beam in a multi-beam bridge, the adjacent members are forced to deflect simultaneously as the load is transferred through the connection to adjacent beams. One of the key parameters investigated in this study is the proportion of the moment carried by the loaded beam. This is analogous to the moment distribution factor that by definition can be calculated using the equation in figure 34.

$$\text{Moment Distribution on Beam 1} = \frac{\text{Moment Carried by Beam 1}}{\text{Moment carried by (Beam 1 + Beam 2 + ... + Beam } N)}$$

Figure 34. Equation. Moment distribution factor for a beam.

When the two beams have the same cross section, material properties, and boundary conditions, the moment carried by each beam is proportional to the deflection or the longitudinal tensile strain at the mid-span. In the four-point bending setup used in these tests, the relationship between the moment, the deflection, and longitudinal tensile strain are given in figure 35 and figure 36, respectively.

$$M = \frac{24\delta EI}{3l^2 - 4b^2}$$

Figure 35. Equation. Moment carried by the beam with respect to the mid-span deflection.

Where:

M = moment at the mid-span.
δ = deflection at the mid-span.
EI = beam stiffness.
l = span length.
b = distance from each end support to each loading point.

$$M = -\frac{\varepsilon EI}{y}$$

Figure 36. Equation. Moment carried by the beam with respect to the longitudinal tensile strain at the mid-span.

Where:

ε = longitudinal tensile strain at the mid-span.
y = distance from where the tensile strain is measured to the neutral axis of the cross section.

Given these relationships, the equation in figure 34 can be rewritten with respect to the mid-span deflection and longitudinal tensile strain for the two-beam system being employed in this study, as shown in figure 37 and figure 38, respectively.

$$\text{Proportion of Moment Carried by Beam A} = \frac{\delta_A}{\delta_A + \delta_B}$$

Figure 37. Equation. Loaded beam proportion of moment factor with respect to the mid-span deflection.

Where:

δ_A = deflection of beam A.
δ_B = deflection of beam B.

$$\text{Proportion of Moment Carried by Beam A} = \frac{\varepsilon_A}{\varepsilon_A + \varepsilon_B}$$

Figure 38. Equation. Loaded beam proportion of moment factor for the loaded beam with respect to the mid-span longitudinal tensile strain.

Where:

ε_A = longitudinal tensile strain in beam A.
ε_B = longitudinal tensile strain in beam B.

An example of the calculated loaded beam proportion of moment based on deflection and strain for the simply supported unstiffened beams with partial-depth conventional grout connection is presented in figure 391 kip = 4.448 kn.
1 kip/ft = 14.59 kn/m.

figure 39. The deflection was recorded by the LVDTs placed at the mid-span, and the strain was measured with the embedded bottom longitudinal strain gauges at the mid-span. A total of 1.5 million cycles was included under three loading ranges. In this figure, beam A was cyclically loaded over three loading ranges spanning from 5 kip (22 kN) up to 59, 77, and 95 kip (262, 342, and 423 kN). The load on beam B was held constant at 5 kip (22 kN). The proportion of moment based on the strain and deflection agreed, showing that beam A carried about 52 percent of the total moment.

| Loading Range (kip): | 54 | 72 | 90 |
| Post-tensioning (kip/ft): | 6.0 | | |
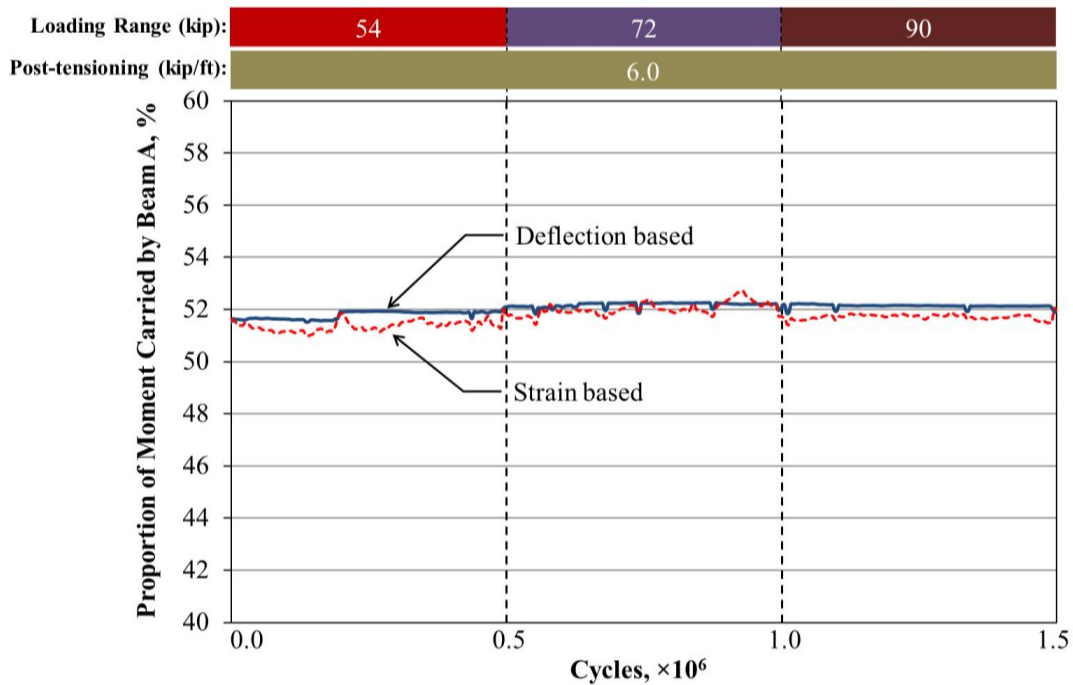
Deflection based

Strain based

Figure 39. Graph. Loaded beam proportion of moment based on deflection and longitudinal tensile strain for unstiffened beams with a partial-depth uncracked conventionally grouted connection.

Source: FHWA.
1 kip = 4.448 kN.
1 kip/ft = 14.59 kN/m.

Figure 40 demonstrates the loaded beam proportion of moment for the same configuration with the addition of the partially stiffened boundary condition. In this case, the two beams still have the same support conditions, and the proportion of moment can be calculated using the equations in figure 35 and figure 36. As shown in figure 40, beam A had a proportion of moment close to 52 percent with the partially stiffened boundary condition, which was nearly identical to the unstiffened case. However, if the longitudinal strains in the beams are different, the moment transferred though the connection must be different. The proportion of moment itself may not reflect the difference, as it measures the ratio of the moments.
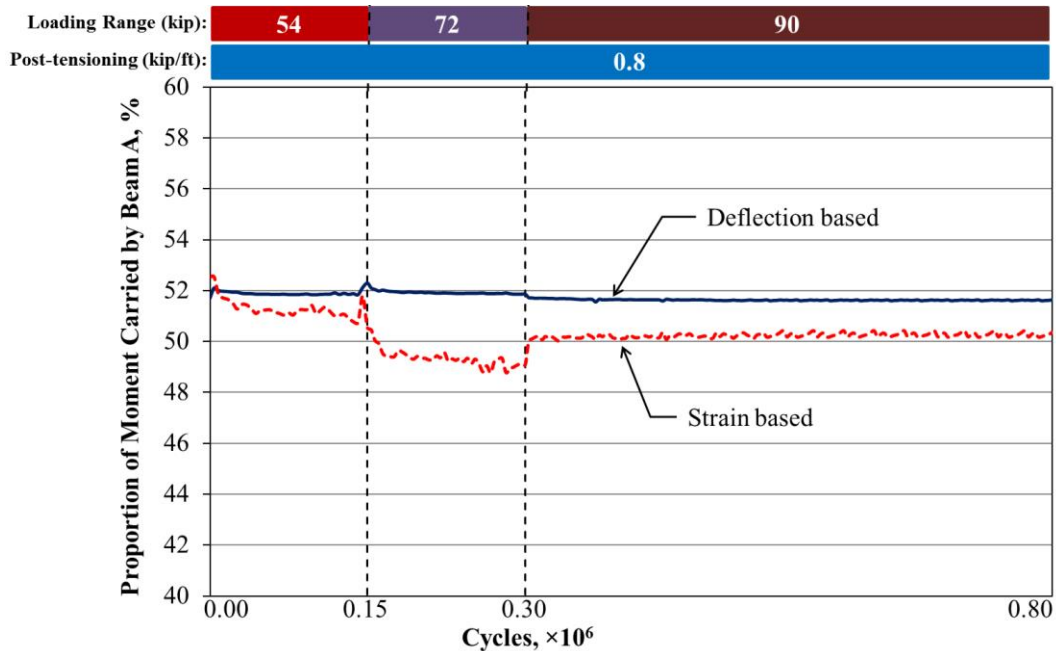
Source: FHWA.
1 kip = 4.448 kN.
1 kip/ft = 14.59 kN/m.

Figure 40. Graph. Loaded beam proportion of moment based on deflection and longitudinal tensile strain for partially stiffened beams with a partial-depth uncracked conventionally grouted connection.

For the fully stiffened configuration, the proportion of moment could not be calculated using the equations in figure 35 and figure 36 because the boundary conditions of the two beams were different. A new parameter, the equivalent moment transferred through the connection ($M_{equivalent}$), must be introduced. This is described further in the following subsection.

EQUIVALENT MOMENT TRANSFERRED THROUGH THE CONNECTION ($M_{equivalent}$)

The concept of $M_{equivalent}$ is demonstrated in the following example with the two simply supported beams loaded at the extreme values of the loading range. When beam A was loaded at the maximum, beam B had less deflection and tensile strain at the mid-span than beam A but more than if it had not been connected to beam A. This extra deflection and tensile strain in beam B was driven by the force transfer through the connection. $M_{equivalent}$ represents the moment being transferred through the connection and can be calculated using the equations in figure 41 and figure 42 as follows:

$$\varepsilon' = \varepsilon_{measured} - \varepsilon_{5kip}$$

Figure 41. Equation. Additional strain in beam B due to $M_{equivalent}$.

32

Where:

ε' = additional strain in beam B due to $M_{equivalent}$.
$\varepsilon_{measured}$ = measured strain in beam B when beam A is loaded at the maximum load and beam B is loaded at the minimum load.
ε_{5kip} = strain in beam B when both beams are loaded at 5 kip (22 kN).

$$M_{equivalent} = -\frac{\varepsilon' EI_{eff}}{y}$$

Figure 42. Equation. $M_{equivalent}$.

Where EI_{eff} is the effective beam stiffness.

ε' can also be thought of as the range of strain experienced during a loading cycle. For the variables in the equations in figure 41 and figure 42, the strains are direct measurements, and y, which was previously defined in the equation in figure 36, is a property of the beam cross section. EI_{eff} can be calculated using the equations in figure 35 and figure 36 with the measured deflection and strain. The calculation of EI_{eff} is demonstrated in the following paragraphs and is compared with the theoretical values based on the sectional and material properties of the beam used.

After the two beams were grouted together, they were loaded, and the deflection and tensile strain at the mid-span were measured. The specimen was loaded with 45 kip (200 kN) on one beam and 55 kip (244 kN) on the other beam, which was equivalent to 50 kip (222 kN) on each beam. The mid-span deflection and tensile strain were recorded. These values were compared with the calculated values obtained using the equations in figure 35 and figure 36. The calculated deflection and tensile strain used an assumed value for the concrete's modulus of elasticity based on an 8,000-psi (55-MPa) compressive strength.

The moment of inertia of the two connected beams was calculated as two times the moment of inertia of an individual beam based on the dimension and reinforcement details. The beam stiffness (EI) for a single beam was calculated to be 434×10^6 kip-inch^2 (1.25×10^6 kN-m^2). The calculated deflection and tensile strain were both slightly larger than the measured values, indicating EI was underestimated. This could be due to the solid diaphragms in the beams and the solid connection. EI_{eff} was then calculated using the equations in figure 35 and figure 36 using the actual measured deflection and strain. The results are listed in table 9. EI_{eff} based on deflection and tensile strain were 442×10^6 and 472×10^6 kip-inch^2 (1.27×10^6 and 1.35×10^6 kN-m^2), respectively, compared to the calculated EI of 434×10^6 kip-inch^2 (1.25×10^6 kN-m^2). The average of the two, 457×10^6 kip-inch (1.31×10^6 kN-m^2), was used as the EI_{eff}.

Table 9. Beam stiffness calculation.

P (kip)	$\delta_{calculated}$ (inches)	$\delta_{measured}$ (inches)	$EI_{eff,\delta}$ ($\times 10^6$ kip-inch^2)	$\varepsilon_{calculated}$ ($\mu\varepsilon$)	$\varepsilon_{measured}$ ($\mu\varepsilon$)	$EI_{eff,\varepsilon}$ ($\times 10^6$ kip-inch^2)
50	0.447	0.439	442	356	328	472

1 kip = 4.448 kN.
1 inch = 25.4 mm.

Where:

P = load at each load point (see figure 22 for loading setup).
$\delta_{calculated}$ = calculated deflection of the beam.
$\delta_{measured}$ = measured deflection in beam B when beam A is loaded at the maximum load and beam B is loaded at the minimum level.
$EI_{eff,\delta}$ = effective beam stiffness based on deflection measurements.
$\varepsilon_{calculated}$ = calculated strain.
$\varepsilon_{measured}$ = measured strain in beam B when beam A is loaded at a maximum load and beam B is loaded at the minimum load.
$EI_{eff,\varepsilon}$ = effective beam stiffness based on strain measurements.

With the new parameter of $M_{equivalent}$, the effect of different boundary conditions was evaluated. For the unstiffened beams with a partial-depth conventionally grouted connection, the measured strain is presented in figure 43, while the strain for the same beams with the partially stiffened boundary condition is presented in figure 44. In both figures, beam A was loaded to 95 kip (423 kN), and beam B was loaded to 5 kip (22 kN). In the unstiffened case, beams A and B had average strains of 162 and 150 µε, respectively. $M_{equivalent}$ was 502 kip-ft (680 kN-m). For the partially stiffened case, beam A had an average strain of 127 µε, and beam B had an average strain of 111 µε. $M_{equivalent}$ was 395 kip-ft (535 kN-m). The proportion of the moment carried by beam A for both boundary conditions was about the same even though the transferred moment differed.
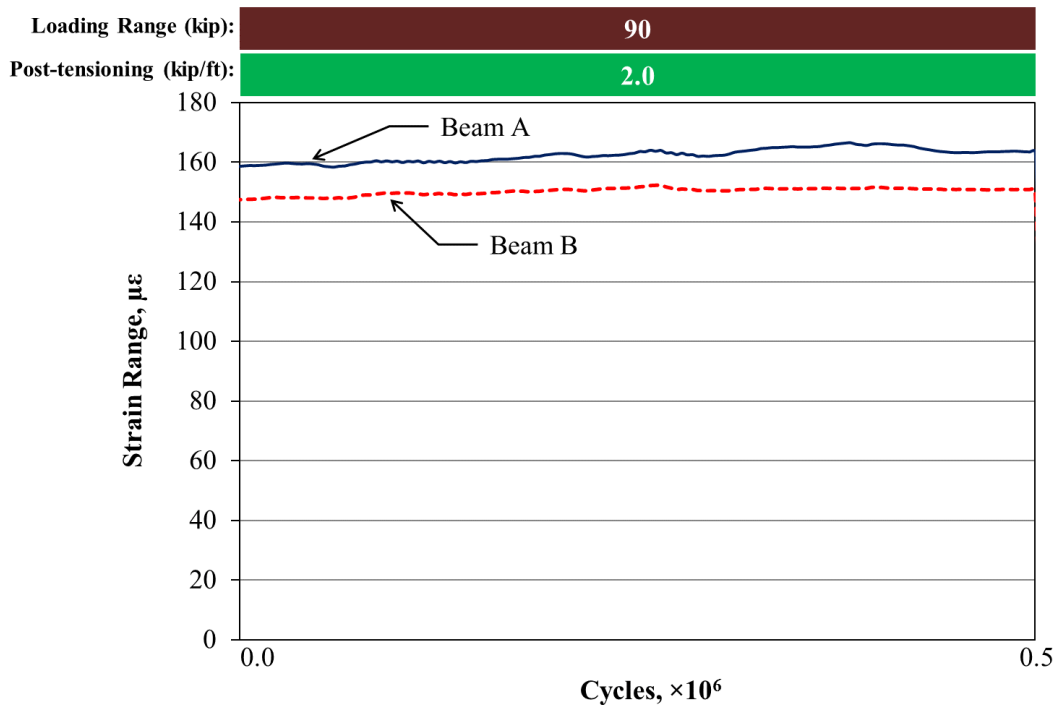
Source: FHWA.
1 kip = 4.448 kN.
1 kip/ft = 14.59 kN/m.

Figure 43. Graph. Longitudinal tensile strain range at the mid-span for unstiffened beams with a partial-depth uncracked conventionally grouted connection.

34
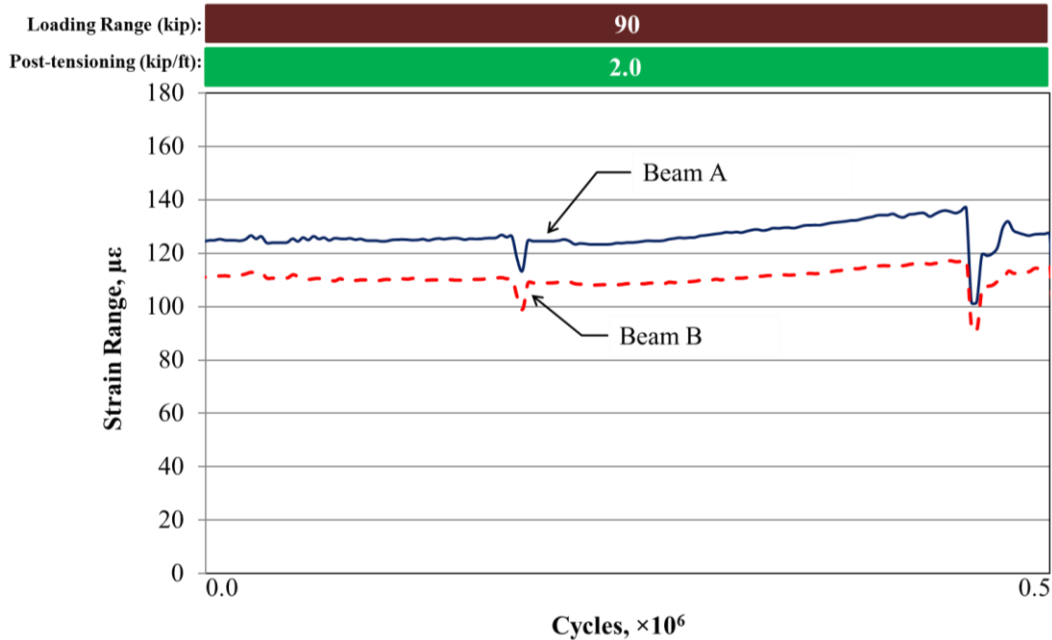
Source: FHWA.
1 kip = 4.448 kN.
1 kip/ft = 14.59 kN/m.

Figure 44. Graph. Longitudinal tensile strain range at the mid-span for partially stiffened beams with a partial-depth uncracked conventionally grouted connection.

Figure 45 presents the strain for the same beams in the same loading range but with the fully stiffened boundary condition. This case was analyzed in two steps. The first step assumed that a single beam with the partially stiffened boundary was loaded with a total force of 95 kip (423 kN). The tensile strain at the mid-span can be reasonably estimated as the sum of the strains in beams A and B with the same boundary condition less the strain induced by a 5-kip (22-kN) load on both beams. ε_{5kip} was measured to be 14 με, which yielded an estimated strain of 220 με. The corresponding moment can then be calculated using the equation in figure 36, which gives an $M_{equivalent}$ of 681 kip-ft (920 kN-m). In the second step, the actual beam A in the case was investigated. The beam had the same boundary condition as in the first step, except a force was transferred through the connection, which generated a moment in the adjacent beam. $M_{equivalent}$ at the mid-span of beam A can be calculated using the equation in figure 42, which was 183 kip-ft (248 kN-m) corresponding to a strain of 59 με. Therefore, the remaining 498 kip-ft (673 kN-m) of the 681 kip-ft (920 kN-m) was transferred through the connection compared to 395 kip-ft (535 kN-m) $M_{equivalent}$ for the partially stiffened case. A more severe loading condition on the connection was created when the deflection of one beam was restrained.

35
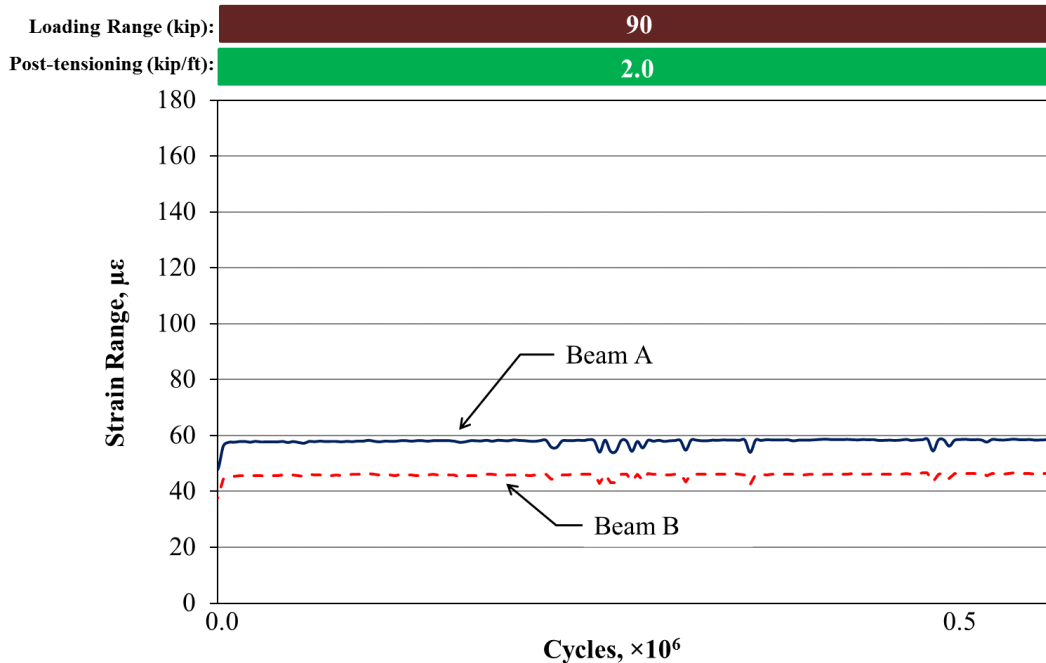
Figure 45. Graph. Tensile strain range at the mid-span for fully stiffened beams with a partial-depth uncracked conventionally grouted connection.

The strain in beam A was reduced by nearly 55 percent from 127 to 59 $\mu\varepsilon$ when the fully stiffened boundary condition was added to beam B compared to the partially stiffened case. This can be viewed as equivalent to the case limiting the end rotation but with 2.2 times of original stiffness. Thus, this loading configuration was similar to a case wherein 4.4 beams were connected in the system. Therefore, the stiffest condition created in the study was considered to approximate the case with 4.4 beams connected with a 95-kip (423-kN) load on a single exterior beam.

DIFFERENTIAL DEFLECTION (Δ_δ)

Δ_δ between adjacent beams is another factor that was evaluated in this study. It is defined by the authors as the difference between the deflections of these two lines at the interface between the two beams. This was done to remove the rigid body rotation of the beams. When connections deteriorate, beams do not deflect uniformly under live loads. Large Δ_δ between adjacent girders may lead to further degradation of grouted connections and reflective cracking in the overlay if one is present. Δ_δ is determined by checking the deflection measurements between the adjacent beams at the mid-span near the connection. Four vertical LVDTs were placed at the mid-span: two on each beam with each LVDT placed 2 inches (51 mm) from the edges of each beam. Δ_δ was determined by drawing two straight lines that define the bottom of each beam. Given where the four LVDTs are located, Δ_δ can be calculated with the equation in figure 46.

36

$$\Delta_\delta = \left[\delta_{AI} - \frac{2}{32}(\delta_{AE} - \delta_{AI})\right] - \left[\delta_{BI} + \frac{2}{32}(\delta_{BI} - \delta_{BE})\right] = \frac{17}{16}(\delta_{AI} - \delta_{BI}) - \frac{1}{16}(\delta_{AE} - \delta_{BE})$$

Figure 46. Equation. Δ_δ between the two beams.

Where:

δ_{AI} = deflection from the loaded beam on the interior LVDT.
δ_{AE} = deflection from the loaded beam on the exterior LVDT.
δ_{BI} = deflection from the unloaded beam on the interior LVDT.
δ_{BE} = deflection from the unloaded beam on the exterior LVDT.

Due to this means of calculation, Δ_δ may become negative if the loaded beam rotates more than the unloaded beam. *Differential rotation* is defined by the authors as the rotation in the unloaded beam subtracted from the rotation in the loaded beam. Figure 47 shows an example of this behavior from the full-depth UHPC connection. It is evident that an increase in differential rotation can yield a decrease in Δ_δ.
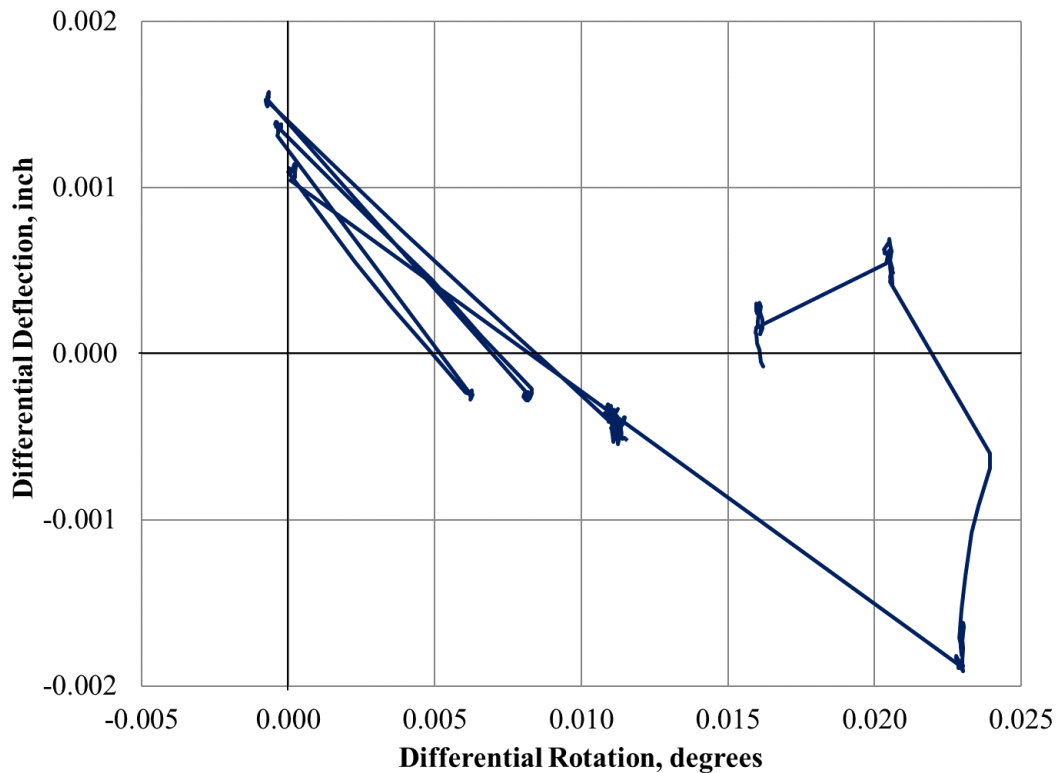
Source: FHWA.
1 inch = 25.4 mm.

Figure 47. Graph. Comparison of Δ_δ and differential rotation for the full-depth UHPC connection.

TRANSVERSE SHEAR IN THE CONNECTION

A fully functioning connection is assumed to effectively transfer the load from one beam to the other. The adjacent beam is expected to have the same deflection as the loaded beam and, therefore, should have a nearly identical deformed shape. The loads that drive this behavior are transferred through the connection. The Canadian Bridge Code assumes that the load is transferred from one beam to another primarily through transverse shear. Transverse flexural rigidity is neglected.[10] This report uses the same assumption.

When two beams are connected and only one beam is loaded, the magnitude of the transverse shear force generated in the connection is related to the deflection of the beams. For a two-beam system where the load is applied to one beam, a greater deflection of the pair will generate more transverse shear in the connection. At locations where there is no potential deflection, such as at the beam ends, no transverse shear force will be generated. For the two beams analyzed in this study, the structurally loaded beam had a nearly uniformly deflected shape. One possible transverse shear distribution (V_y) is presented in figure 48. If V_y and the moment transferred through the shear key are known, the shear force transferred through the connection can be calculated. As the variable of interest for design is the maximum distributed shear force (v'_{max}) in the connection, the shear force calculation can be simplified by assuming a triangular shear distribution (V'_y). v'_{max} of V'_y should be larger than the maximum value of V_y. v'_{max} can be calculated using the equation in figure 49.
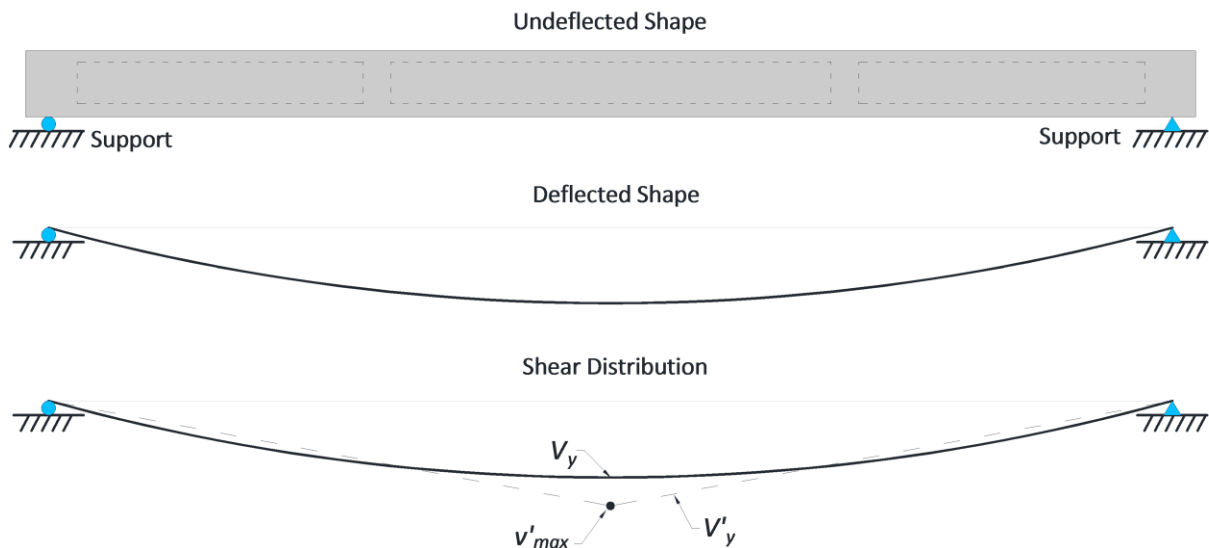
Source: FHWA.

Figure 48. Illustration. Transverse shear stress distribution through the connection.

$$v'_{max} = \frac{M_{max} \times 12}{l^2}$$

Figure 49. Equation. v'_{max} through the connection.

Where:

M_{max} = maximum moment transferred through the connection.
l = span length.

For the tests conducted in this study, M_{max} was 478 kip-ft (646 kN-m), and v'_{max} was calculated to be 207 lb/inch (36.3 kN/m).

The Canadian Bridge Design Code provides charts to determine the required transverse shear force to be resisted based on the study by Bakht et al.[10,39] In the method proposed by Bakht et al., the shear force is determined using the orthotropic plate theory based on the bridge width, span length, and a factor related to the longitudinal, flexural, and torsional rigidity of the beam section.[39] In general, bridges with greater torsional rigidity, larger bridge widths, and shorter spans generate higher transverse shear. Using the Canadian Bridge Design Code chart that aligns with the beams tested in this study, v'_{max} due to the AASHTO HS-20 truck is calculated to be approximately 207 lb/inch (36.3 kN/m).[10,5] This used the minimum bridge width available in the charts, which is 25 ft (7.6 m).

The shear stress in the shear key can be calculated for the partial-depth conventionally grouted shear key. The depth of the shear key is 8.875 inches (225 mm), and v'_{max} is 207 lb/inch (36.3 kN/m). Therefore, the shear stress is 23 psi (161 kPa).

The interface shear strength of the conventional grout to the precast concrete has been reported by other researchers. For example, a study by Buyukozturk et al. found that the shear strength at the interface between grout and concrete for a flat connection was 85 psi (590 kPa) under 100 psi (0.69 MPa) of confining pressure and increased to 210 psi (1.4 MPa) with 300 psi (2.07 MPa) of confining pressure.[40] They also found that the shear strength of a keyed connection would be 10 times greater than a flat connection under the same confinement pressure. Other studies found that the shear strength for keyed connections in the absence of transverse confinement can range from 150 to 358 psi (1.03 to 2.47 MPa).[41,42] Based on these values, the shear strength of a conventionally grouted connection is sufficient to transfer the estimated shear stress found in this study.

De la Varga et al. conducted ASTM C882 slant shear tests to determine the interface shear strength of UHPC materials.[17,43] They found that the bond between UHPC and concrete with an EA surface usually failed the concrete substrate. This suggests that the interface bond is stronger in shear compared to the precast concrete.

CHAPTER 4. TEST RESULTS

The results from the thermal and cyclic loading are presented in this chapter. The prewetting and curing procedures adopted in this study prevented shrinkage cracking and debonding during and after construction of the connections. The specimens were kept inside the laboratory throughout the testing program, with each specimen first being subjected to the thermal cycling followed by the cyclic structural loading.

EFFECTS FROM THERMAL LOADING

The specimens were thermally loaded to create a temperature gradient between the top and bottom flanges of approximately 50 °F (28 °C). A total of 10 thermal cycles were applied to each test specimen except for the full-depth connection specimens, which only underwent 8 cycles. The thermal loading generated an upward deflection at the mid-span of between 0.425 and 0.570 inch (10.8 and 14.5 mm). The deflection versus temperature gradient curves for the conventionally grouted connections in the study are presented in figure 50, and the curves for the UHPC connections are shown in figure 51.
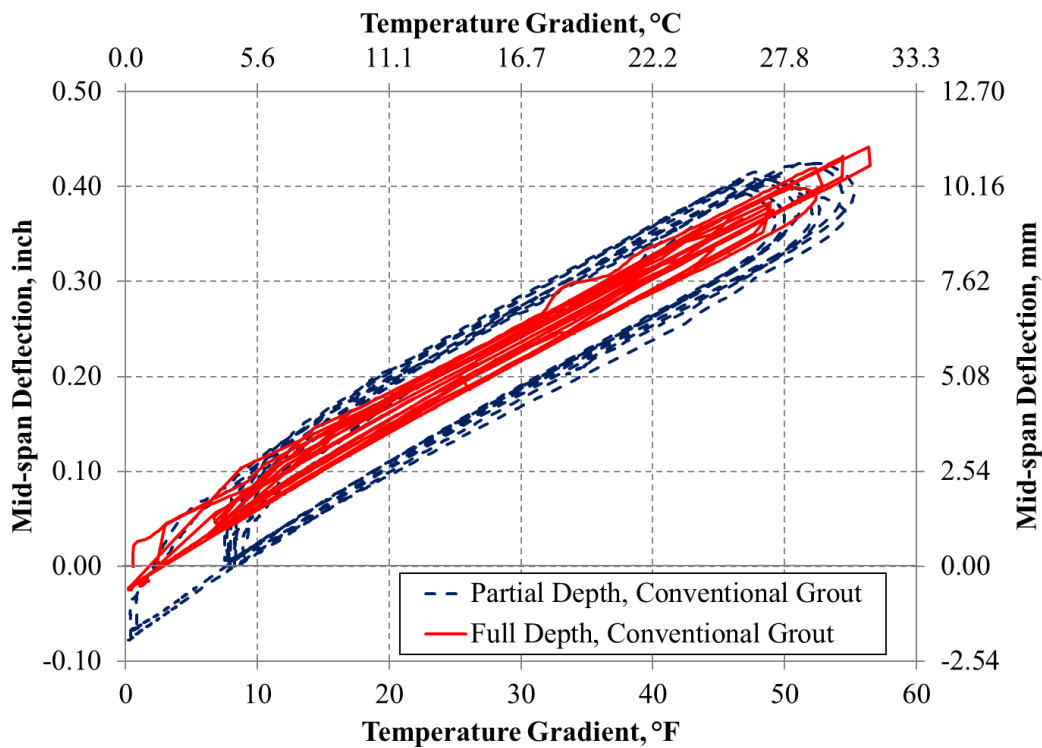
Source: FHWA.
1 inch = 25.4 mm.
1 °F = 0.556 °C.

Figure 50. Graph. Relationship between upward deflection and temperature gradient in beams with conventionally grouted connections.
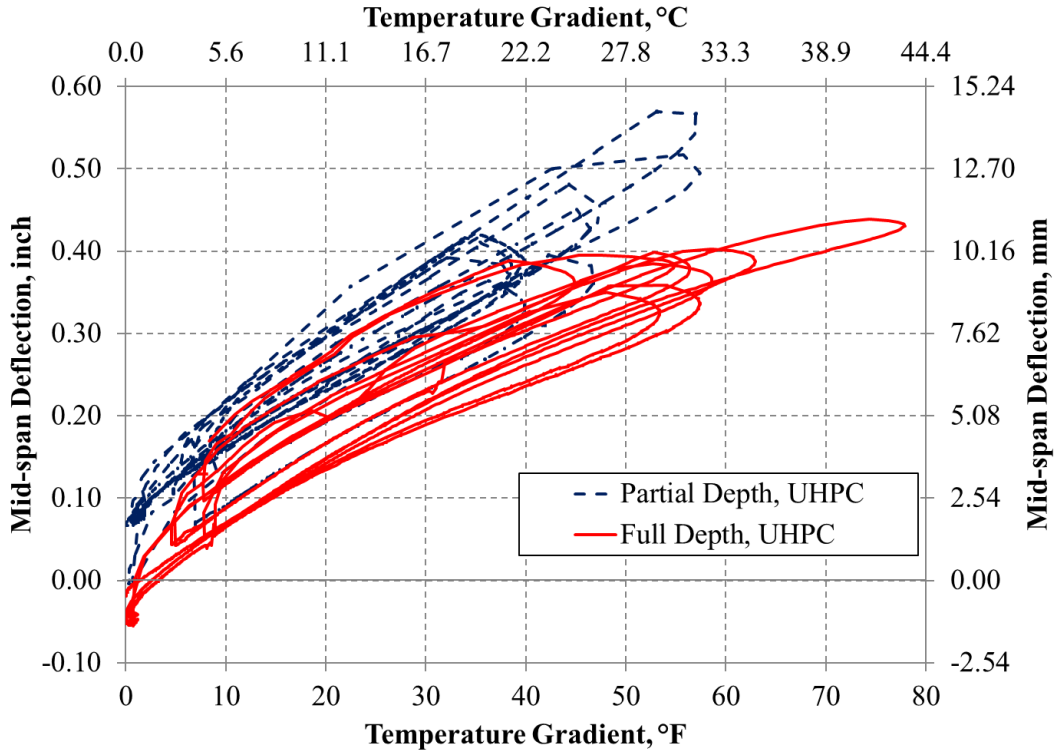
Source: FHWA.
1 inch = 25.4 mm.
1 °F = 0.556 °C.

Figure 51. Graph. Relationship between upward deflection and temperature gradient in beams with UHPC connections.

Table 10 summarizes the thermal loading and unloading data. The behavior of the beams used in the tests was generally the same. All of the tests had approximately the same deflection rate due to the thermal stress. The only exception was for the full-depth UHPC connection, which had a somewhat lower deflection rate. Despite reaching a gradient that was 20 °F (11 °C) higher than the other tests, the deflection was similar. The partial-depth UHPC connection had the greatest deflection, likely due to the largest heating rate. A visual inspection was conducted after the thermal loading. Only minor, non-structural cracking was observed in the partial-depth conventional grouted connection; the most severe is shown in figure 52. No debonding was caused by thermal loading for any of the connections.

Table 10. Data summary of the thermal tests.

Connection Type	Maximum Deflection (inches)	Maximum Gradient (°F)	Heating Rate (inch/°F)	Cooling Rate (inch/°F)	Average Rate (inch/°F)	Mean Deviation (inch/°F)
Partial-depth grout	0.425	55.3	7.68×10^{-3}	7.97×10^{-3}	7.82×10^{-3}	0.28×10^{-3}
Full-depth grout	0.442	56.5	7.34×10^{-3}	7.63×10^{-3}	7.48×10^{-3}	0.24×10^{-3}
Partial-depth UHPC	0.570	57.5	8.11×10^{-3}	6.88×10^{-3}	7.50×10^{-3}	0.66×10^{-3}
Full-depth UHPC	0.439	77.9	6.01×10^{-3}	6.13×10^{-3}	6.07×10^{-3}	0.44×10^{-3}

1 inch = 25.4 mm.
1 °F = 0.556 °C.
1 inch/°F = 45.72 mm/°C.
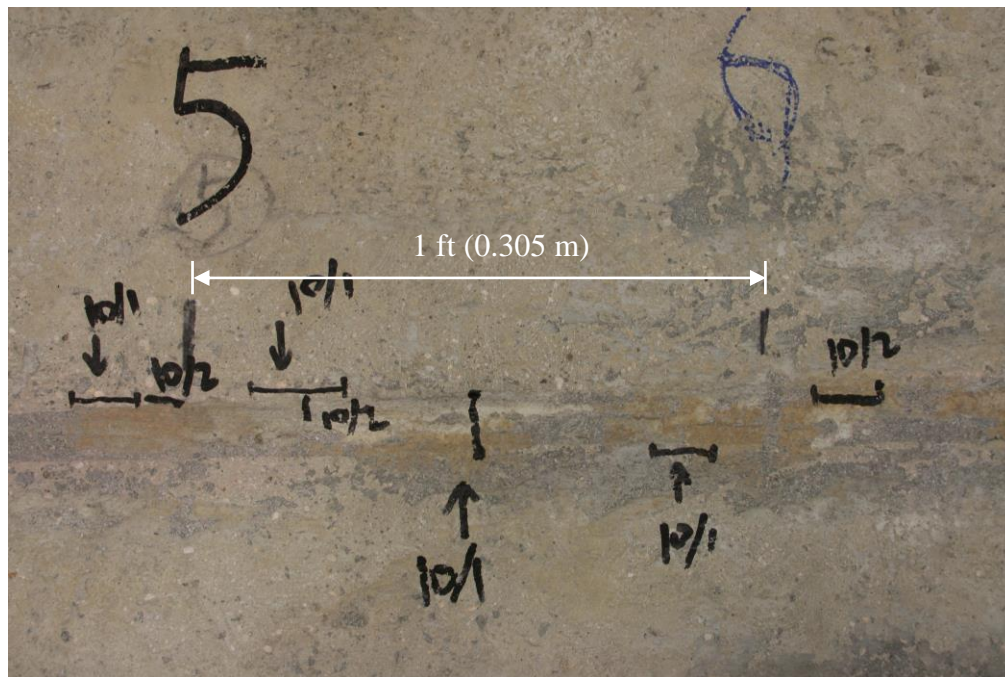
Source: FHWA.
1 ft = 0.305 m.

Figure 52. Photo. Representative cracking observed in the partial-depth conventional grout connection after thermal loading.

EFFECTS FROM CYCLIC STRUCTURAL LOADING

The partial-depth conventional grout connection was first tested in this study, followed by the full-depth conventional grout connection, then the partial- and full-depth UHPC connections. The boundary conditions, loading range, and loading cycles used on each connection are presented in table 4 through table 7.

To effectively evaluate the connection performance and efficiency under different conditions, this study adopted three parameters to measure the performance of the connection. The first two are the proportion of moment factor for the loaded beam and longitudinal strains in the beams, respectively. These demonstrate the ability of the connection to transfer loads between beams. The third is $\varDelta_\delta$, which provides an early indication of degradation of the connection. To be consistent between all tests, the longitudinal strain reported in graphs and used for proportion of moment are those from the embedded bottom strain gauges. The deflection measurements for proportion of moment are the average of both the vertical LVDTs on the beams, while $\varDelta_\delta$ is calculated using the method defined in chapter 3.

Proportion of Moment and $\varDelta_\delta$ Between the Beams

The proportion of moment carried by each beam and $\varDelta_\delta$ between the two beams was also assessed for each of the four connection details.

Partial-Depth Conventional Grout Connection

The full 100-kip (445-kN) transverse PT force was applied at each PT point 7 d after casting the shear key, generating PT distribution of 8 kip/ft (117 kN/m). The beams were then thermally loaded. The thermal loading did not initiate any local or global distress in the connection. Before the cyclic structural loading, the connection was checked, and only minor non-structural cracks were observed.

The beams were first tested in the unstiffened configuration. Loading ranges started at 18 kip (80 kN) and increased to 36, 54, 72, and 90 kip (160, 240, 320, and 400 kN). In total, 3 million cycles were performed; the existing cracks were not observed to propagate in the connection, and no new cracks formed. The transverse PT was then reduced from 8 to 6, 4, 2, and 0.8 kip/ft (117 to 87, 58, 29, and 12 kN/m). At each of these reduced transverse PT levels, the beams were cyclically loaded with the 54-, 72-, and 90-kip (240-, 320-, and 400-kN) loading ranges. An additional 3.9 million cycles were completed with no new cracks forming or existing cracks propagating. The longitudinal tensile strain at the mid-span, the loaded beam proportion of moment, and $\varDelta_\delta$ in these loading configurations are presented in figure 53 through figure 55, respectively. The tensile strain data were only available for the 90-kip (400-kN) loading range under the 8-kip/ft (117-kN/m) PT level.
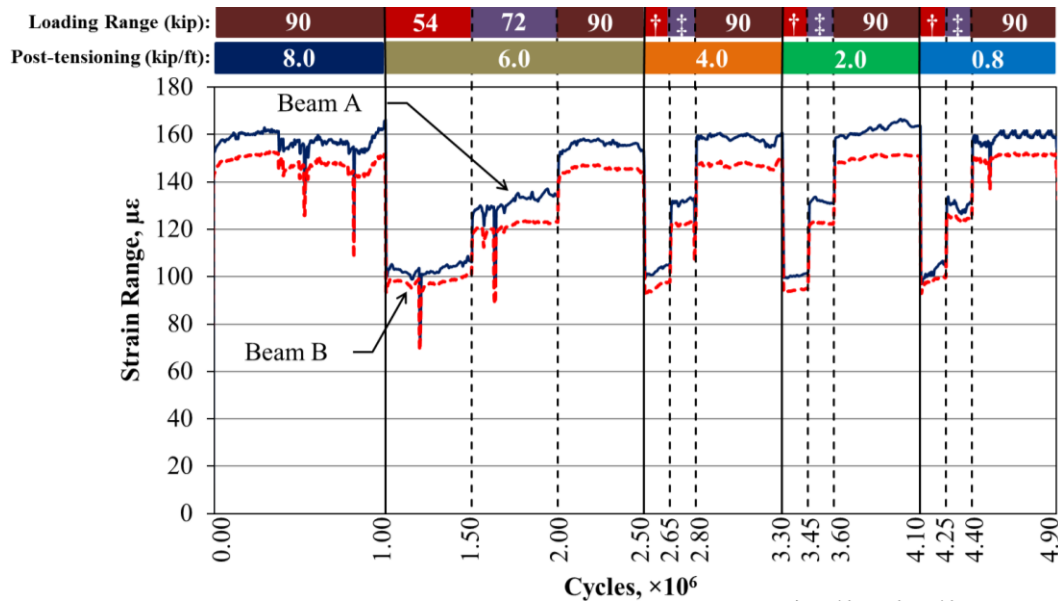
Source: FHWA.
1 kip = 4.448 kN.
1 kip/ft = 14.59 kN/m.
† = 54-kip loading range.
‡ = 72-kip loading range.

Figure 53. Graph. Longitudinal tensile strain measured at the mid-span in unstiffened beams with a partial-depth uncracked conventionally grouted connection.
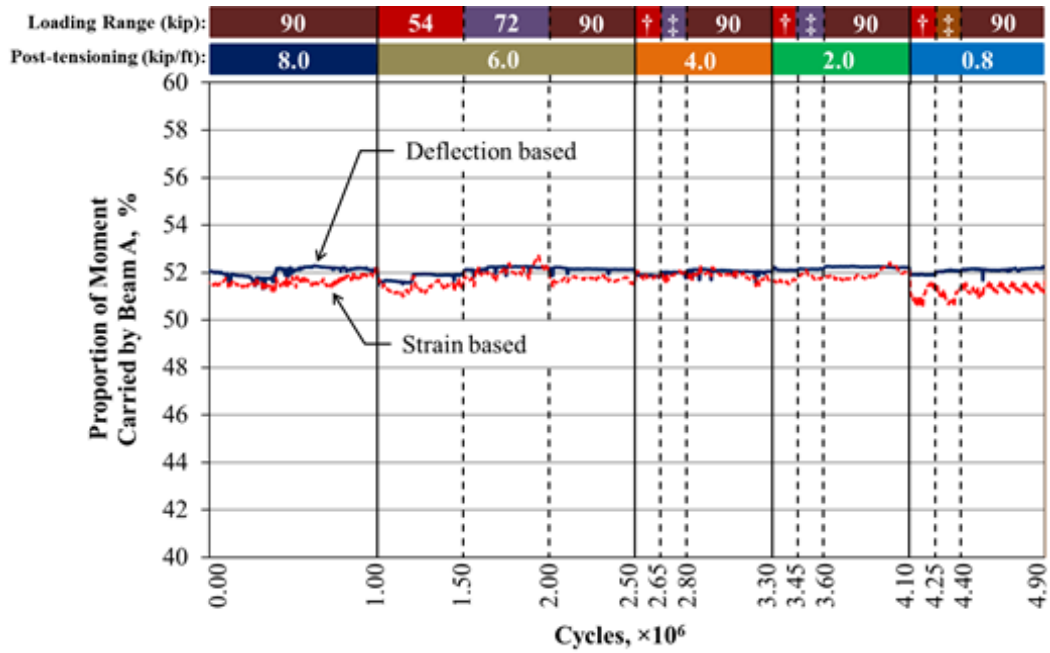
Source: FHWA.
1 kip = 4.448 kN.
1 kip/ft = 14.59 kN/m.
† = 54-kip loading range.
‡ = 72-kip loading range.

Figure 54. Graph. Proportion of moment based on the mid-span strain and deflection for unstiffened beams with a partial-depth uncracked conventionally grouted connection.
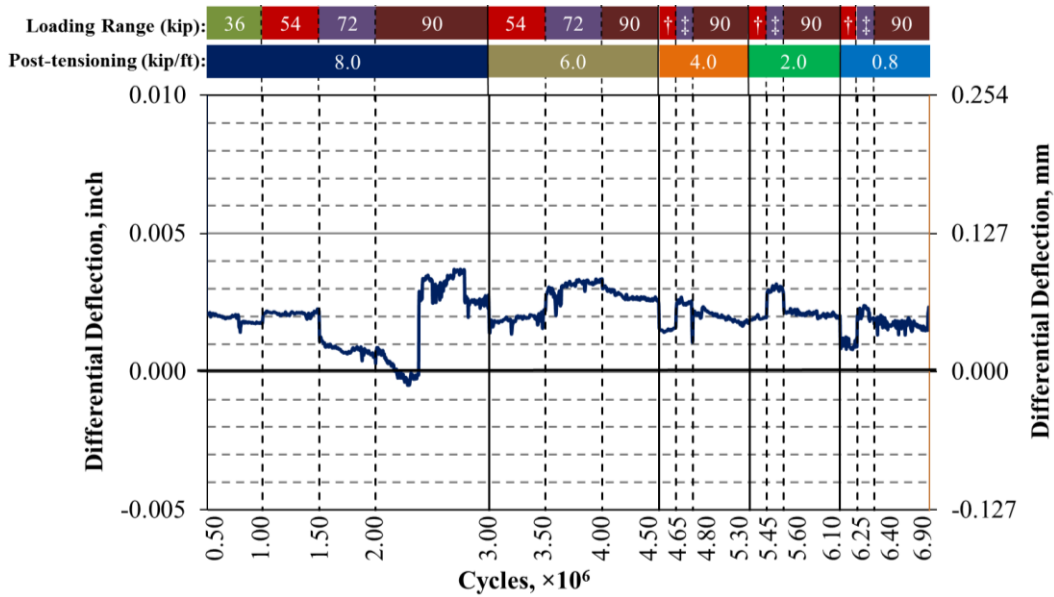
Source: FHWA.
1 kip = 4.448 kN.
1 kip/ft = 14.59 kN/m.
1 inch = 25.4 mm.
† = 54-kip loading range.
‡ = 72-kip loading range.
Note: Data for the first 500,000 cycles were not collected properly and therefore were not included.

Figure 55. Graph. Δ_δ measured at the mid-span in unstiffened beams with a partial-depth uncracked conventionally grouted connection.

The level of the three variables remained nearly constant within a particular loading range regardless of the level of transverse PT applied. Specifically, the longitudinal strain while in the 90-kip (400-kN) loading range remained 160 and 145 με for the loaded and unloaded beams, respectively. The proportion of moment on the loaded beam was consistently around 52 percent regardless of the loading range or the level of PT applied. Δ_δ was about 0.0025 inch (0.064 mm) in the largest loading range regardless of level of PT. These results indicate that the amount of transverse PT did not seem to have an effect on system performance when the connection was intact without any apparent cracking or debonding. Further discussion of the effect of transverse PT is provided in the Transverse PT section in chapter 5.

The specimen was stiffened using the two methods previously discussed, and 1.6 and 1.75 million cycles were performed with the partially and fully stiffened connections, respectively. The results for the partially stiffened boundary condition are shown in figure 56 through figure 58. Increasing the stiffness was found to decrease the longitudinal strain in the beams. When less PT force was used, strains were found to be lower, a more even load distribution was calculated, and lower Δ_δ was recorded. An error in an LVDT resulted in the deflection-based proportion of moment to be based solely on the exterior LVDT for the unloaded beam in this configuration.

47
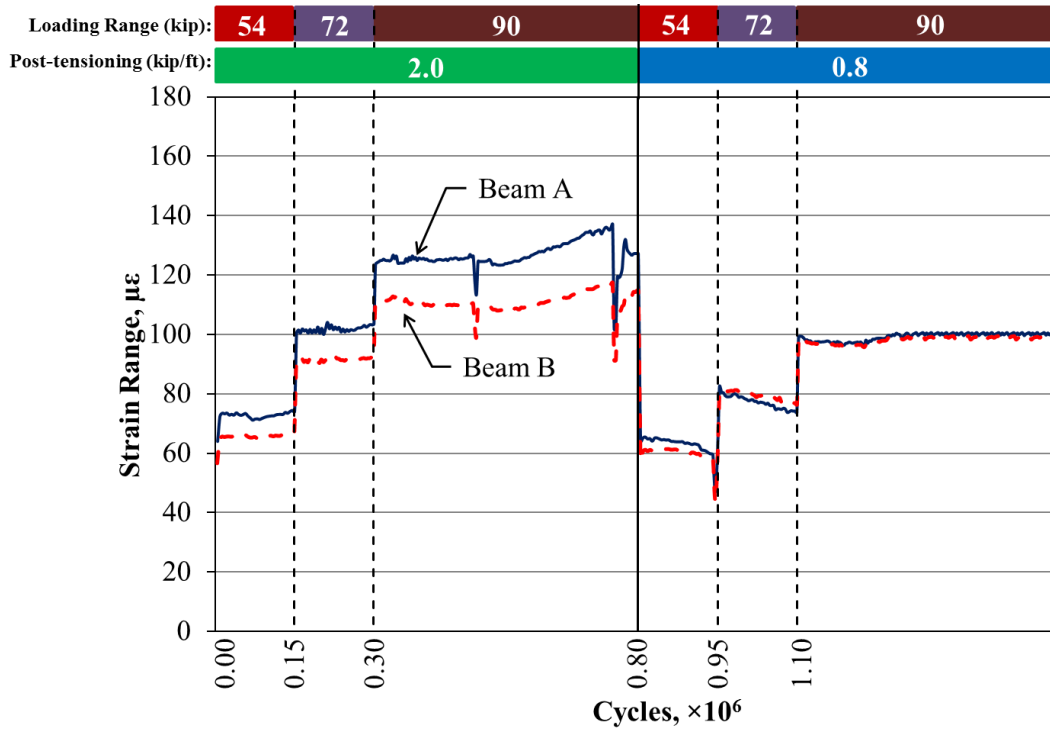
Source: FHWA.
1 kip = 4.448 kN.
1 kip/ft = 14.59 kN/m.

Figure 56. Graph. Longitudinal tensile strain measured at the mid-span in partially stiffened beams with a partial-depth uncracked conventionally grouted connection.
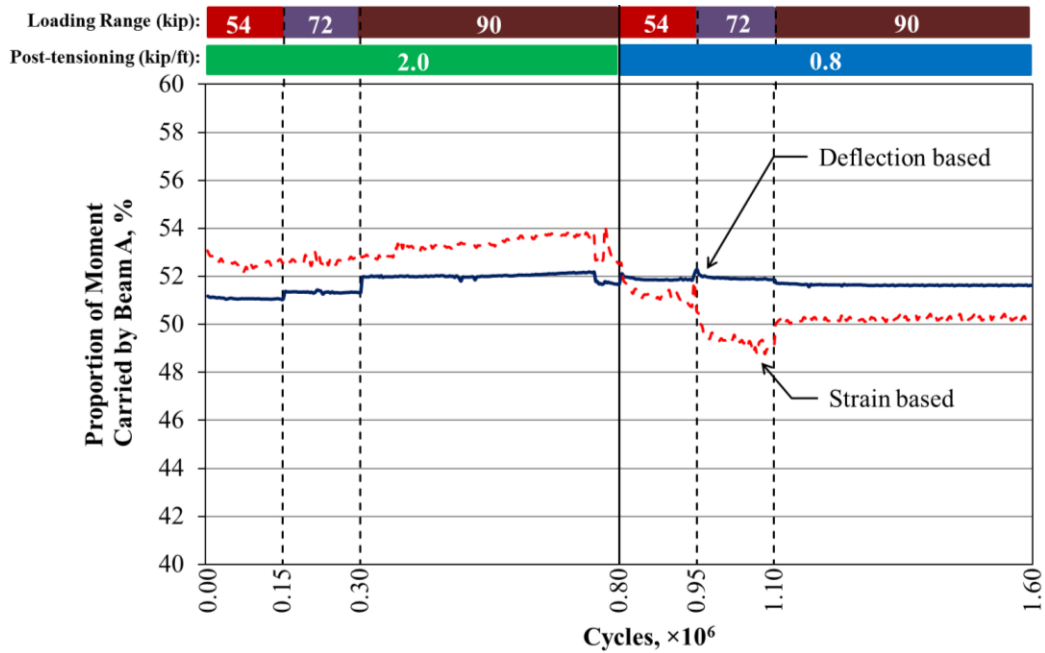
Source: FHWA.
1 kip = 4.448 kN.
1 kip/ft = 14.59 kN/m.

Figure 57. Graph. Loaded proportion of moment based on the mid-span strain and deflection for partially stiffened beams with a partial-depth uncracked conventionally grouted connection.
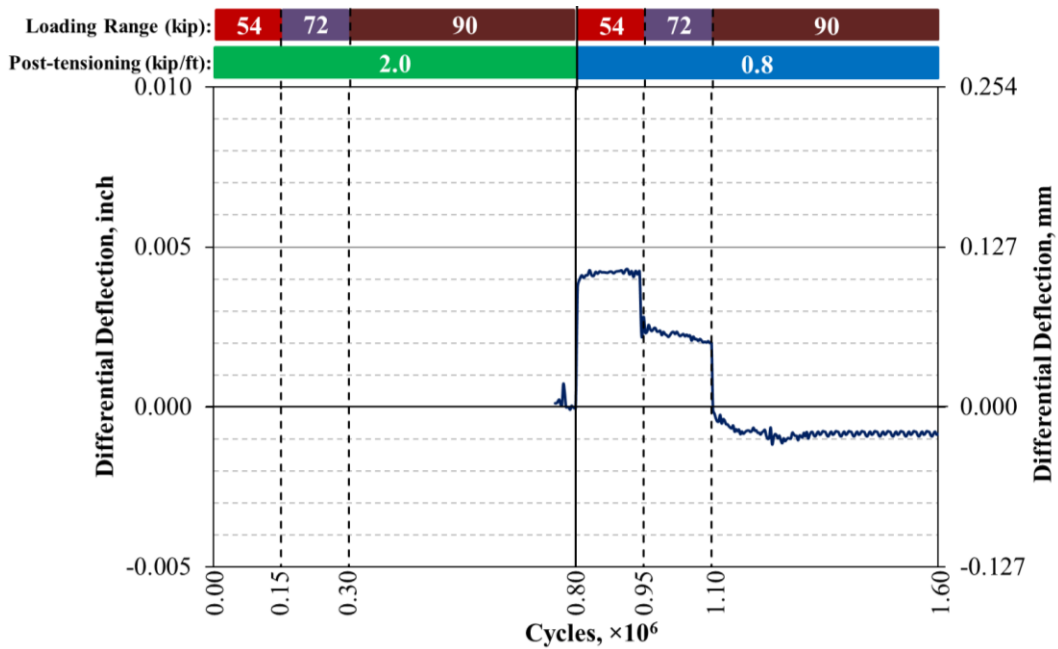
Source: FHWA.
1 kip = 4.448 kN.
1 kip/ft = 14.59 kN/m.
1 inch = 25.4 mm.

Figure 58. Graph. Δ_δ measured at the mid-span in partially stiffened beams with a partial-depth uncracked conventionally grouted connection.

After the partially stiffened cycles were completed, the fully stiffened configuration was tested. The results for the fully stiffened boundary condition are shown in figure 59 and figure 60. The values reported were the strain range and deflection, as calculated from figure 41. For the final 360,000 cycles, the transverse PT force was eliminated. The fully stiffened boundary condition further lowered the longitudinal tensile strain experienced by the beams. Δ_δ was also lower— about 0.001 inch (0.025 mm)—compared to the simply supported case. The thermal cracks observed were not seen to propagate in the connection, indicating that the transverse PT force had a minimal impact on system performance as long as the connection remained in good condition.

Source: FHWA.
1 kip = 4.448 kN.
1 kip/ft = 14.59 kN/m.
§ = 15,000 cycles at both the 54- and 72-kip loading ranges.
◊ = 90-kip loading range.
† = 54-kip loading range.
‡ = 72-kip loading range.

Figure 59. Graph. Longitudinal tensile strain range measured at the mid-span in fully stiffened beams with a partial-depth uncracked conventionally grouted connection.

51
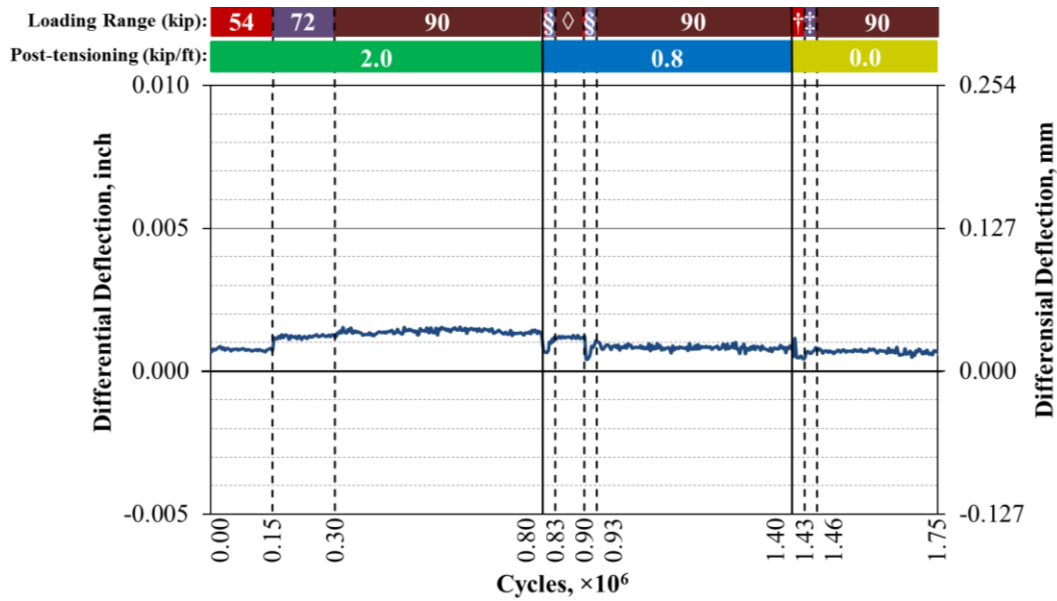
Source: FHWA.
1 kip = 4.448 kN.
1 kip/ft = 14.59 kN/m.
§ = 15,000 cycles at both the 54- and 72-kip loading ranges.
◊ = 90-kip loading range.
† = 54-kip loading range.
‡ = 72-kip loading range.

Figure 60. Graph. Δ_δ measured at the mid-span in fully stiffened beams with a partial-depth uncracked conventionally grouted connection.

More than 10 million cycles of structural loading were applied to the beams with a partial-depth conventional grout connection. At its most severe, the structural loading applied an $M_{equivalent}$ of 478 kip-ft (646 kN-m) transferred through the connection. No distress was observed.

The connection was then mechanically cracked by applying a direct tensile force on top of the connection, as shown in figure 61. Cracks at the interface between the grout and box beam concrete were initiated and extended about 32 ft (9.8 m). The extent to which the cracks extended into the connection was checked by ponding water on the connection. Water was observed to penetrate the connection, indicating the connection had debonded along the length of the observed cracking.

A. Cracking setup.   B. Cracked connection.

Figure 61. Photos. Mechanical cracking of the partial-depth conventionally grouted connection, including the cracking setup and the cracked connection.

The beams were again cyclically loaded using the fully stiffened boundary condition. Transverse PT forces ranging from 8 to 0 kip/ft (117 to 0 kN/m) were tested, and 830,000 cycles were completed. The cracks were found to propagate along the connection regardless of the transverse PT force applied but propagated more quickly under lower levels of PT. After the 8- and 4-kip/ft (117- and 87-kN/m) PT cycles, the end of the crack was seen to extend about 9 inches (230 mm), and additional cracks propagated within the already cracked connection. The most extensive cracking occurred after the 0.8- and 0-kip/ft (12- and 0-kN/m) levels of PT cycles. After the 0.8-kip/ft (12-kN/m) cycles, the crack extended 4 ft (1.2 m) to a total cracked length of 37 ft (11.3 m). The cycles with no PT further extended the crack to 40 ft (12.2 m). The crack propagation can be seen in figure 62. Red marker indicates the extent of the mechanical cracking, while green, blue, and orange markers show propagation after the 4-, 0.8-, and 0-kip/ft (87-, 12-, and 0-kN/m) PT levels, respectively.
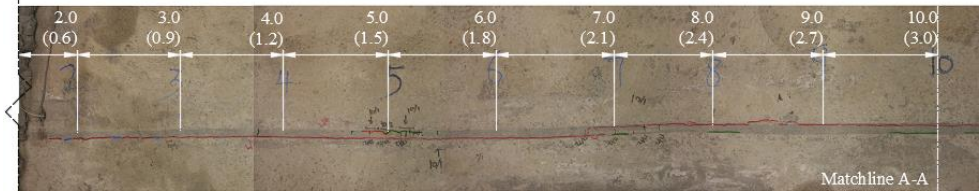
Source: FHWA.

A. Connection from the 2- to 10-ft (0.61- to 3.05-m) mark.
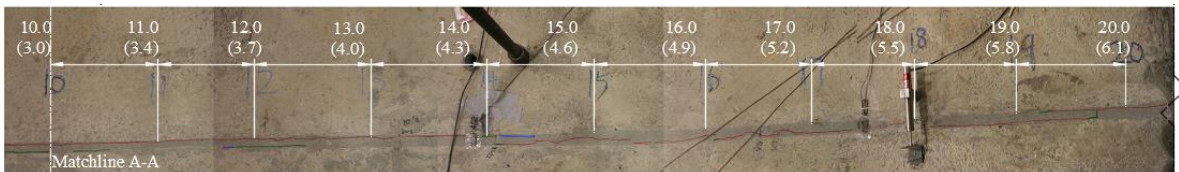
Source: FHWA.

B. Connection from the 10- to 20-ft (3.05- to 6.10-m) mark.
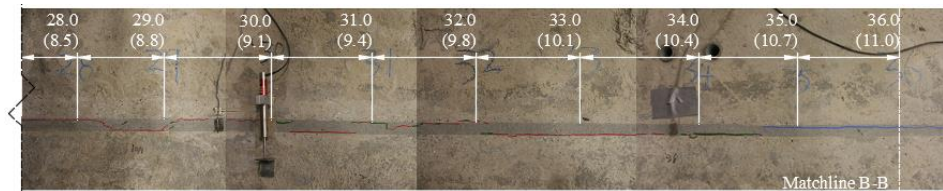
Source: FHWA.

C. Connection from the 28- to 36-ft (8.53- to 10.97-m) mark.
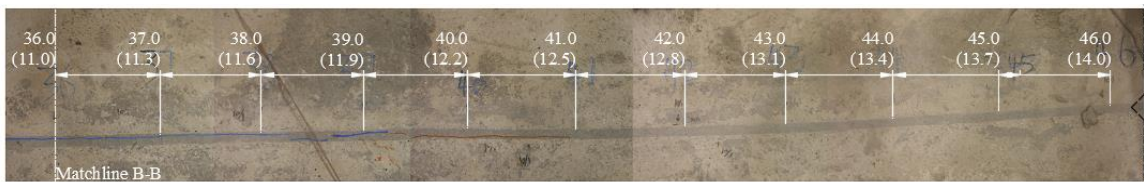
Source: FHWA.

D. Connection from the 36- to 46-ft (10.97- to 14.02-m) mark.

Note: Numbers in the photos reflect distance from the west end in feet where 1 ft = 0.305 m.

Figure 62. Photos. Propagation of the end of the connection crack induced by cyclic structural loading.

The longitudinal tensile strain range and Δ_δ between the two adjacent beams at the mid-span for the partially cracked connections are presented in figure 63 and figure 64. The partially cracked connection could still effectively transfer the load from one beam to the other, likely through friction between the grout and the box beam concrete; however, a slightly larger Δ_δ was observed. A jump can be seen during the 90-kip (400-kN) range of the cycles without PT around 800,000 cycles. This may correspond to the propagation of the crack seen in figure 62.
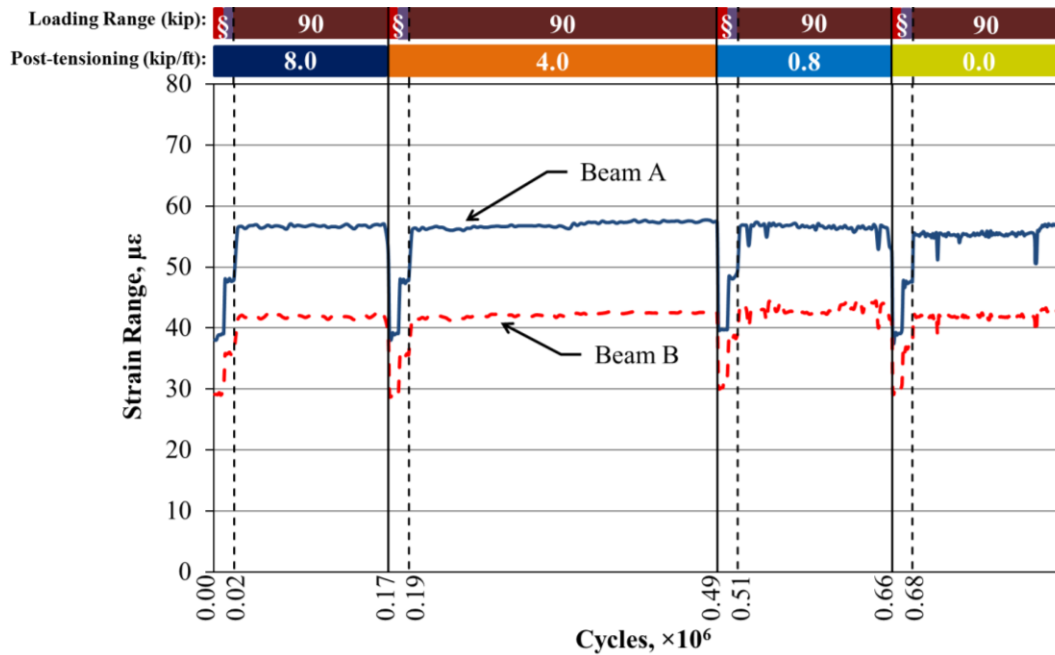
Source: FHWA.
1 kip = 4.448 kN.
1 kip/ft = 14.59 kN/m.
§ = 10,000 cycles at both the 54- and 72-kip loading ranges.

Figure 63. Graph. Longitudinal tensile strain range measured at the mid-span in fully stiffened beams with a partial-depth partially cracked conventionally grouted connection.
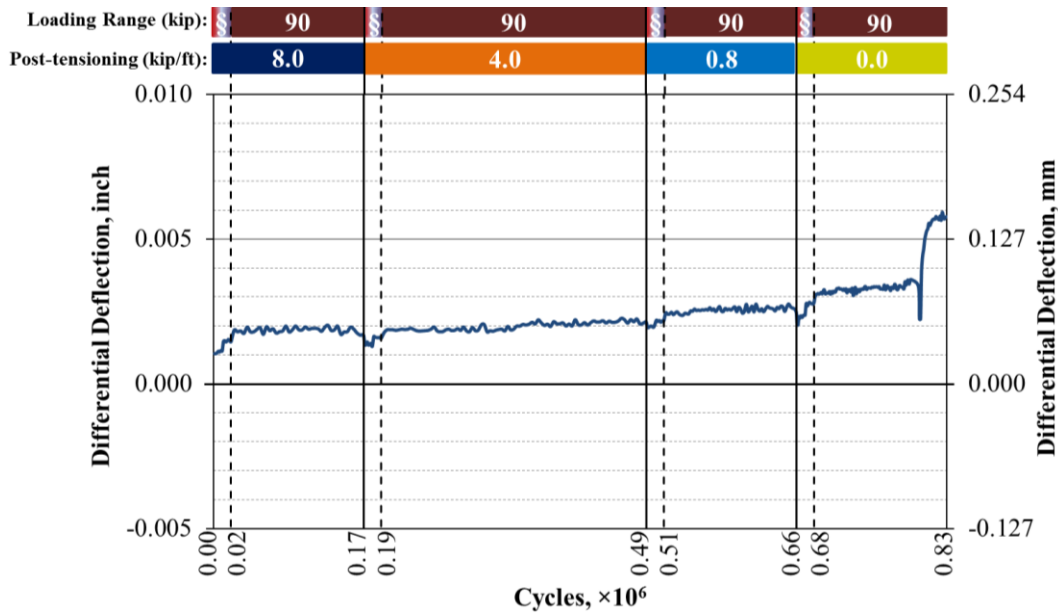
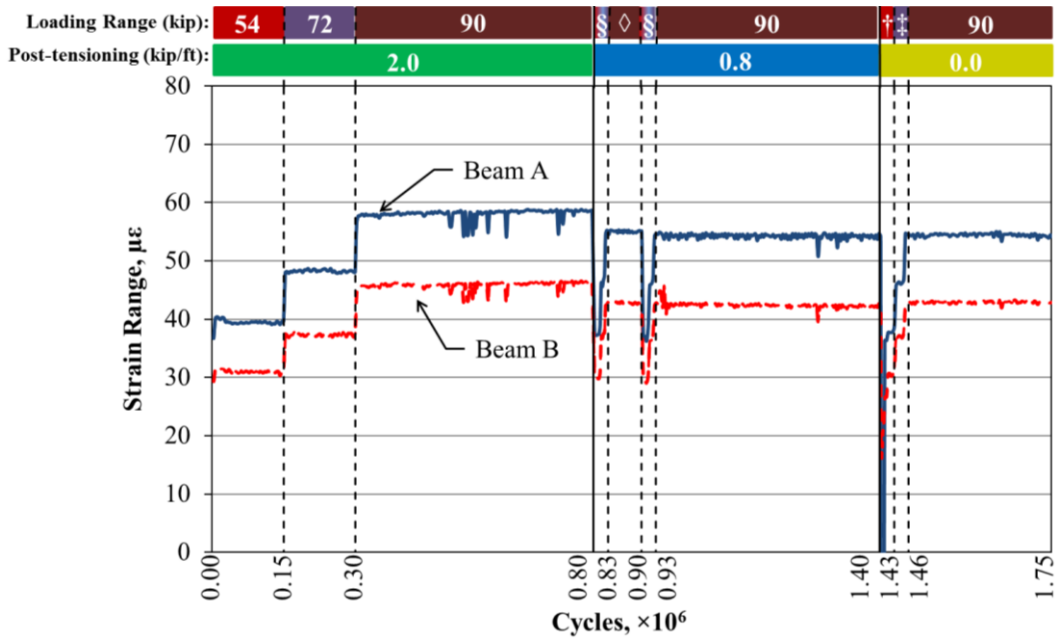Source: FHWA.
1 kip = 4.448 kN.
1 kip/ft = 14.59 kN/m.
1 inch = 25.4 mm.
§ = 10,000 cycles at both the 54- and 72-kip loading ranges.

Figure 64. Graph. $\varDelta_\delta$ measured at the mid-span in fully stiffened beams with a partial-depth partially cracked conventionally grouted connection.

The connection was then mechanically cracked so the full length of the connection was cracked. The beams were then subjected to further cyclic loading with the stiffest boundary condition. A total of 200,000 cycles were performed with the transverse PT forces ranging from 8 to 0 kip/ft (117 to 0 kN/m).

The longitudinal tensile strain range and $\varDelta_\delta$ between the two adjacent beams at the mid-span for the fully-cracked connection are presented in figure 65 and figure 66. Larger $\varDelta_\delta$ and longitudinal strains were observed in the fully cracked connection.
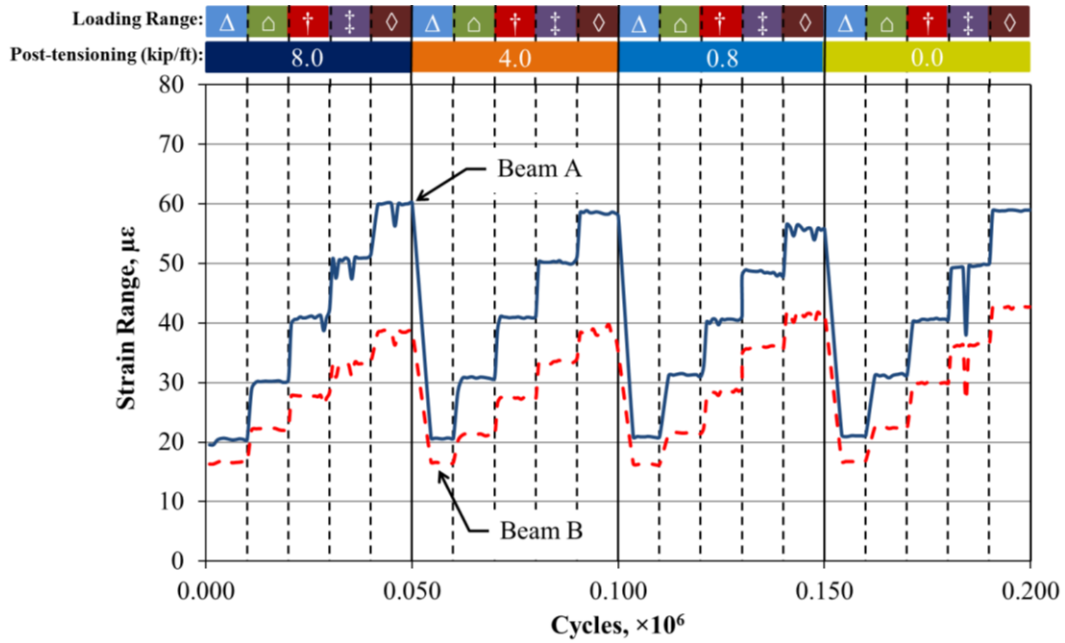
Source: FHWA.
1 kip = 4.448 kN.
1 kip/ft = 14.59 kN/m.
Δ = 18-kip loading range.
⌂ = 36-kip loading range.
† = 54-kip loading range.
‡ = 72-kip loading range.
◊ = 90-kip loading range.

Figure 65. Graph. Longitudinal tensile strain range measured at the mid-span in fully stiffened beams with a partial-depth fully cracked conventionally grouted connection.
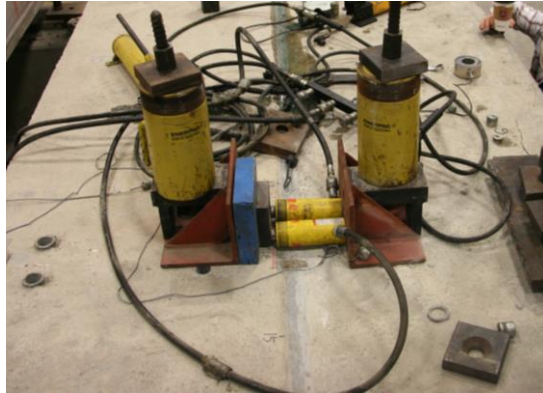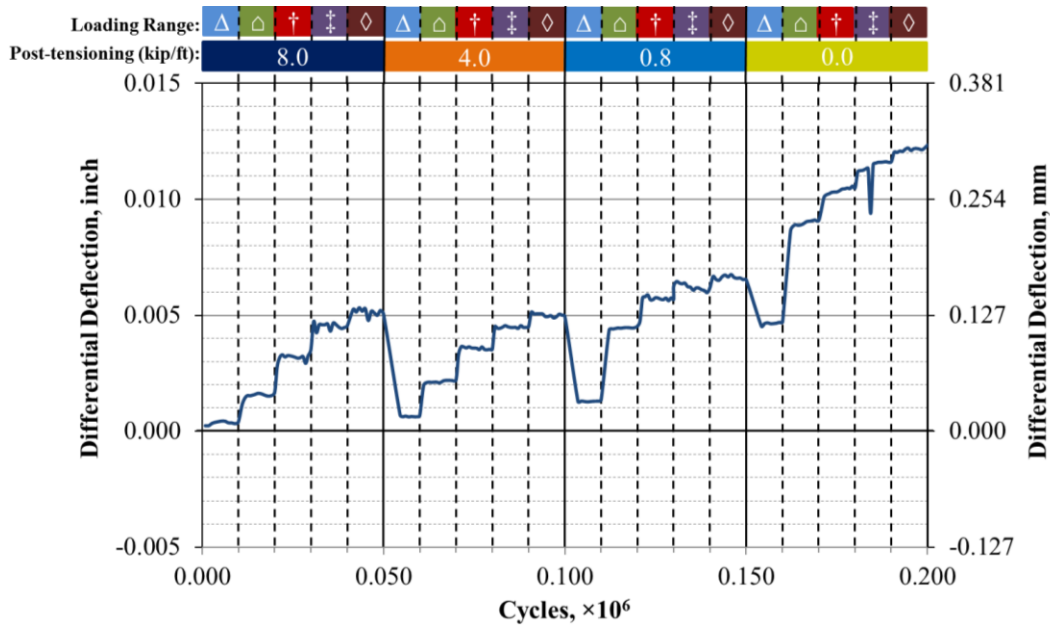
Source: FHWA.
1 kip = 4.448 kN.
1 kip/ft = 14.59 kN/m.
Δ = 18-kip loading range.
⌂ = 36-kip loading range.
† = 54-kip loading range.
‡ = 72-kip loading range.
◊ = 90-kip loading range.

Figure 66. Graph. Δ_δ measured at the mid-span in fully stiffened beams with a partial-depth fully cracked conventionally grouted connection.

The transverse PT force did not have much effect on the longitudinal strain at the mid-span. The transverse PT force varied from 8 to 0 kip/ft (117 to 0 kN/m) in the partially and fully cracked connections. The transverse PT affected Δ_δ. When it was removed from the fully cracked connection, Δ_δ was noted to increase within the 50,000 cycles conducted in this study.

Full-Depth Conventional Grout Connection

The same construction procedure used for partial-depth conventionally grouted connection was adopted for the full-depth conventionally grouted connection. Approximately two-thirds of the length of the connection cracked when the wrench-tight PT force was removed. The transverse curvature (i.e., sweep) of the beams with the full-depth connection may have varied enough to cause cracking to develop, as illustrated in figure 67. When the PT forces were applied, the beams aligned from the applied force. After the grout was cast and the transverse force was removed, the beams tried to return to their original shape. This introduced a tensile force across the connection and could lead to connection cracking if the bond strength between the grout and the box beams were not sufficiently large. This would imply that the differential transverse curvature on the beams with the full-depth shear keys was larger than that on the beams with the partial-depth shear keys. This caused the full-depth shear key to crack upon release of the PT force, while the partial-depth shear key did not.

58
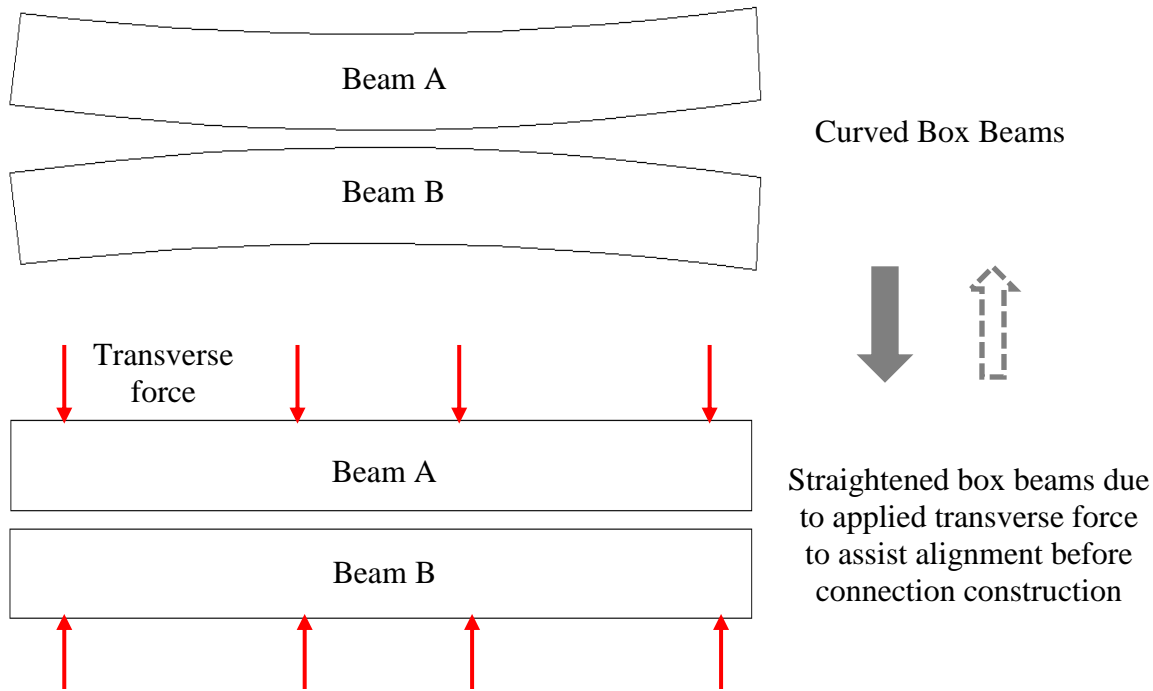
Figure 67. Illustration. Exaggerated transverse curve in box beams.

Cyclic loading was applied to the specimen with the partially cracked connection using the unstiffened configuration and varying levels of transverse PT. A total of 2.25 million cycles were completed, and the existing cracking in the connection was observed to propagate. However, the crack did not extend the entire length of the beam. The connection was further cracked with the same method used for the partial-depth connection so that the connection interface cracks extended the entire length of the specimen. The beams were then loaded for another 150,000 cycles. The longitudinal tensile strain at the mid-span and the proportion of moment carried by the loaded beam are presented in figure 68 and figure 69, respectively. Δ_δ between the two beams is presented in figure 70. With transverse PT forces of 8, 4, and 0.8 kip/ft (117, 58, and 12 kN/m), the partially cracked connection could still effectively transfer the moment, having a proportion of moment factor of about 54 percent. When the transverse PT was removed, the proportion of moment factor remained about 54 percent under the 54-kip (240-kN) loading range but increased to over 57 percent when the loading range increased to 72 and 90 kip (320 and 400 kN).

Similar observations were noted with Δ_δ. As shown in figure 70, Δ_δ was constantly within 0.001 inch (0.025 mm) for all loading ranges while having any level of transverse PT. It jumped to around 0.015 inch (0.381 mm) for the partially cracked connection under the 72-kip (320-kN) loading range. Both the partially and fully cracked connections had Δ_δ of around 0.018 inch (0.457 mm) in the 90-kip (400-kN) loading range.
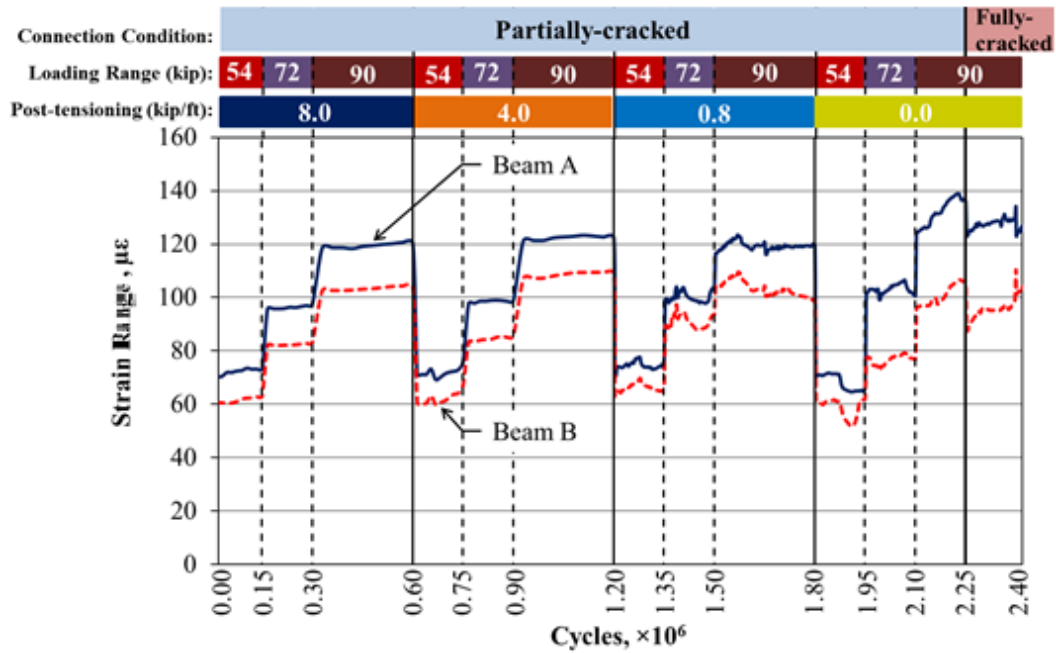
Source: FHWA.
1 kip = 4.448 kN.
1 kip/ft = 14.59 kN/m.

Figure 68. Graph. Tensile strain at the mid-span showing full-depth connection, conventional grout, unstiffened boundary, and partially and fully cracked conditions.
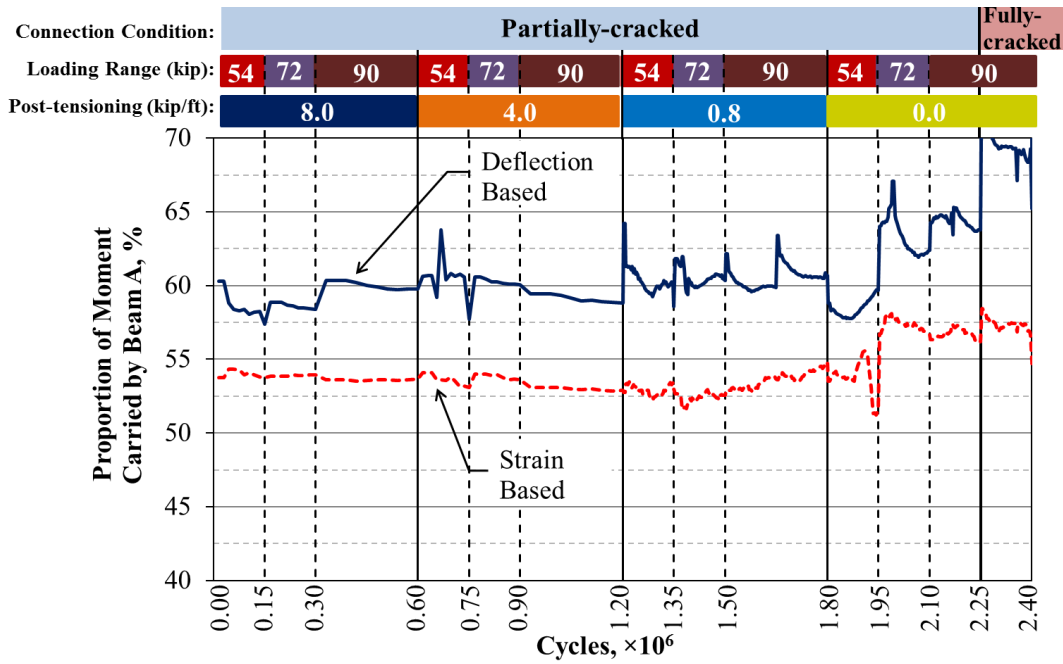
Figure 69. Graph. Proportion of moment carried by the loaded beam based on the mid-span strain and deflection for the full-depth partially and fully cracked conventionally grouted connections.

Source: FHWA.
1 kip = 4.448 kN.
1 kip/ft = 14.59 kN/m.
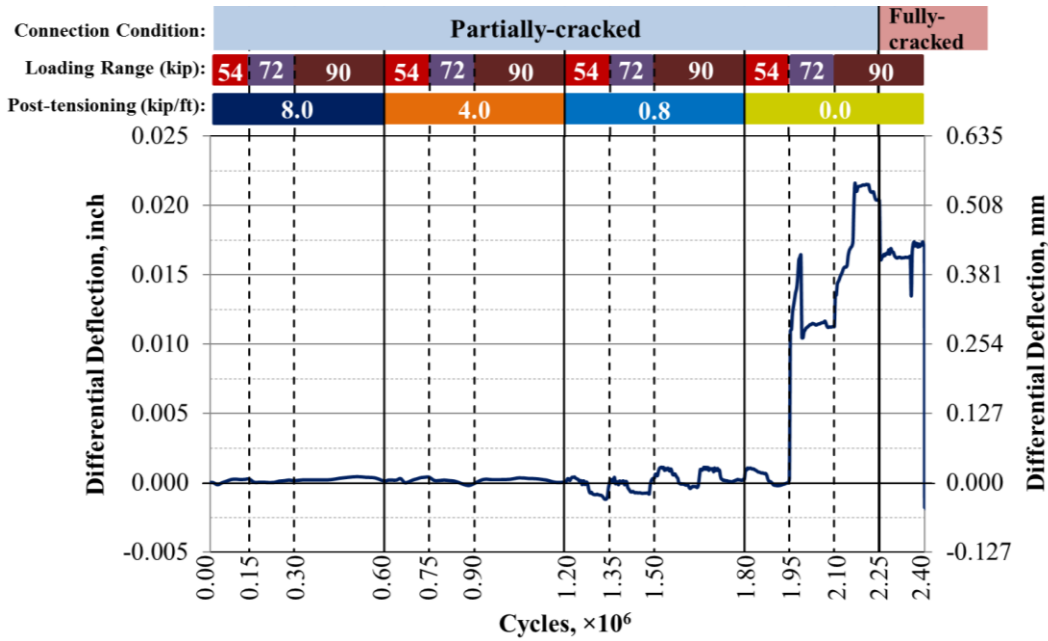
Source: FHWA.
1 kip = 4.448 kN.
1 kip/ft = 14.59 kN/m.
1 inch = 25.4 mm.

Figure 70. Graph. Δ_δ measured at the mid-span in the full-depth partially and fully cracked conventionally grouted connections.

Partial-Depth UHPC Connection

After the conventional grout connections were tested, the pair of beams were separated and repositioned to construct the UHPC connections. Both UHPC connections were constructed successfully, and no cracks were observed before the cyclic structural loading.

The beams with the partial-depth UHPC connection were loaded with the partially stiffened and fully stiffened boundary conditions. A total of 1.55 million cycles were performed, and no cracking was observed in the specimen. The longitudinal tensile strain at the mid-span for beams with partial-depth UHPC connection is presented in figure 71. Values for the tensile strain for the fully stiffened portion of the plot are the range of longitudinal strains. Proportion of moment on the loaded beam for the partially stiffened connection is presented in figure 72. Δ_δ for the connection is presented in figure 73. Under the 54-, 72-, and 90-kip (240-, 320-, and 400-kN) loading ranges, the loaded beam had a proportion of moment around 50 percent with the partially stiffened boundary, and Δ_δ was limited to within 0.005 inch (0.127 mm).
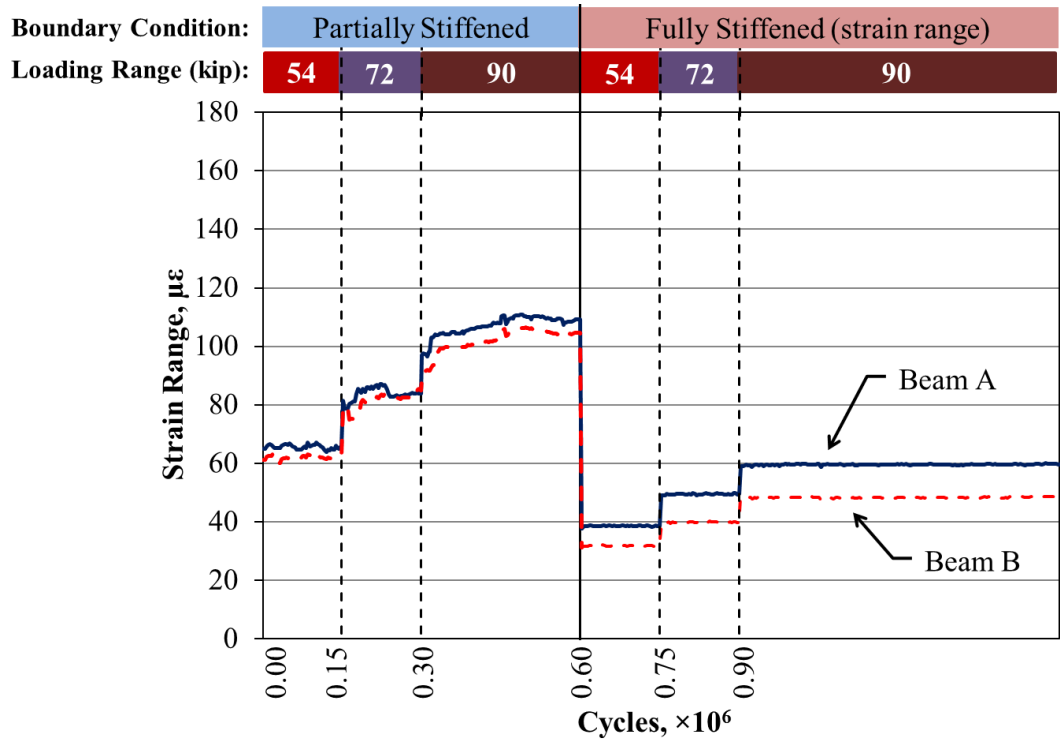
Figure 71. Graph. Longitudinal tensile strain measured at the mid-span in partially and fully stiffened beams with a partial-depth UHPC connection.

Source: FHWA.
1 kip = 4.448 kN.
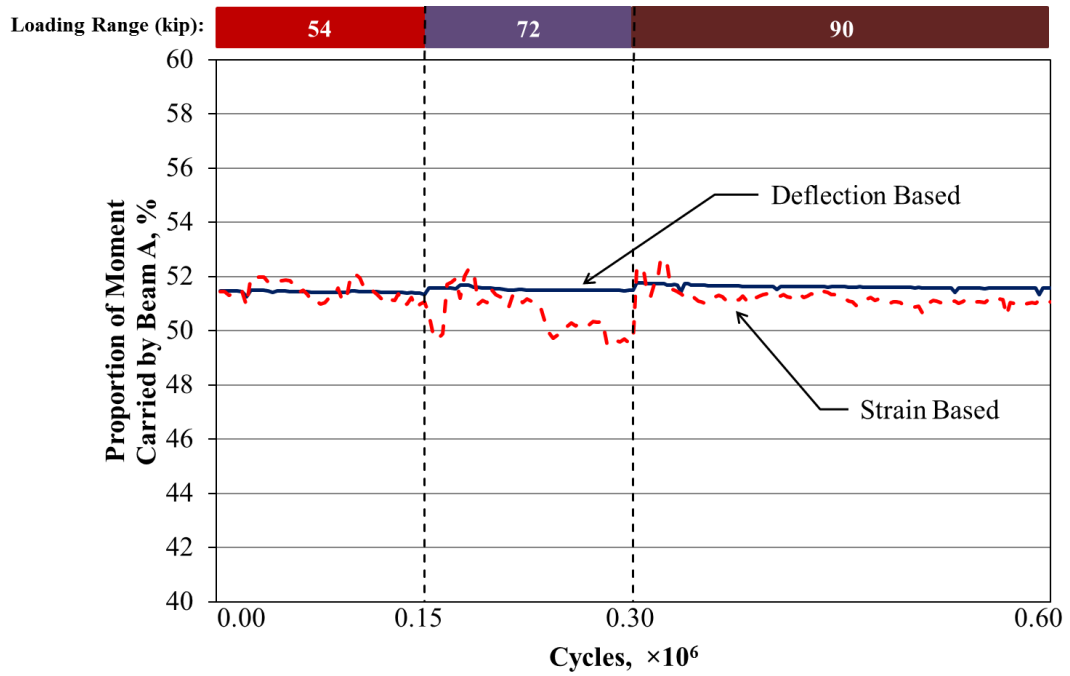
Source: FHWA.
1 kip = 4.448 kN.

Figure 72. Graph. Proportion of moment carried by the loaded beam based on the mid-span strain and deflection for partially stiffened beams with a partial-depth UHPC connection.
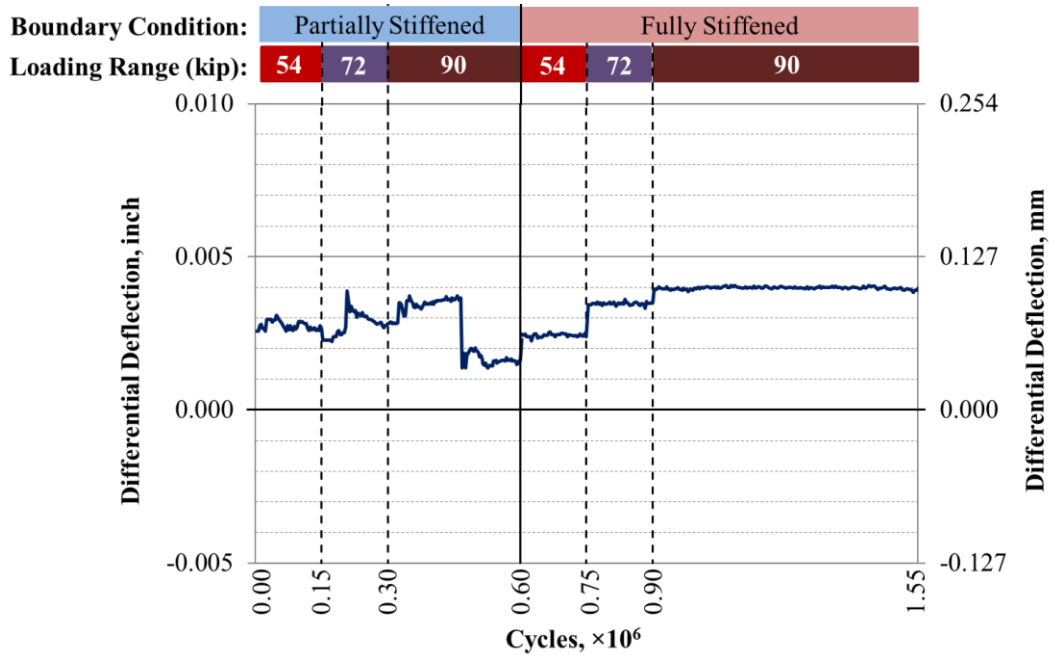
Figure 73. Graph. Δ_δ measured at the mid-span in partially and fully stiffened beams with a partial-depth UHPC connection.

An attempt to induce cracking in the connection with the same method as the conventional grout specimens was performed. When the transverse tensile force was applied across the connection, cracks developed in the box beam rather than in the UHPC or the connection interface, as shown in figure 74. This suggests that the interface bond strength between the UHPC and EA interface concrete was similar to or greater than the tensile strength of the box beam concrete. This behavior demonstrates that UHPC can create a connection whose behavior is comparable to or exceeds the tensile cracking strength of monolithically cast concrete box beams due to the tensile strength, interface bond strength, and reinforcement development ability of the UHPC.
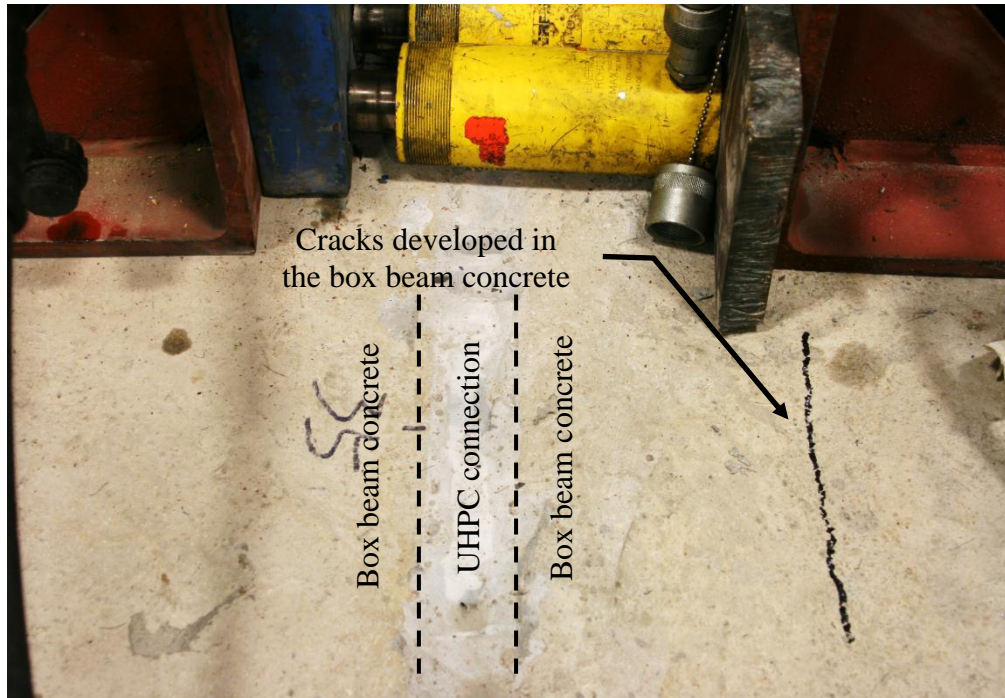
Figure 74. Photo. Crack development in the box beam during an attempt to mechanically induce a crack in the UHPC connection.

Full-Depth UHPC Connection

The partial-depth UHPC connection exhibited performance that could be expected to be comparable to a monolithic bridge system. Given the similarities between the partial- and full-depth UHPC connections, it was anticipated that the full-depth UHPC connection would exhibit similar performance.

The longitudinal tensile strain for the unstiffened and partially stiffened cases is presented in figure 75, the loaded beam proportion of moment for these cases is given in figure 76, and Δ_δ is presented in figure 77. The partially stiffened boundary condition caused the strains measured at mid-span to decrease. The proportion of moment on the loaded beam stayed constant around 51 percent. Δ_δ between the beams were minor, between −0.002 and 0.001 inch (−0.051 and 0.025 mm), across both boundary conditions and all loading ranges.
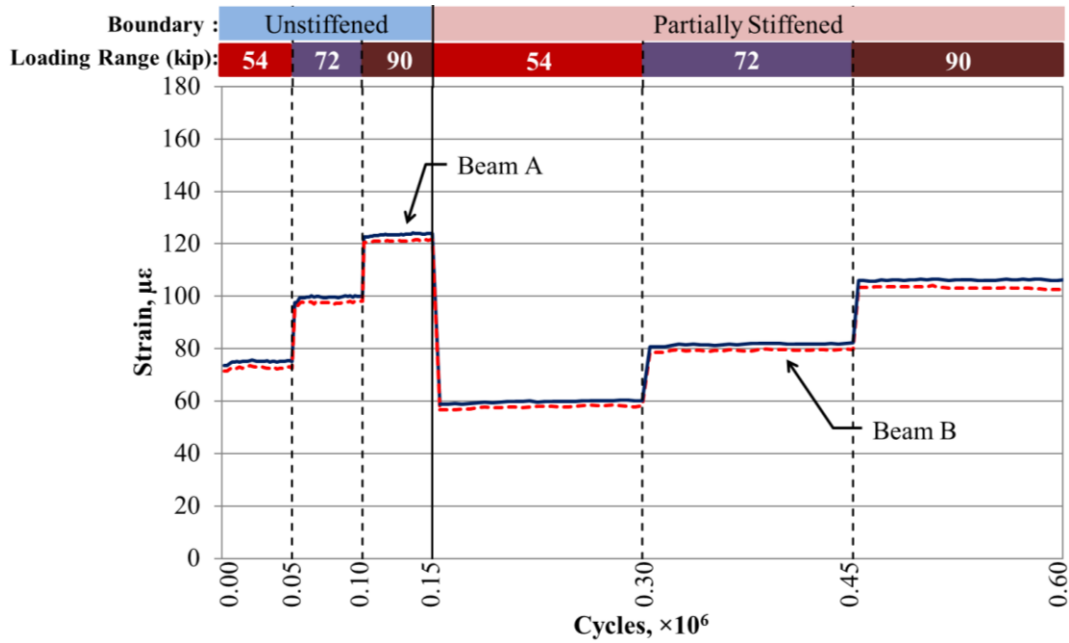
Figure 75. Graph. Longitudinal tensile strain measured at the mid-span in unstiffened and partially stiffened beams with a full-depth UHPC connection.
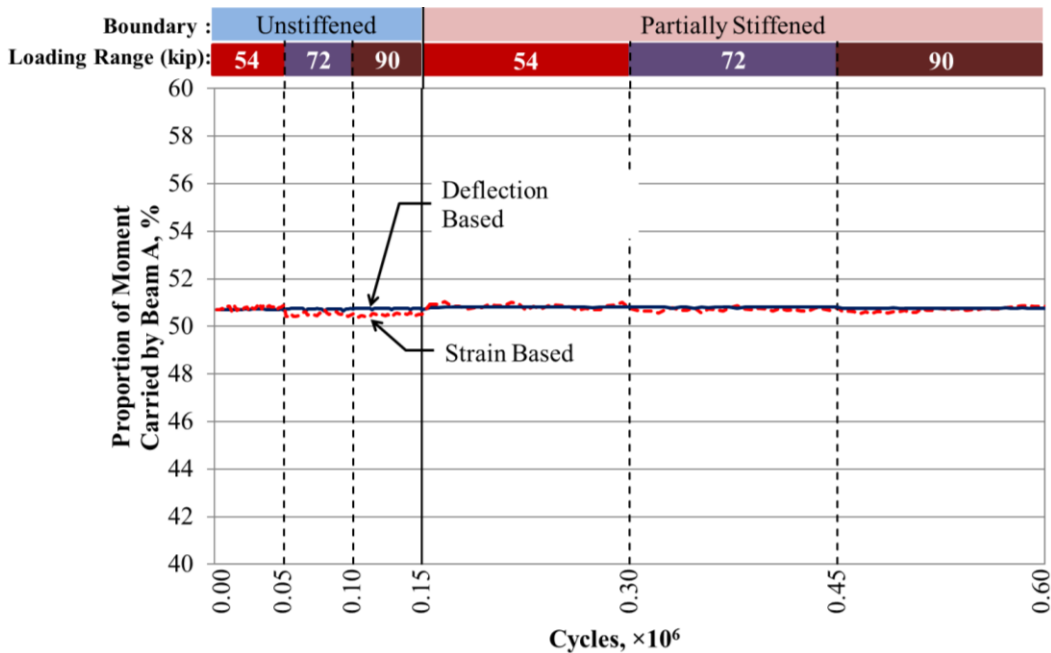
Figure 76. Graph. Proportion of the moment carried by the loaded beam based on the mid-span strain and deflection for unstiffened and partially stiffened beams with a full-depth UHPC connection.
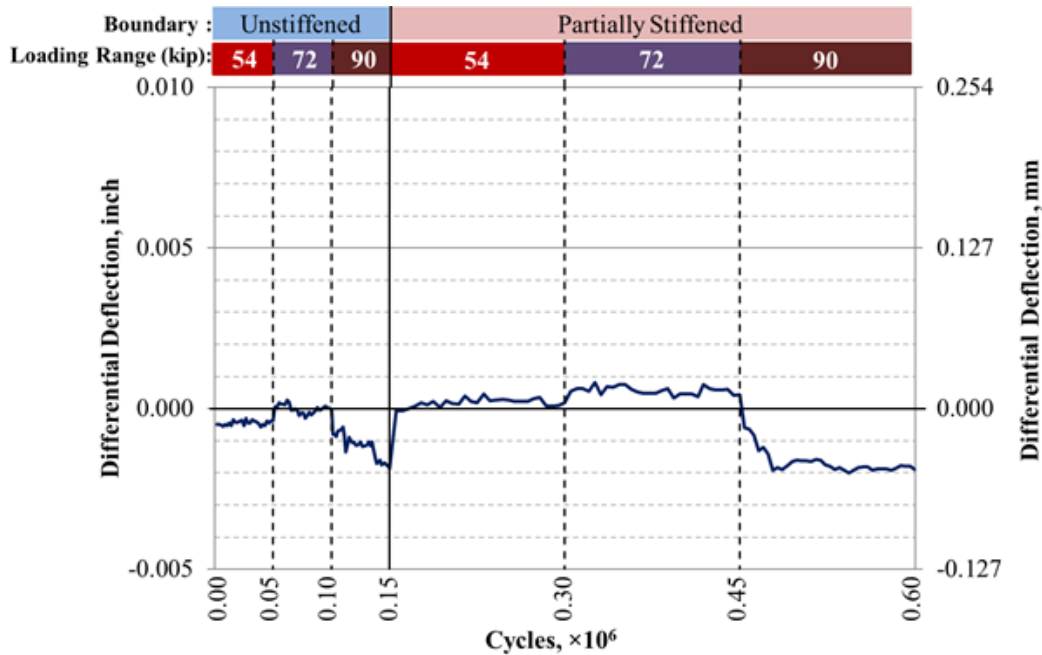
Source: FHWA.
1 kip = 4.448 kN.
1 inch = 25.4 mm.

Figure 77. Graph. $\varDelta_\delta$ measured at the mid-span in unstiffened and partially stiffened beams with a full-depth UHPC connection.

The longitudinal tensile strain range and $\varDelta_\delta$ for the uncracked full-depth UHPC connection with the fully stiffened boundary condition are presented in figure 78 and figure 79, respectively, and a total of 915,000 cycles were conducted. No cracks were initiated. The connection limited $\varDelta_\delta$ to within ±0.0015 inch (±0.038 mm).
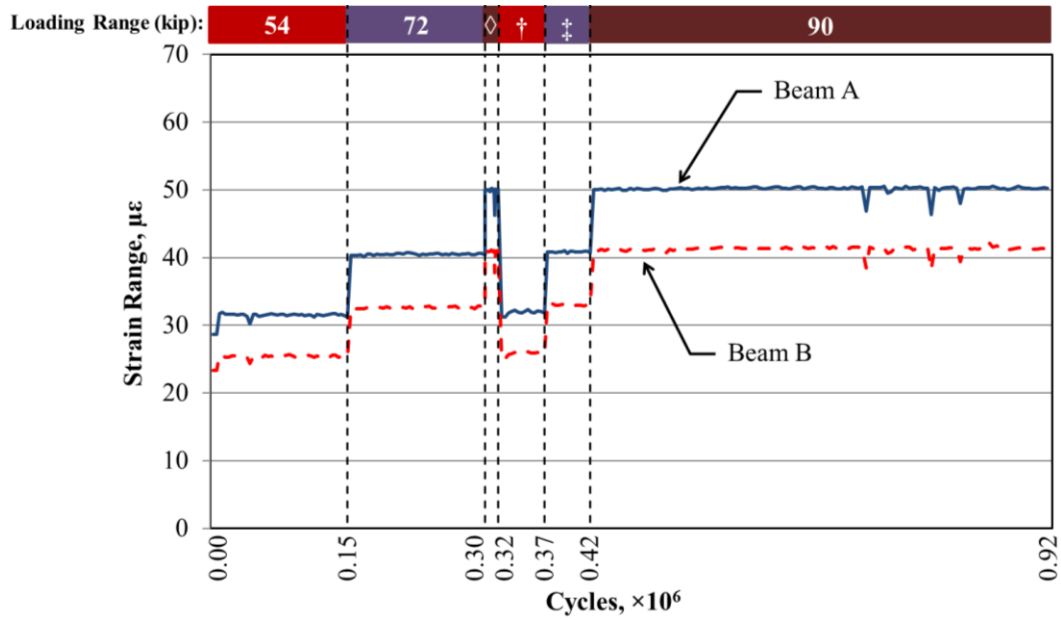
Source: FHWA.
1 kip = 4.448 kN.
◊ = 90-kip loading range.
† = 54-kip loading range.
‡ = 72-kip loading range.

Figure 78. Graph. Longitudinal tensile strain range measured at the mid-span in fully stiffened beams with a full-depth UHPC connection.

Source: FHWA.
1 kip = 4.448 kN.
1 inch = 25.4 mm.
◊ = 90-kip loading range.
† = 54-kip loading range.
‡ = 72-kip loading range.

Figure 79. Graph. Δ_δ measured at the mid-span in fully stiffened beams with a full-depth UHPC connection.

Transverse Strain in the Beams

Connections mainly transfer a load from one beam to another through transverse shear, which drives adjacent beams to effectively have the same deflection. The connections also need to provide transverse flexural rigidity to resist transverse tensile forces due to eccentrically placed wheel loads and superimposed dead loads. The results of the transverse strain due to structural loading are presented here.

Figure 80 presents a reference for the transverse strain gauges used in this section. The simulated structural loading was intentionally placed 6 inches (152 mm) off the centerline of the beams (refer to figure 22 for the test setup) to increase the transverse tensile stress.

Source: FHWA.
1 ft = 0.305 m.

Figure 80. Illustration. Location of all possible transverse strain gauges in this study.

Figure 81 through figure 90 present the recorded transverse tensile strains for the uncracked partial-depth conventional grout and the partial- and full-depth UHPC connections. Specifically, figure 81 shows transverse strains measured by the embedded gauges for the simply supported partial-depth conventional grout connections. Some of the embedded strain gauges did not function properly during the tests; therefore, only those with valid data were reported. A transverse strain between 30 and 42 $\mu\varepsilon$ was measured in beam A, while beam B had a transverse strain between 25 and 35 $\mu\varepsilon$ in the 90-kip (400-kN) loading range. The beams were then loaded with the fully stiffened boundary condition. The transverse strain range is reported in figure 82 and figure 83. The stiffer boundary condition reduced the transverse tensile strain in the embedded strain gauges with values between 10 and 20 $\mu\varepsilon$ in the 90-kip (400-kN) loading range. Surface tensile strain on the connection surface was similar to the embedded gauges in the beams.
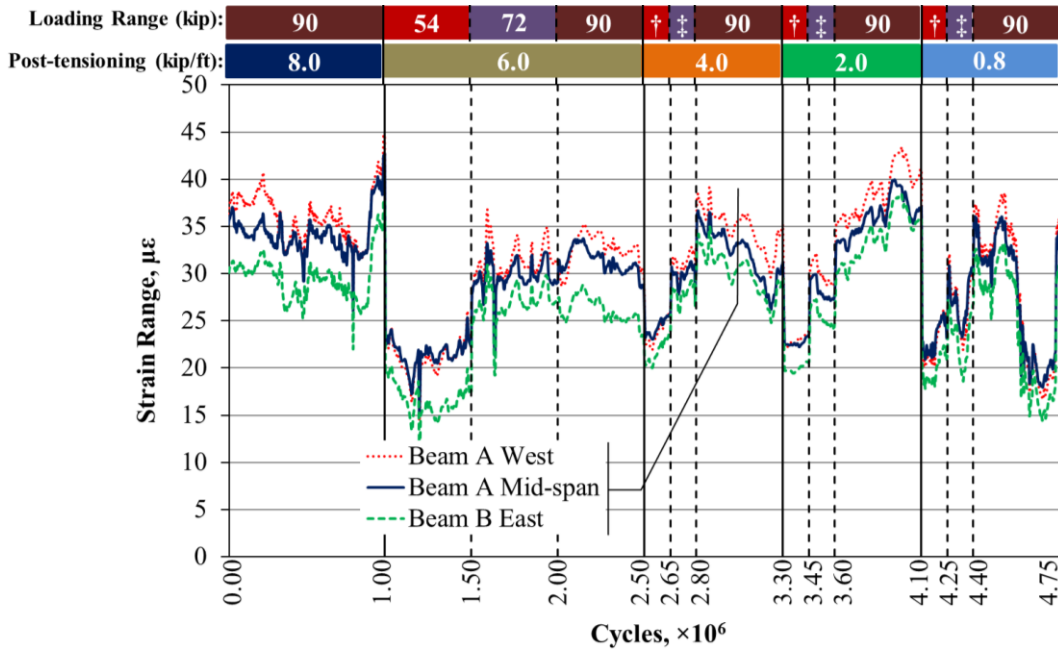
Source: FHWA.
1 kip = 4.448 kN.
1 kip/ft = 14.59 kN/m.
† = 54-kip loading range.
‡ = 72-kip loading range.

Figure 81. Graph. Top transverse strain ranges recorded by internal strain gauges in two beams for unstiffened beams with a partial-depth uncracked conventionally grouted connection.
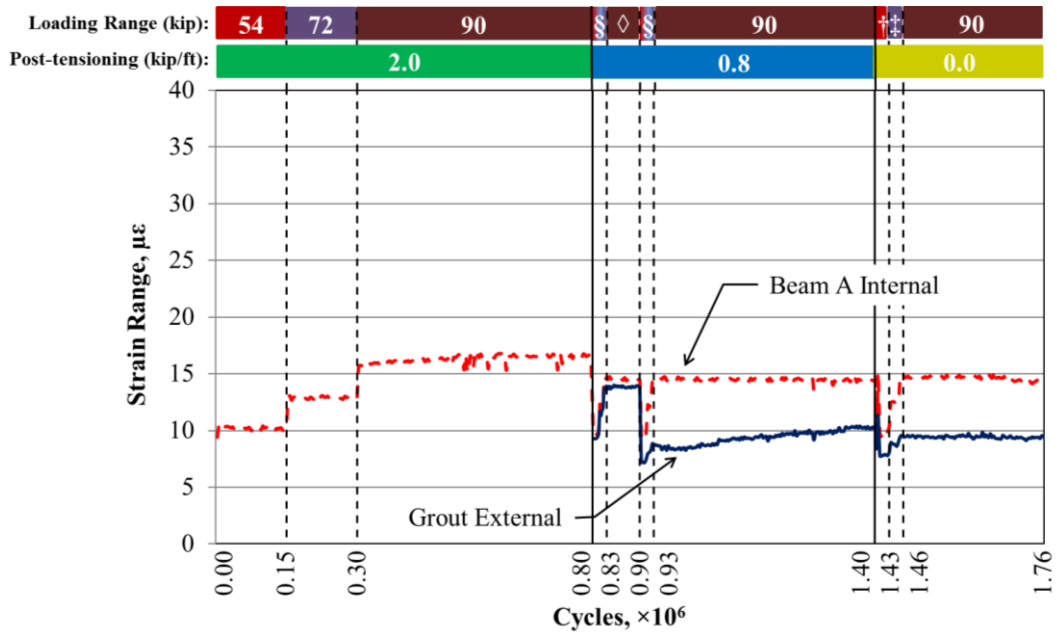
Source: FHWA.
1 kip = 4.448 kN.
1 kip/ft = 14.59 kN/m.
§ = 15,000 cycles at both the 54- and 72-kip loading ranges.
◊ = 90 kip loading range.
† = 54 kip loading range.
‡ = 72 kip loading range.

Figure 82. Graph. Top transverse strain ranges recorded at the mid-span for fully stiffened beams with a partial-depth uncracked conventionally grouted connection.
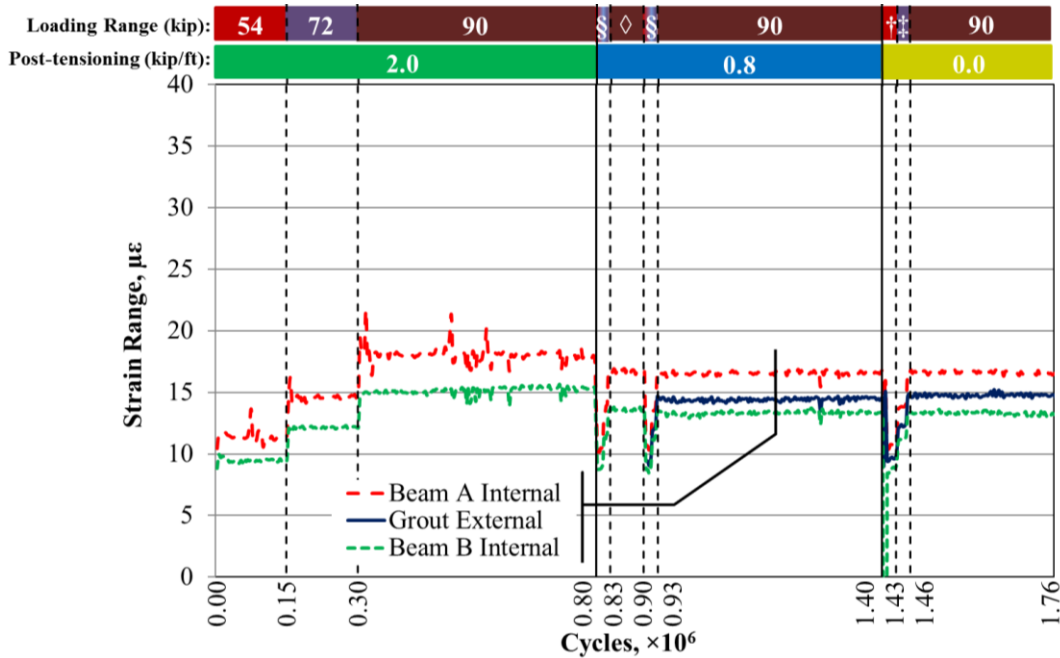
Source: FHWA.
1 kip = 4.448 kN.
1 kip/ft = 14.59 kN/m.
§ = 15,000 cycles at both the 54- and 72-kip loading ranges.
◊ = 90 kip loading range.
† = 54 kip loading range.
‡ = 72 kip loading range.

Figure 83. Graph. Top transverse strain ranges recorded 6 ft (1.8 m) east of the mid-span for fully stiffened beams with a partial-depth uncracked conventionally grouted connection.

For the partial-depth UHPC connections, surface strain gauges were installed on the connection and the box beam surfaces at the mid-span and 6 ft (1.8 m) from the mid-span. More surface strain gauges were installed on the connection at transverse PT locations. The transverse tensile strain in the UHPC was generally less than or equal to 20 $\mu\varepsilon$, which was the same as with the conventional grouted connection. The results are presented in figure 84 through figure 86.

74
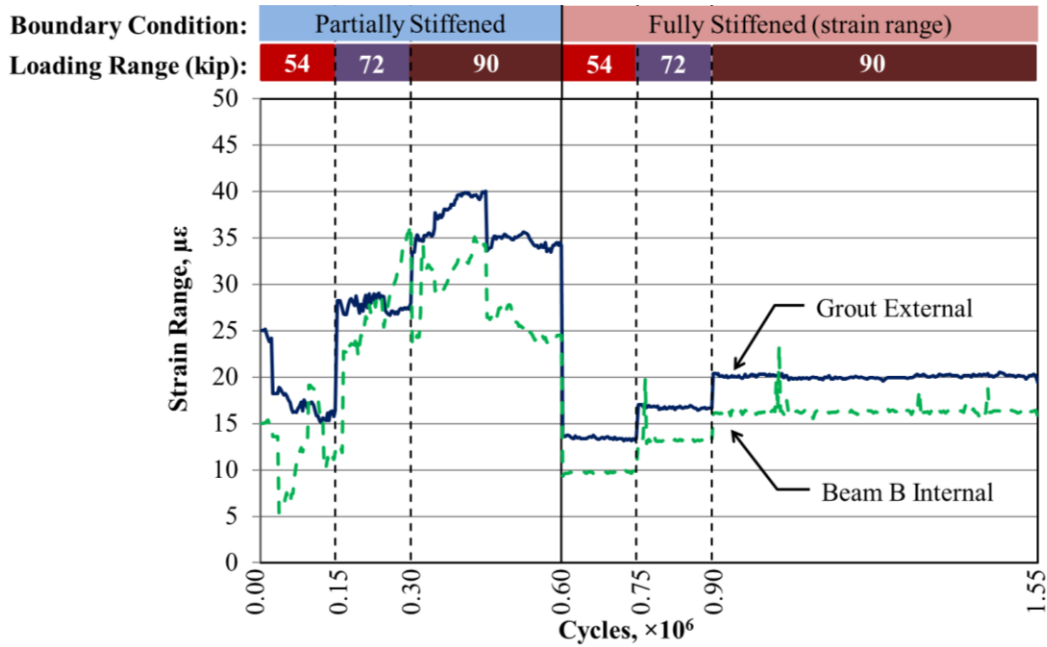
Figure 84. Graph. Top transverse strain ranges recorded at the mid-span for partially and fully stiffened beams with a partial-depth uncracked UHPC connection.
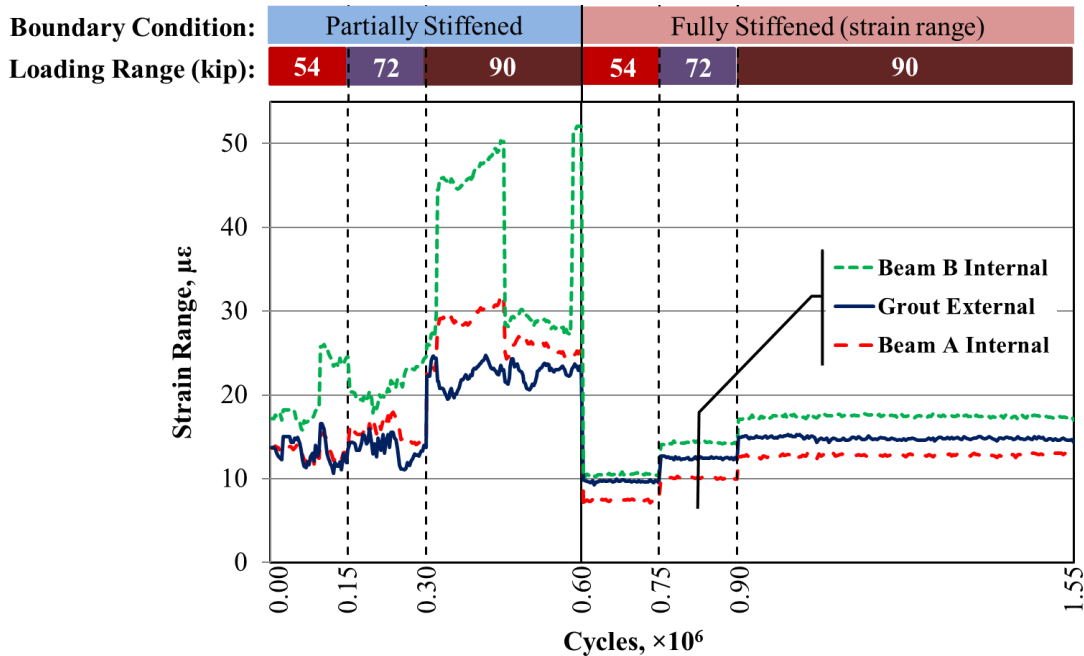
Source: FHWA.
1 kip = 4.448 kN.

Figure 85. Graph. Top transverse strain ranges recorded 6 ft (1.8 m) east of the mid-span for partially and fully stiffened beams with a partial-depth uncracked UHPC connection.

Source: FHWA.
1 kip = 4.448 kN.

75
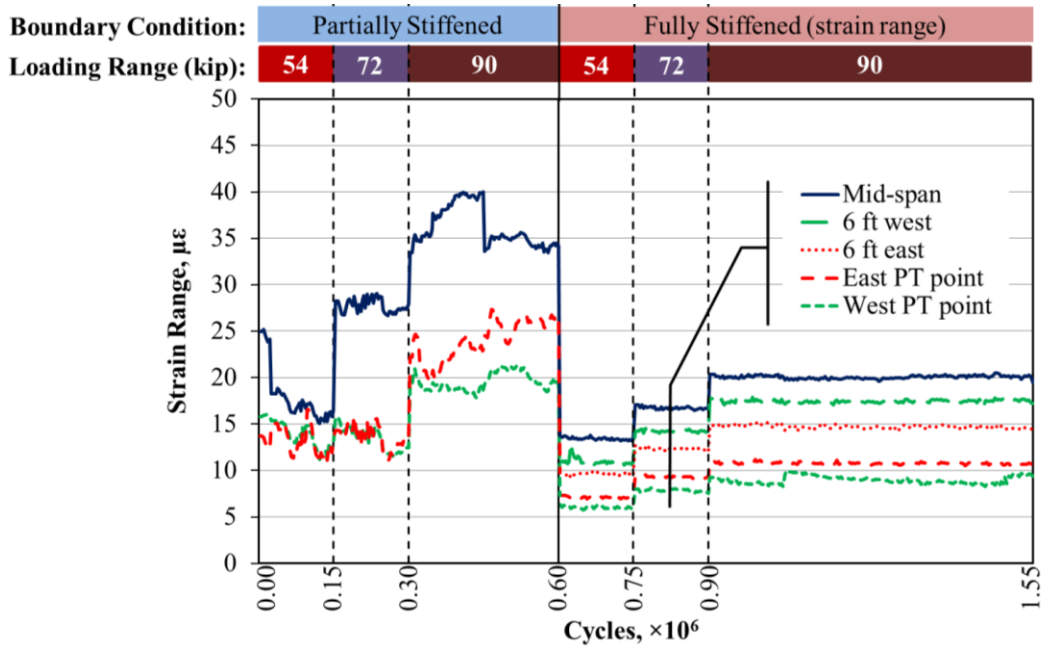
Source: FHWA.
1 kip = 4.448 kN.
1 ft = 0.305 m.

Figure 86. Graph. Top transverse strain ranges recorded along the length of the connection for partially and fully stiffened beams with a partial-depth uncracked UHPC connection.

When the full-depth UHPC connection was tested, additional surface strain gauges were installed along the cross section at the same longitudinal locations on the beam. Not all of the strain gauges functioned properly; only those with valid data were reported in figure 87 through figure 90. The simply supported case showed the highest transverse tensile strain of all the cases studied. The strain gauges placed next to the connection usually had more transverse strain. The only exception was for the strain gauge located on the outside edge of the loaded beam 6 ft (1.8 m) from the mid-span, as shown in figure 88.
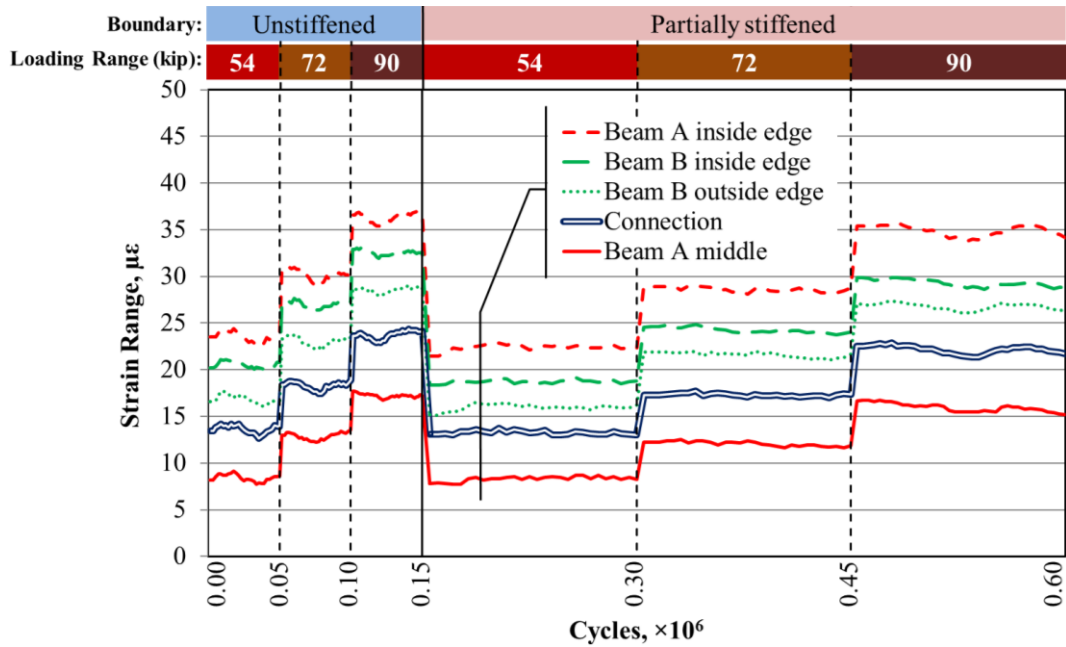
Source: FHWA.
1 kip = 4.448 kN.

Figure 87. Graph. Distribution of top transverse strain ranges recorded along the top of the unstiffened and partially stiffened beams with a full-depth uncracked UHPC connection at the mid-span.
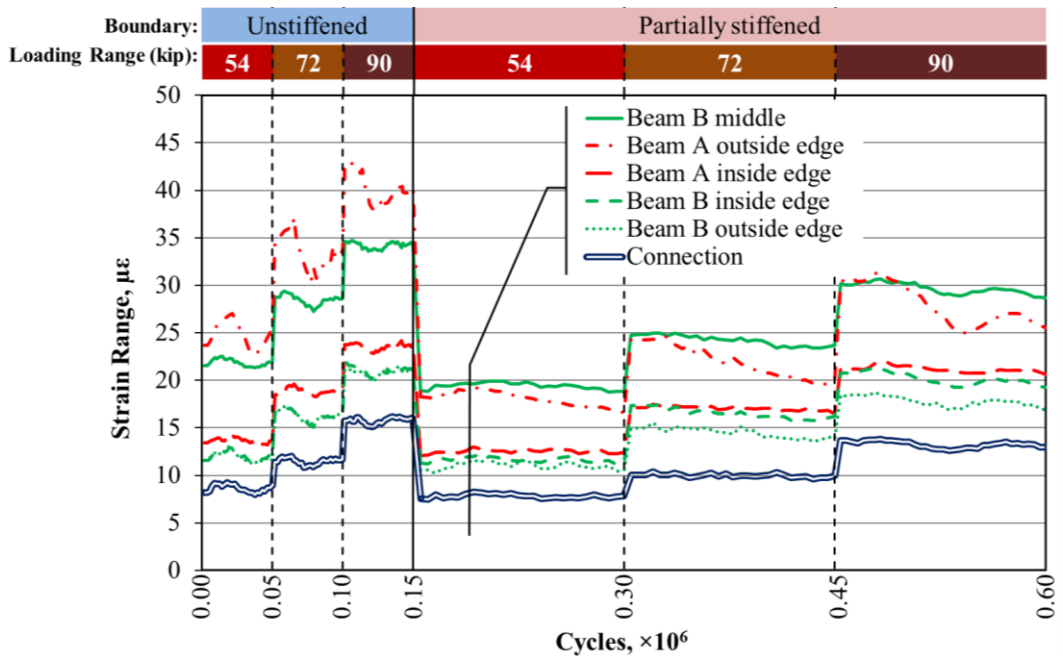
Source: FHWA.
1 kip = 4.448 kN.

Figure 88. Graph. Top transverse strain ranges recorded along the top of unstiffened and partially stiffened beams with a full-depth uncracked UHPC connection 6 ft (1.8 m) from the mid-span.
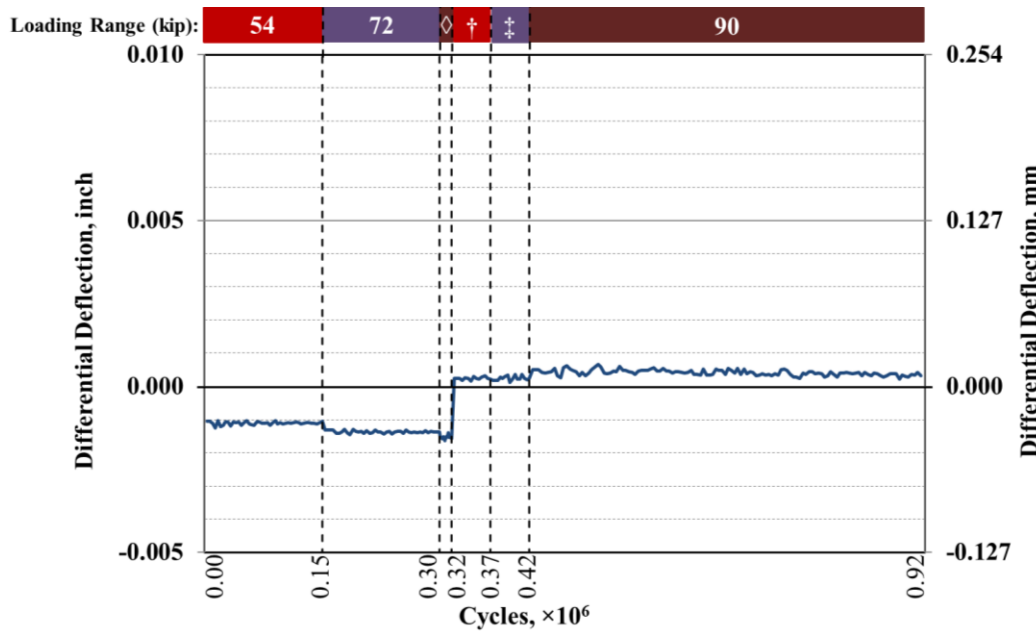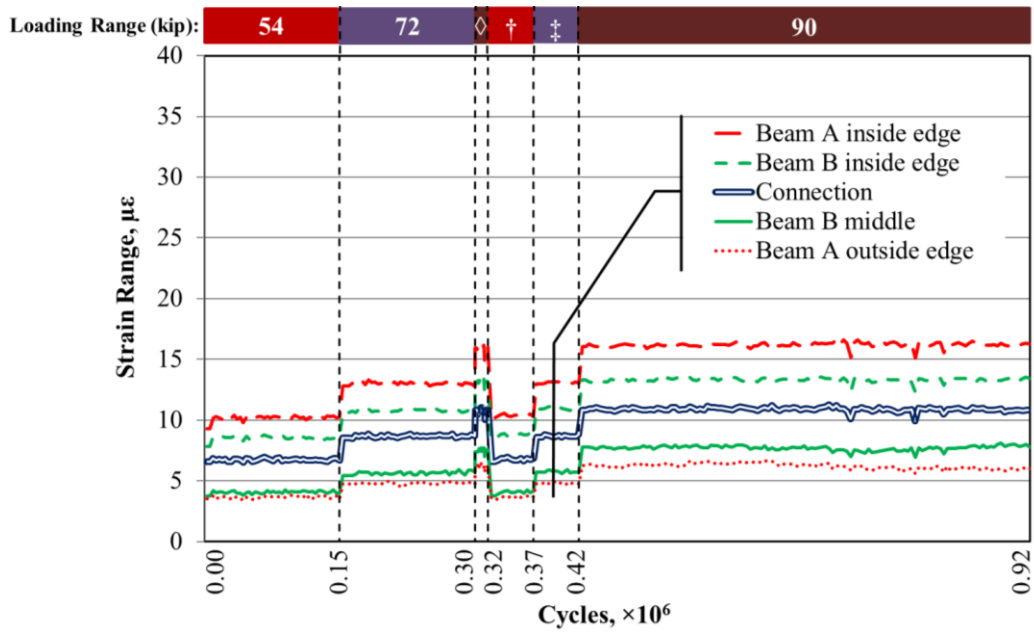
Source: FHWA.
1 kip = 4.448 kN.
◊ = 90-kip loading range.
† = 54-kip loading range.
‡ = 72-kip loading range.

Figure 89. Graph. Top transverse strain ranges recorded along the top of fully stiffened beams with a full-depth uncracked UHPC connection at the mid-span.
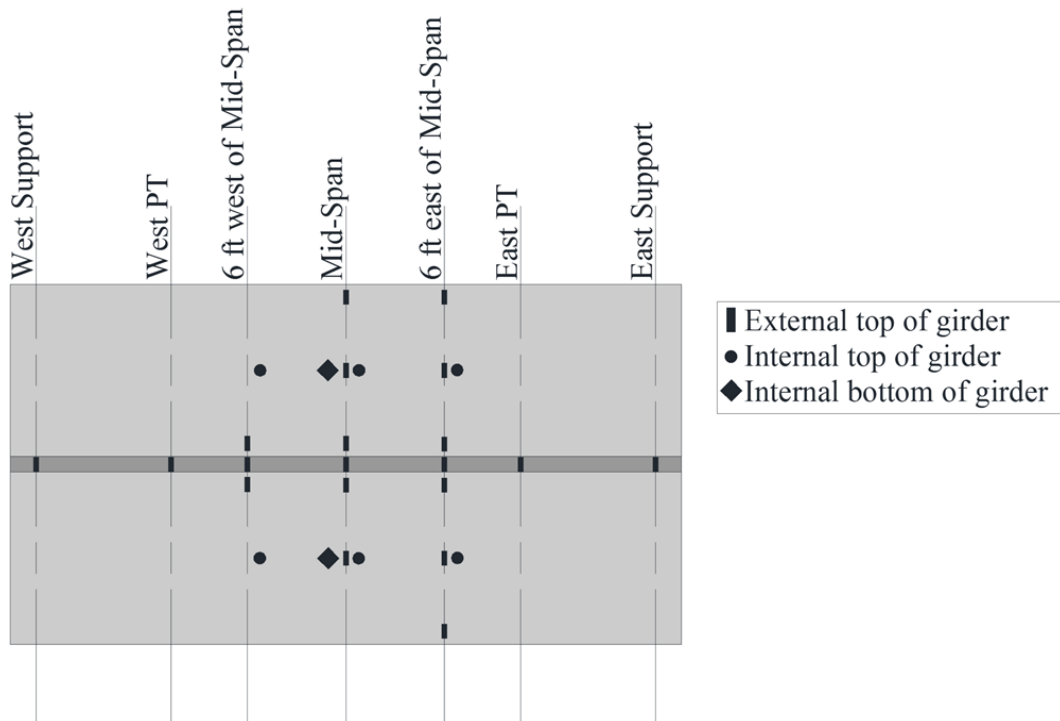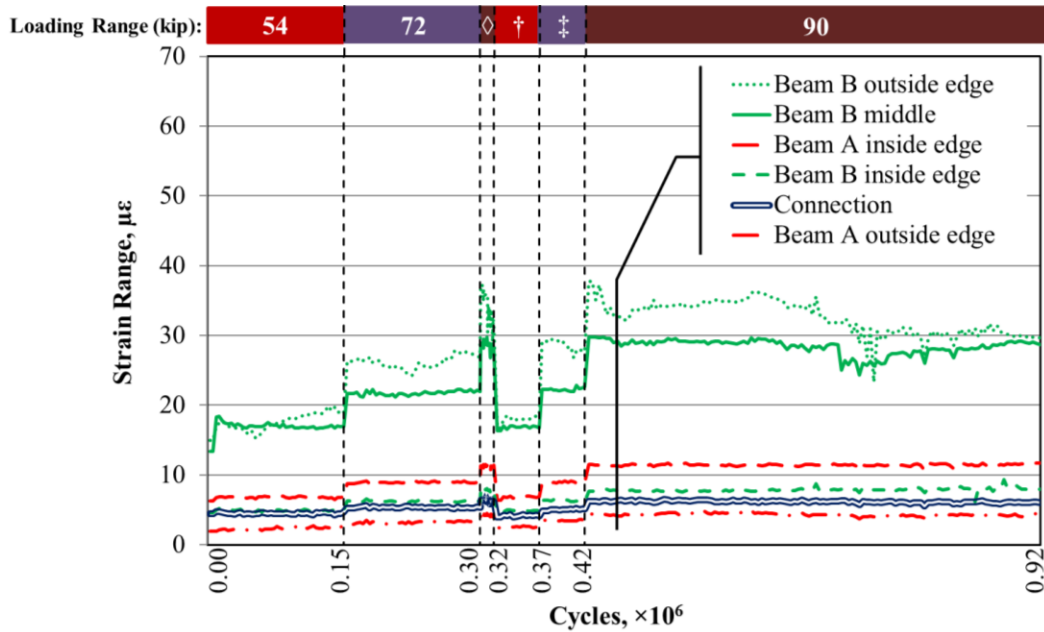
Source: FHWA.
1 kip = 4.448 kN.
◊ = 90-kip loading range.
† = 54-kip loading range.
‡ = 72-kip loading range.

Figure 90. Graph. Top transverse strain ranges recorded along the top of fully stiffened beams with a full-depth uncracked UHPC connection 6 ft (1.8 m) east of the mid-span.

Independent of the connection design and boundary conditions, the transverse tensile strain generated by the structural loading was observed to be less than 40 με. If a maximum transverse tensile strain of 40 με in the box beam concrete close to the connection is assumed, the interface bond between the grout and box beam concrete should have enough strength to resist this strain. A 40-με deformation in a 6,000-psi (41-MPa) concrete produces a stress of approximately 150 psi (1 MPa).

Proper selection of a grout, a connection surface preparation technique, and curing methodology can mitigate interface cracking by ensuring that the tensile resistance of the connection is at least as strong as the precast concrete. It must be recognized that the early age dimensional stability of the grout is also important as shrinkage strains can be large, potentially resulting in cracking of the grout and interface debonding.

When a direct tensile force was applied to the UHPC connections, as demonstrated in figure 74, the box beam concrete cracked rather than the connection interface or the UHPC itself. This indicates that the interface bond between the UHPC and the box beam with an EA surface preparation and rebar in a non-contact lap splice is of similar or greater tensile strength as compared to the tensile strength of the box beam concrete. This was also observed in a study by De la Varga et al. where interface bond between different grout materials and concrete was investigated.[17] They found that, for connections with UHPC and EA, the failure primarily occurs in the concrete rather than at the interface or within UHPC itself. This is not true for conventional grout connections, as the interface often fails under the same conditions. Note that

79

the discrete steel reinforcement that is distributed along the length of the UHPC connections provides further advantages in terms of increasing local shear and tensile strengths and limiting the crack width if any cracks should develop at the interface.

CHAPTER 5. DISCUSSION

This chapter discusses the effect of certain connection parameters, including the depth of the connection, condition of the connection, the level of transverse PT applied, and the material used in the connection. The data are presented using bar graphs of the average values, with the error bars indicating the minimum and maximum values observed. The average, minimum, and maximum values are based on a five-point moving average of the recorded values.

PARTIAL- VERSUS FULL-DEPTH CONNECTION

Because tests on partial- and full-depth conventional grouted connections were not performed with the same level of cracking and boundary conditions, a meaningful analysis isolating the effect of the connection depth was not possible. Therefore, this section focuses on the comparison between the partial- and full-depth UHPC connections only.

The effect on the longitudinal strains in the bottom flange of the beams is shown in figure 91. When the partially stiffened end condition was used, little effect can be seen as the strains in the loaded and unloaded beams were virtually identical between the partial- and full-depth connections. However, when the fully stiffened boundary condition was employed, the range of strains in each of the full-depth beams decreased around 10 $\mu\varepsilon$. This may have been caused by a higher *EI* due to a larger area of material in the connection. The larger drop in strain between the full- and partial-depth connections in the fully stiffened boundary configuration could be caused by the full-depth connection limiting transverse bending through the connection. This could lead to increased deflection and, therefore, increased longitudinal strain.
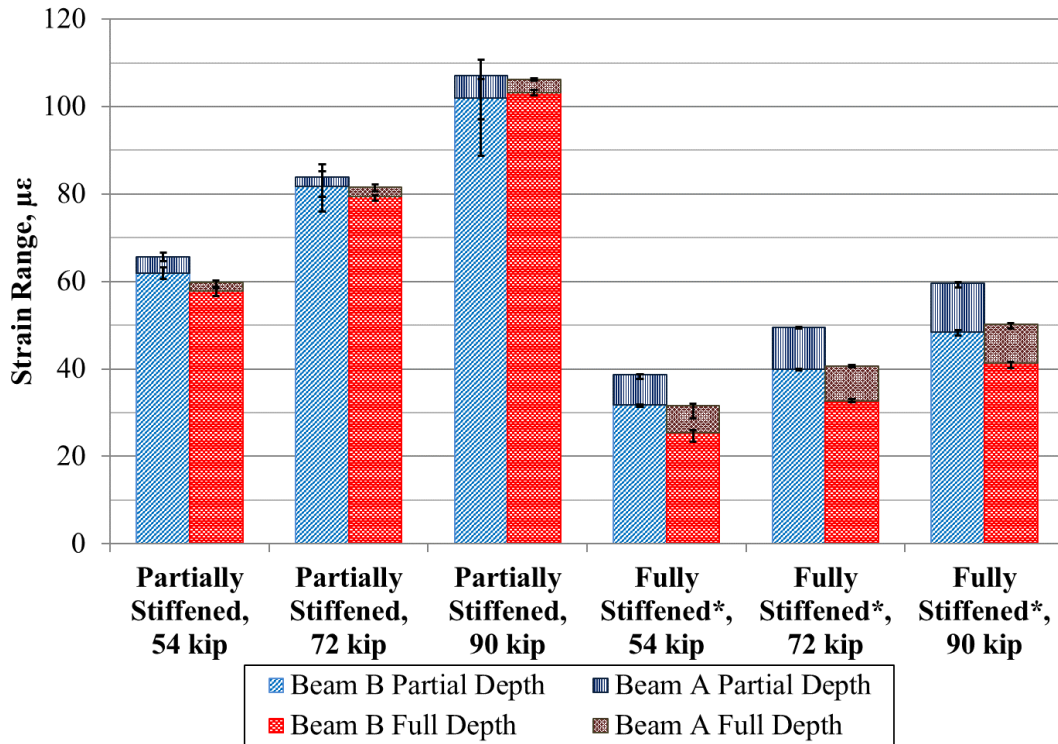
Source: FHWA.
1 kip = 4.448 kN.
*Fully stiffened strain is reported as the strain range.

Figure 91. Graph. Comparison of the longitudinal strain ranges for the partial- and full-depth UHPC connections.

The loaded beam proportion of moment for the two connection depths under the partially stiffened boundary condition can be seen in figure 92. The moment was well distributed with both the partial- and full-depth connections, with more equitable distribution occurring when a full-depth shear key was used. This could be caused by increased torsional stiffness provided with a full-depth connection. This increased stiffness allows the beams to deflect more evenly and results in more uniform Δ_δ and strains in the two beams. This is shown in both the deflection- and strain-based measures of proportion of moment.
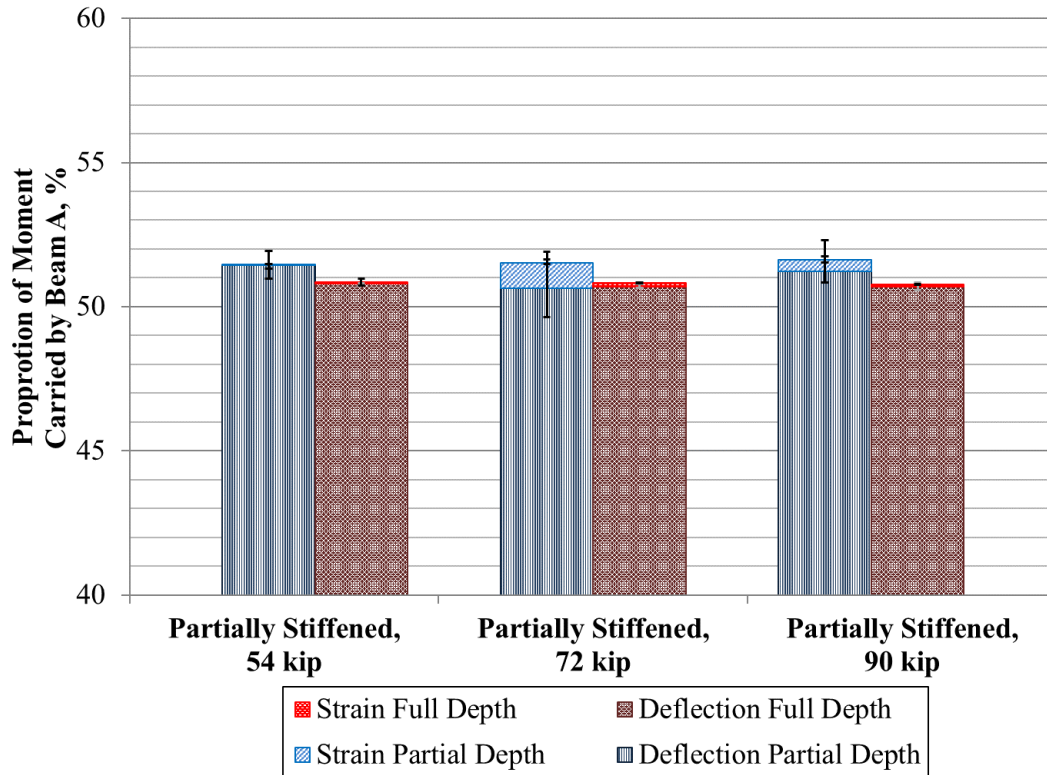
Source: FHWA.
1 kip = 4.448 kN.

Figure 92. Graph. Comparison of the loaded beam proportion of moment between the partial- and full-depth UHPC connections.

As with the performance with longitudinal strains, both connection depths were able to minimize Δ_δ between the beams, limiting the differential movement to 0.004 inch (0.102 mm) in both cases. The full-depth connection again performed slightly better, limiting observed values between the beams to within 0.002 inch (0.051 mm). A plot showing the Δ_δ for the two connection depths is shown in figure 93.
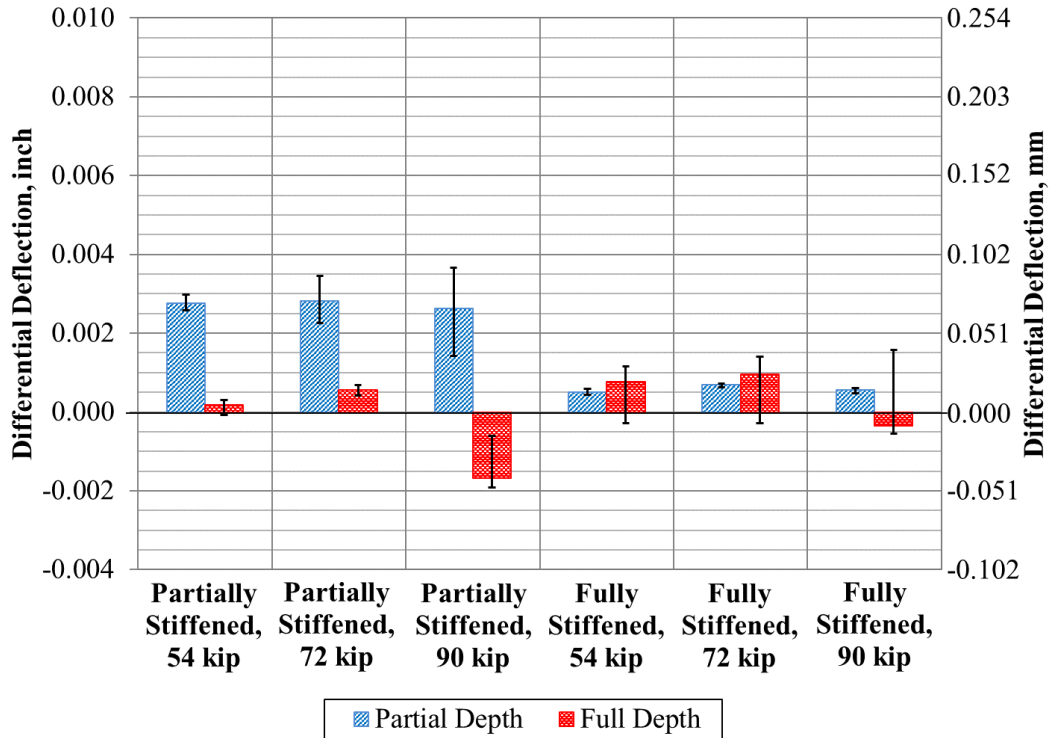
Figure 93. Graph. Comparison of Δ_δ of the partial- and full-depth UHPC connections.

Figure 94 shows the transverse strains in the connection at the mid-span as well as 6 ft (1.8 m) to the east side of the mid-span. This graph shows that the transverse strains in the connection were lower for the full-depth connection. Transverse strains were generated in the connection as it transferred the moment acting like a transverse beam. The full-depth connection was 2.5 times deeper than the partial-depth connection. This resulted in lower transverse strains in the extreme fibers of the full-depth connection.
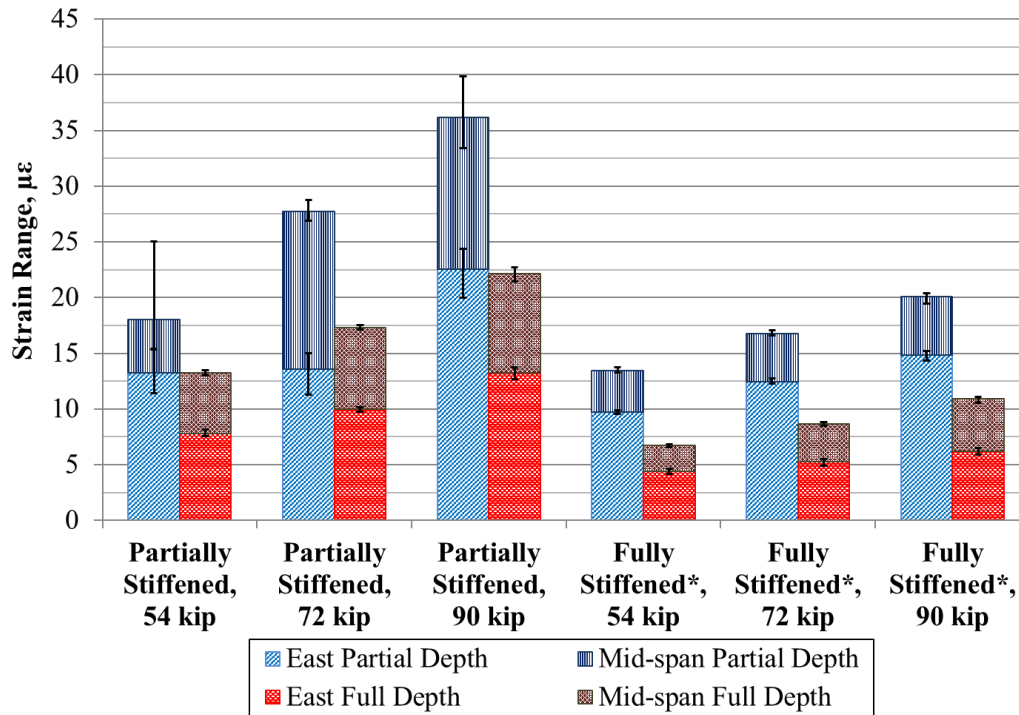
Figure 94. Graph. Comparison of the top transverse strain ranges in the partial- and full-depth UHPC connections.

The performance of both the partial- and full-depth connections was satisfactory within the context of the metrics discussed here. The increased depth of the full-depth connection resulted in somewhat better load sharing and more uniform deformations; however, increasing the depth of the connection increases construction costs, especially if a more expensive material such as UHPC is being utilized in the connection.

CONDITION OF THE CONNECTION

This section discusses the performance of the partial-depth conventional grout connection with respect to the condition of the connection. This was the only configuration that was run in uncracked, partially cracked, and fully cracked connections. The responses of the beams are shown in the 54-, 72-, and 90-kip (240-, 320-, and 400-kN) loading ranges for the 0.8- and 0-kip/ft (12- and 0-kN/m) PT levels.

The beams exhibited a nearly identical strain response to the loading cycles regardless of the condition of the connection, as can be seen in the comparison in figure 95. The cracked connections could still effectively transfer the load from one beam to the other when a level of PT was utilized likely through friction between the grout and the box beam concrete. Ranges of strain in the loaded beam were only about 2 $\mu\varepsilon$ higher for beams with a cracked connection. When no PT was used, the strains on the unloaded beam remained the same regardless of crack condition, while strains on the loaded beam were seen to increase, especially on the beam with the fully cracked connection.

85
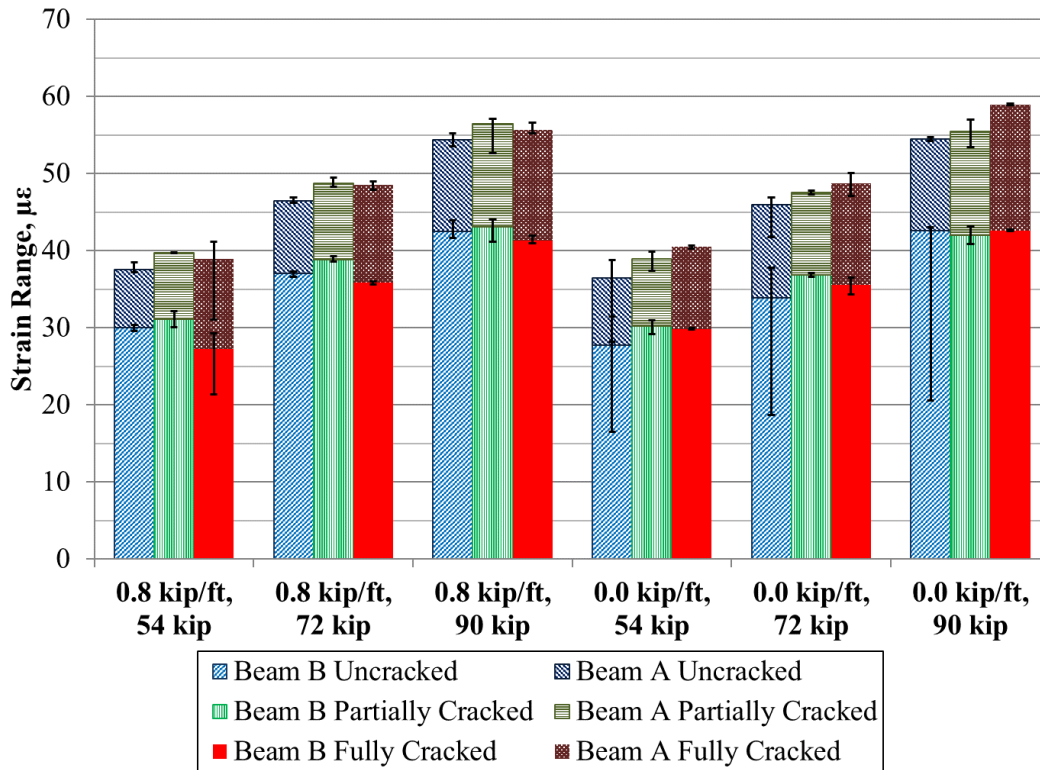
Source: FHWA.
1 kip = 4.448 kN.

Figure 95. Graph. Comparison of longitudinal strain ranges based on the extent of cracking in the connection.

As shown in figure 96, Δ_δ was affected by the condition of the connection. The uncracked section was able to maintain a Δ_δ below 0.001 inch (0.025 mm). With the introduction of cracks in the connection, Δ_δ increased to between 0.002 and 0.004 inch (0.051 and 0.102 mm) for the partially cracked connection. When the connection was entirely debonded, Δ_δ of over 0.012 inch (0.305 mm) was observed in the 90-kip (400-kN) loading cycle. This demonstrates that the connection condition has the potential to have a significant impact on Δ_δ between adjacent beams.
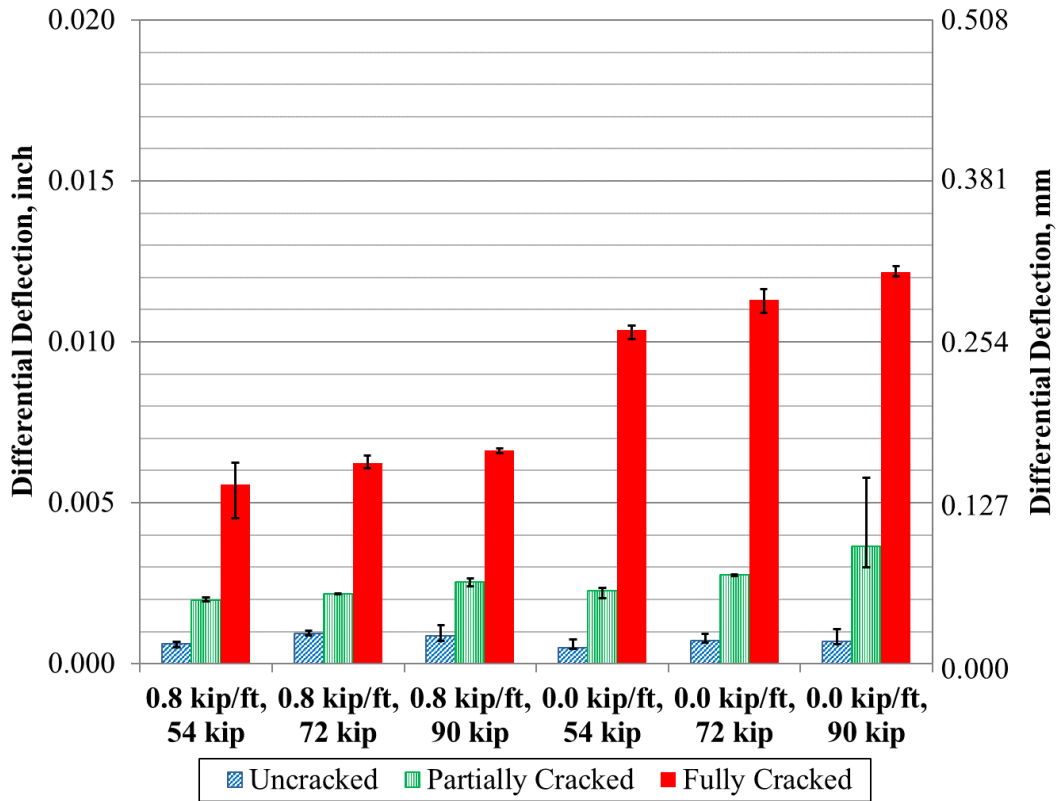
Source: FHWA.
1 inch = 25.4 mm.
1 kip/ft = 14.59 kN/m.
1 kip = 4.448 kN.

Figure 96. Graph. Comparison of Δ_δ between the beams based on the extent of cracking in the connection.

Figure 97 and figure 98 show a comparison of transverse strains in the connection and in the beams, respectively, based on the condition of the connection. Overall, there was not a large difference between the transverse strains in the connection. As for the internal transverse strains in the beams, the strains in the loaded beams were found to increase, while the strains in the unloaded beams were found to decrease. This is intuitive because when the connection is not intact, it cannot transfer loads as effectively.
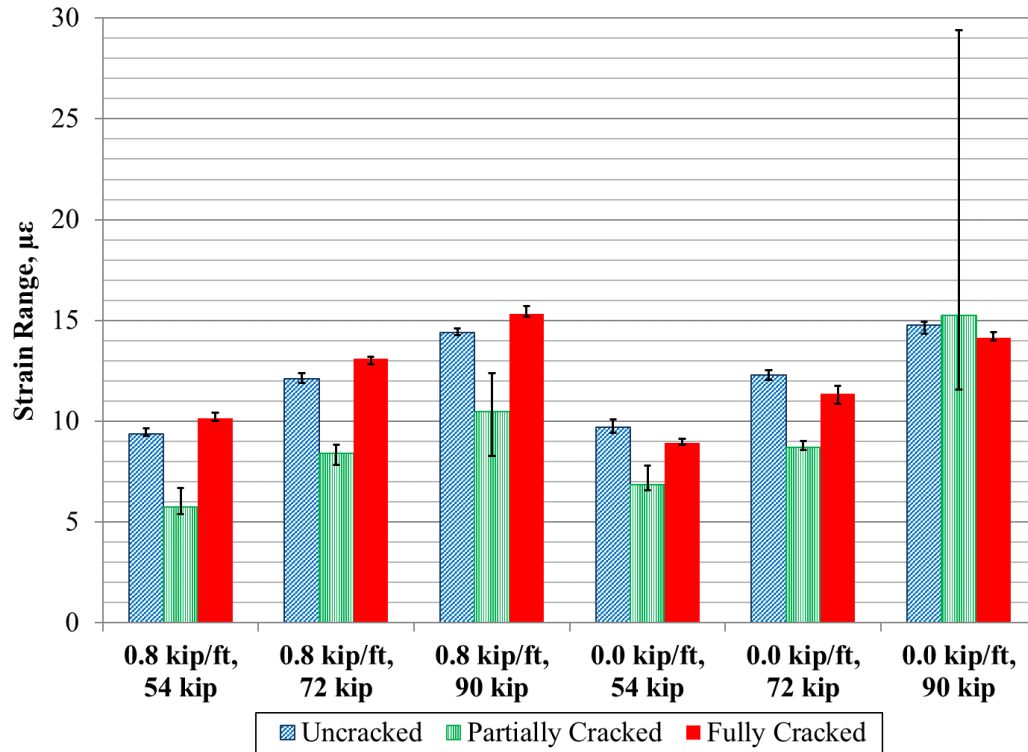
Source: FHWA.
1 kip/ft = 14.59 kN/m.
1 kip = 4.448 kN.

Figure 97. Graph. Comparison of the top transverse strain ranges at the mid-span in the connection based on the extent of cracking in the connection.
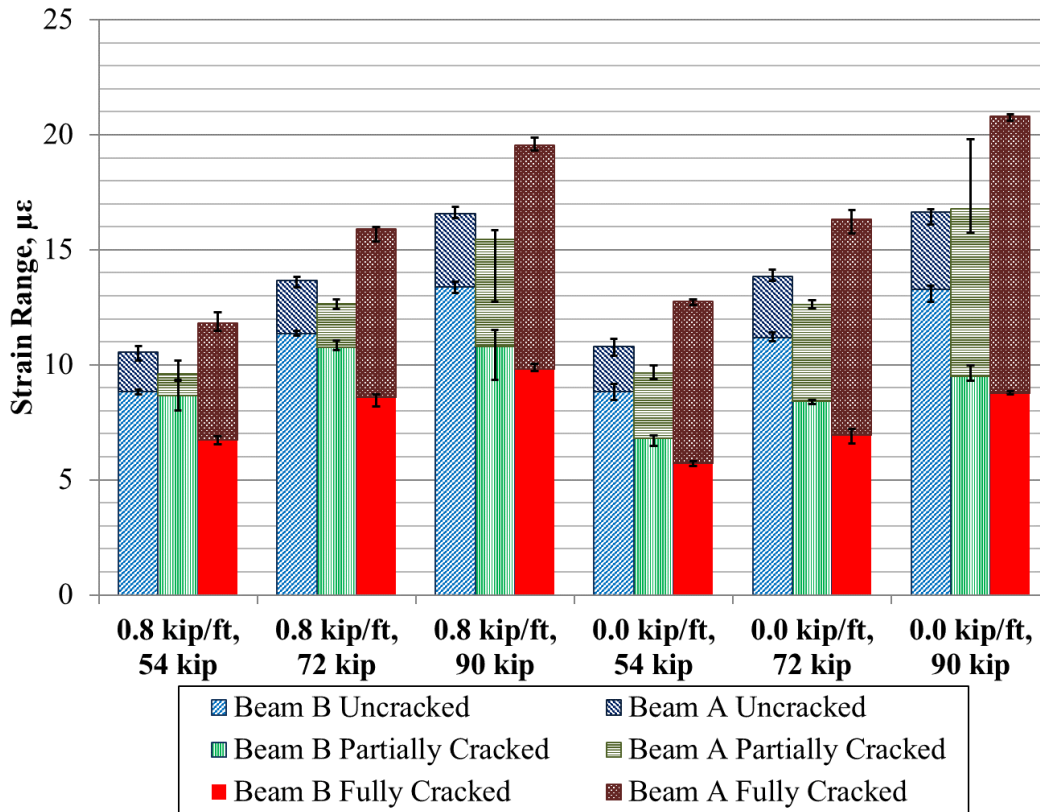
Source: FHWA.
1 kip/ft = 14.59 kN/m.
1 kip = 4.448 kN.

Figure 98. Graph. Comparison of the top transverse strain ranges in the beams based on the extent of cracking in the connection.

The condition of the connection was found to have an impact on the performance of the connection, particularly when the PT force was removed. Loaded beam longitudinal and transverse strains and $\varDelta_\delta$ were seen to increase, while unloaded beam transverse strains were found to decrease. This shows that the condition of the connection plays an important role in force transfer.

TRANSVERSE PT

This section investigates the effect of transverse PT, which was evaluated using the loaded beam proportion of moment and $\varDelta_\delta$ between the two beams under different levels of transverse PT force.

Figure 99 and figure 100 show the measured longitudinal tensile strains at the mid-span and the calculated proportion of moment carried by the loaded beam, respectively, for the beams with an unstiffened partial-depth conventionally grouted connection. The two beams were loaded under different levels of transverse PT force distribution from 8 to 0.8 kip/ft (117 to 12 kN/m). The measured tensile strains in the two beams did not noticeably change under different levels of transverse PT applied. The calculated proportion of moment on the loaded beam were consistently between about 51 and 52 percent throughout all the PT levels.
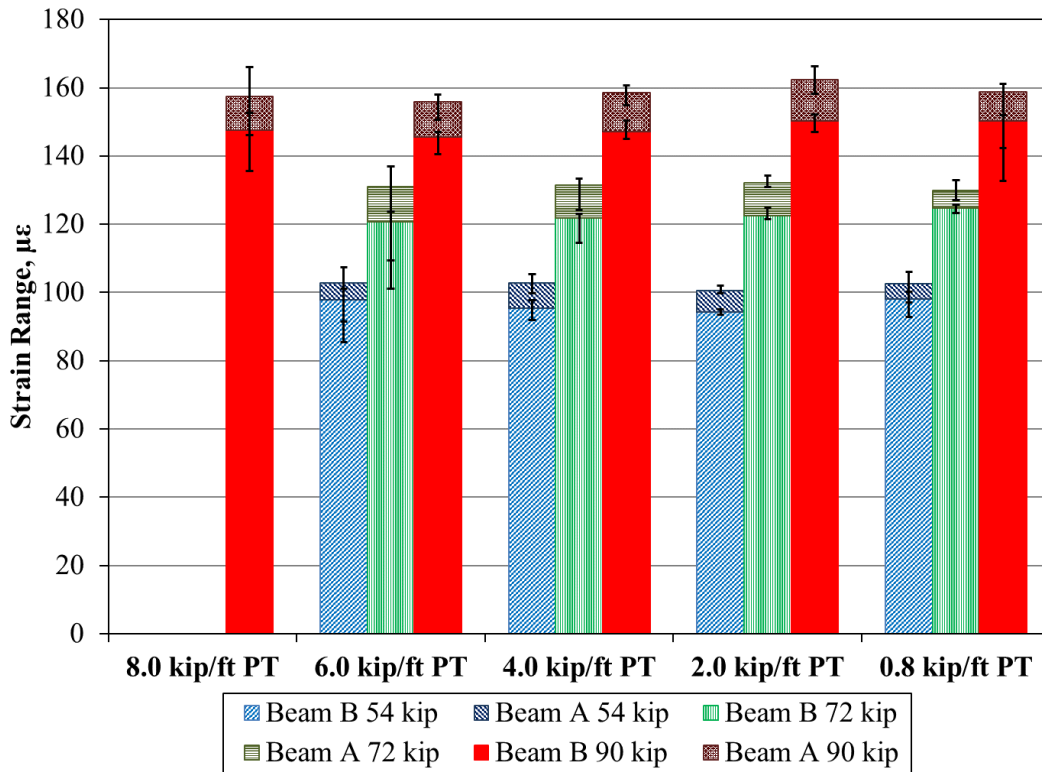
Source: FHWA.
1 kip/ft = 14.59 kN/m.
1 kip = 4.448 kN.

Figure 99. Comparison of the longitudinal strain ranges for the unloaded and loaded beams with unstiffened uncracked partial-depth conventional connections based on the level of PT.
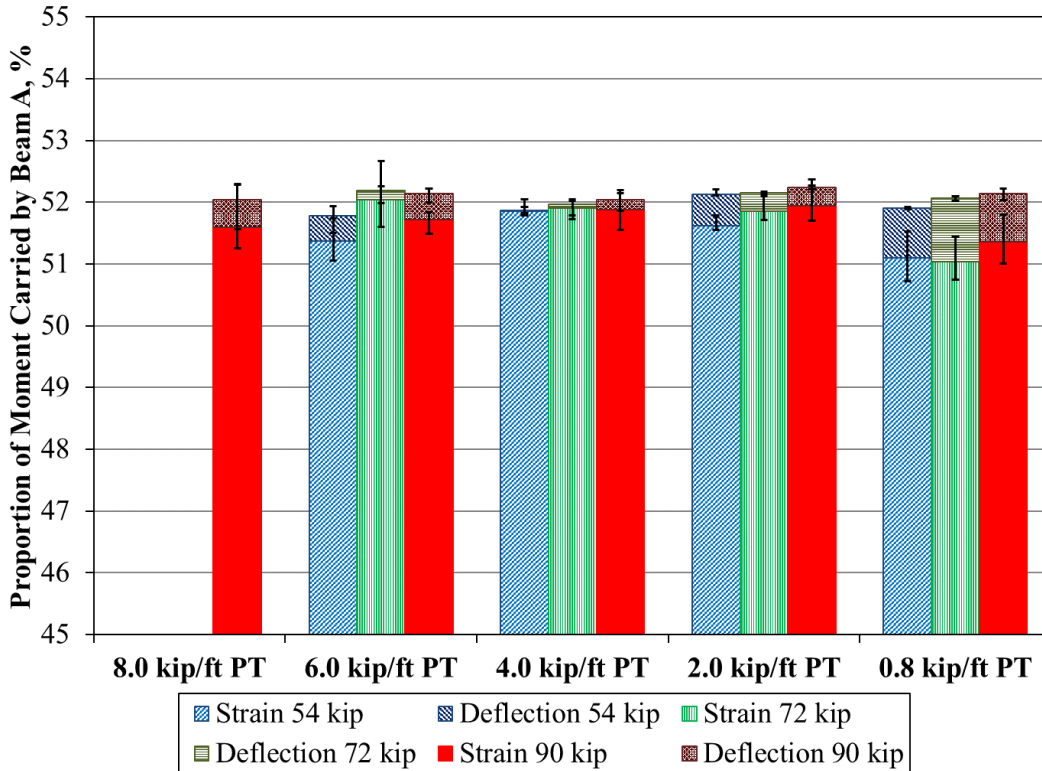
Figure 100. Graph. Comparison of the loaded beam proportion of moment in the beams with unstiffened uncracked partial-depth connections based on the level of PT force.

Figure 101 shows Δ_δ for the beams connected with an unstiffened partial-depth conventionally grouted connection. Δ_δ also showed little variance, maintaining a value of approximately 0.002 inch (0. 051 mm). For comparison, the *Precast Prestressed Concrete Bridge Design Manual* includes a discussion that the acceptable amount of Δ_δ between adjacent box beams is 0.020 inch (0.508 mm) for spans up to 100 ft (30.5 m).[3]
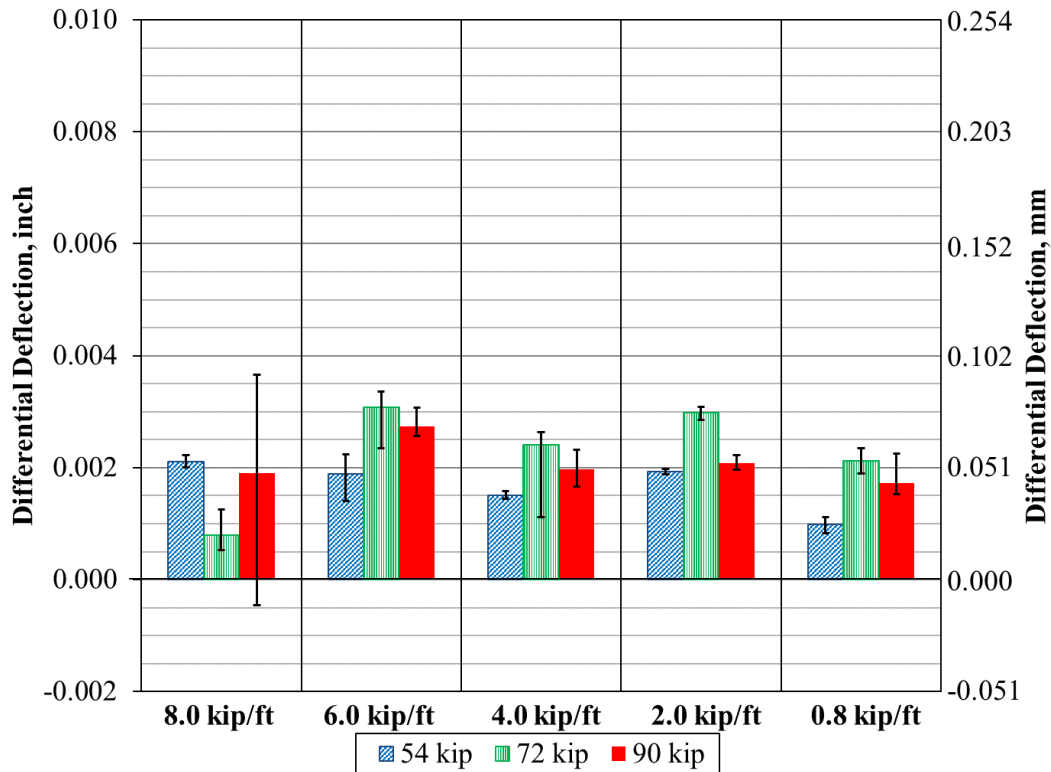
Source: FHWA.
1 inch = 25.4 mm.
1 kip = 4.448 kN.
1 kip/ft = 14.59 kN/m.

Figure 101. Graph. Comparison of Δ_δ in the beams with unstiffened uncracked partial-depth connections based on the level of PT force.

The beams with the partial-depth conventional grout connection were loaded with the stiffest boundary condition, with uncracked, partially cracked, and fully cracked connections. The partially and fully cracked conventionally grouted connections were loaded under transverse PT forces ranging from 8 to 0 kip/ft (117 to 0 kN/m). The results of the longitudinal tensile strain and Δ_δ are presented in figure 102 and figure 103, respectively. The intact connection did not see a notable effect on the longitudinal strain ranges between different levels of transverse PT. Similar observations were made for the partially and fully cracked connections. Δ_δ in the partially and fully cracked connection, however, was affected by the level of PT used in the beams. It can be seen that the uncracked connection maintained a Δ_δ of around 0.001 inch (0.025 mm) regardless of the level of PT force. The partially cracked connection had a Δ_δ under 0.0025 inch (0.064 mm) for PT levels less than 2 kip/ft (29 kN/m) and over 0.006 inch (0.152 mm) with the PT force removed. The difference was even more dramatic with the fully cracked connection, with Δ_δ doubling from 0.006 to 0.012 inch (0.152 to 0.305 mm) when the PT force was removed.
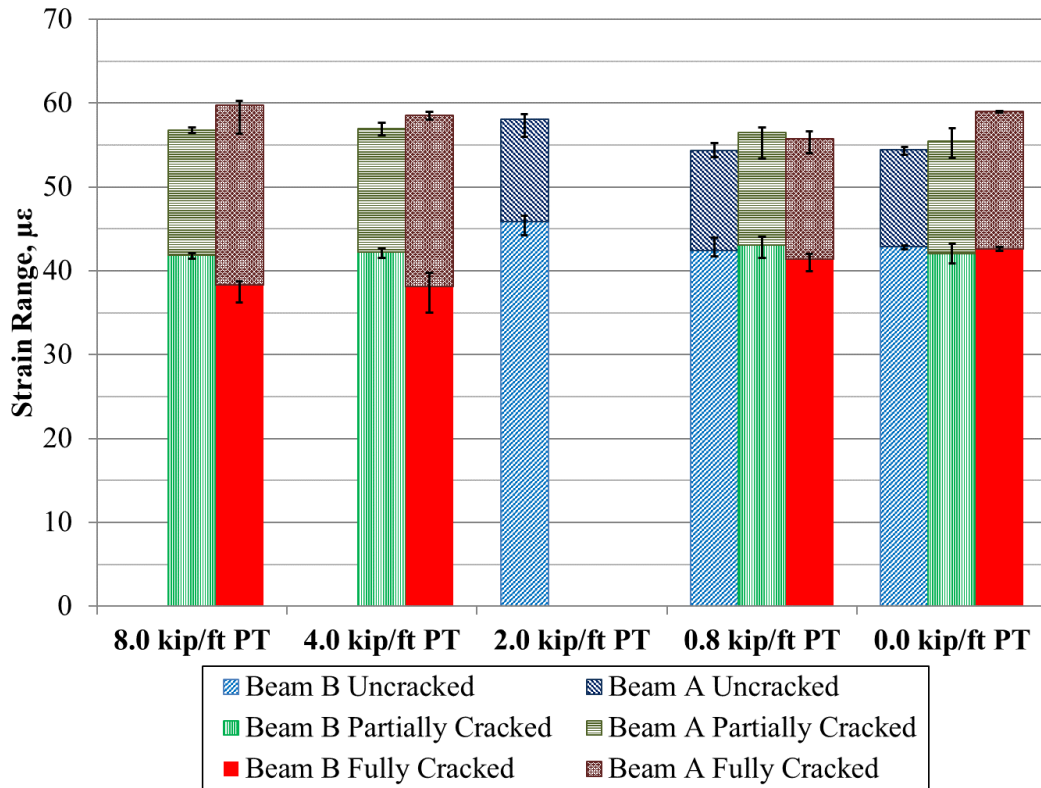
Source: FHWA.
1 kip/ft = 14.59 kN/m.

Figure 102. Graph. Comparison of longitudinal strain ranges in beams with fully stiffened partial-depth connections based on the level of PT force.
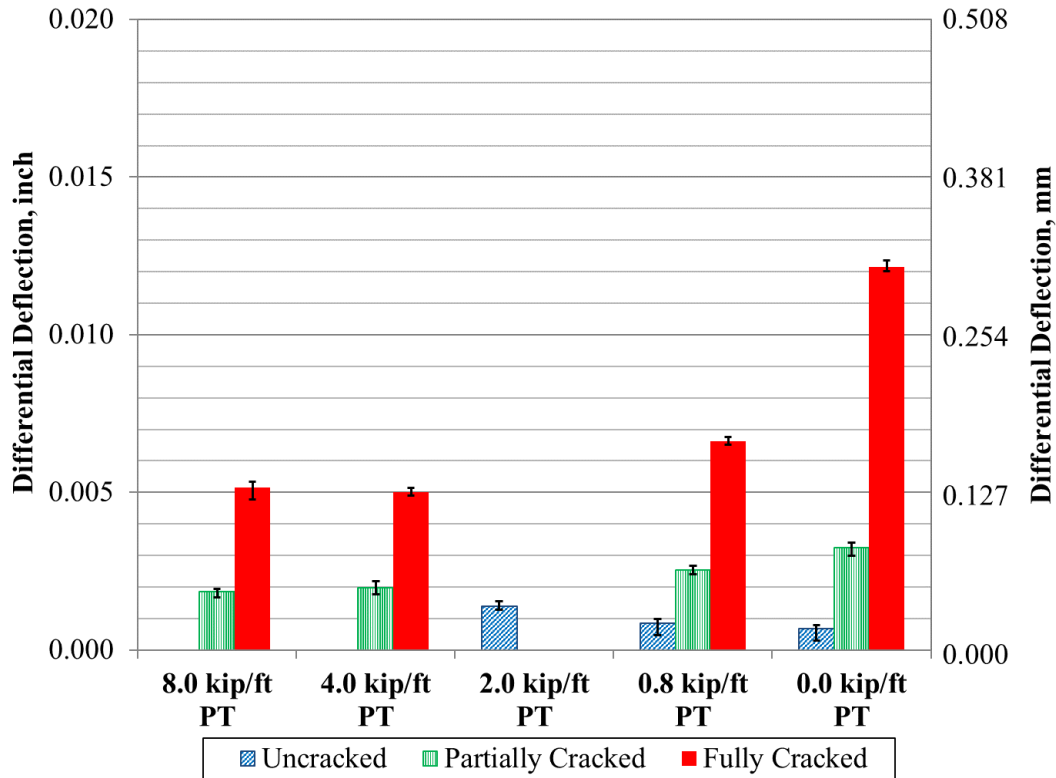
Source: FHWA.
1 inch = 25.4 mm.
1 kip/ft = 14.59 kN/m.

Figure 103. Graph. Comparison of Δ_δ in beams with fully stiffened partial-depth connections based on the level of PT force.

Figure 104 through figure 106 show the longitudinal strain, proportion of moment, and Δ_δ for the partially cracked full-depth conventionally grouted connection, respectively. It can still effectively transfer the loads between adjacent beams and limit Δ_δ as long as PT is present. Once the PT force was removed, changes were seen in all three measured variables. Longitudinal strain in the loaded beam increased by over 10 με, while the unloaded beam decreased by 5 με. This led to a 3 percent increase in the strain-based proportion of moment carried by the loaded beam. The deflection-based proportion of moment was also seen to increase by nearly 4.5 percent. Δ_δ increased from 0.0005 inch (0.013 mm) at 0.8 kip/ft (12 kN/m) of PT force to 0.019 inch (0.483 mm) with no PT applied.
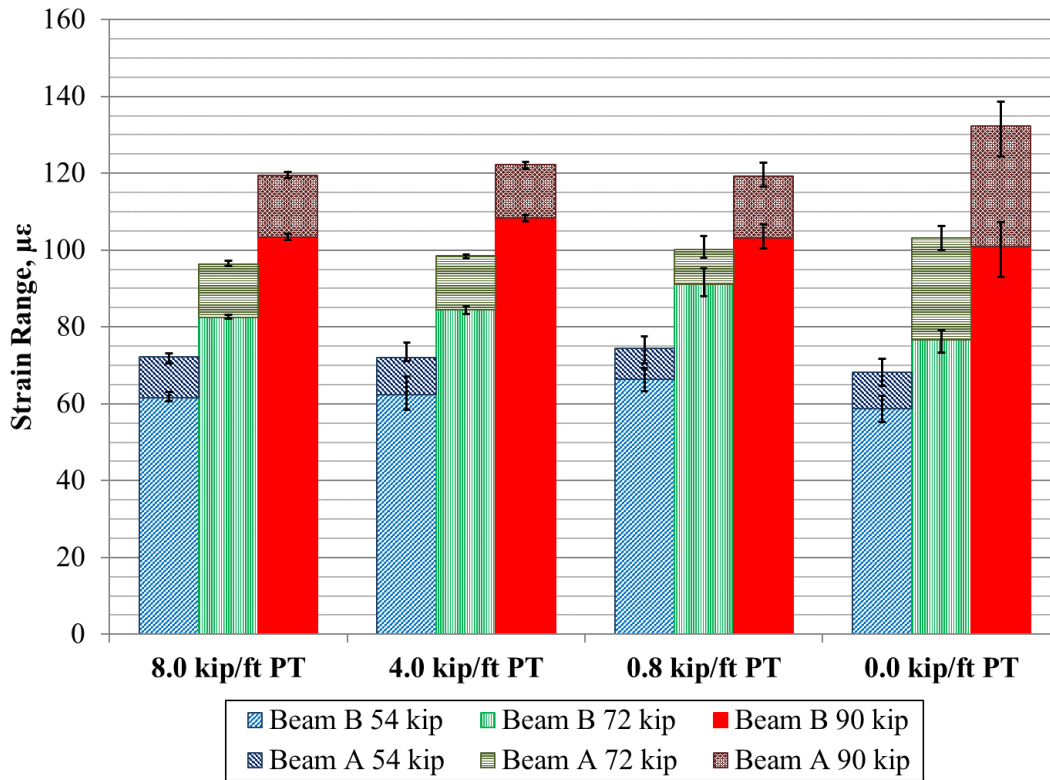
Source: FHWA.
1 kip = 4.448 kN.
1 kip/ft = 14.59 kN/m.

Figure 104. Graph. Comparison of longitudinal strain ranges in beams with partially cracked unstiffened full-depth conventional connections based on the level of PT force.
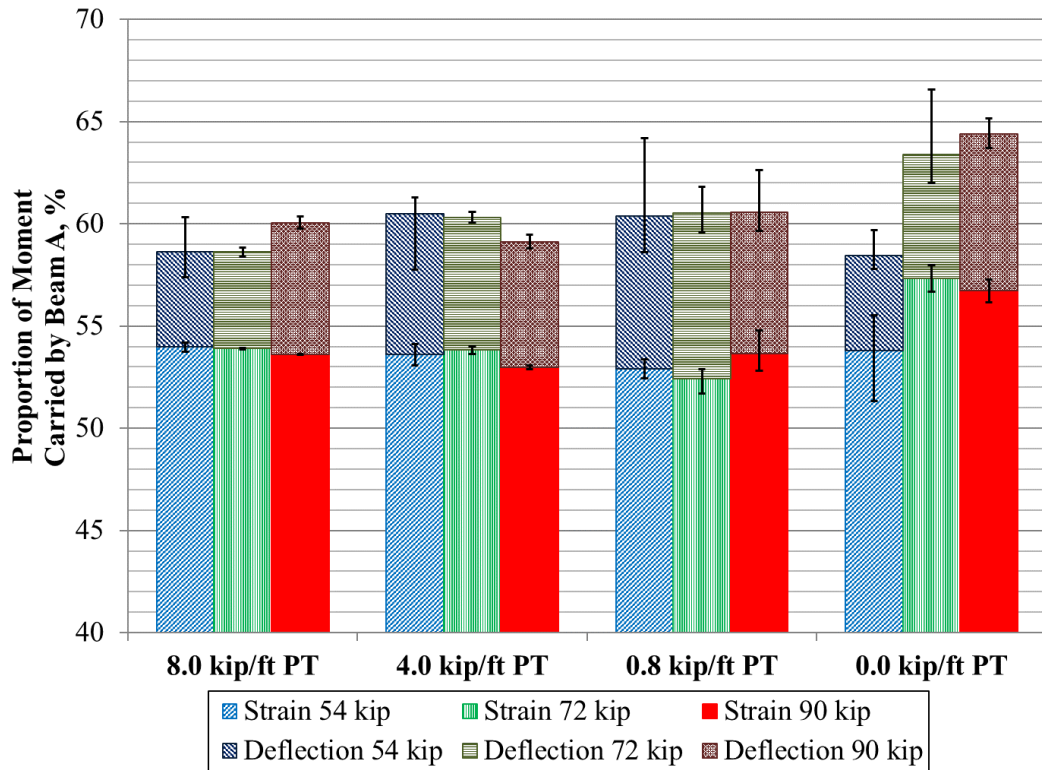
Source: FHWA.
1 kip = 4.448 kN.
1 kip/ft = 14.59 kN/m.

Figure 105. Graph. Comparison of loaded beam proportion of moment in beams with partially cracked unstiffened full-depth conventional connections based on the level of PT force.
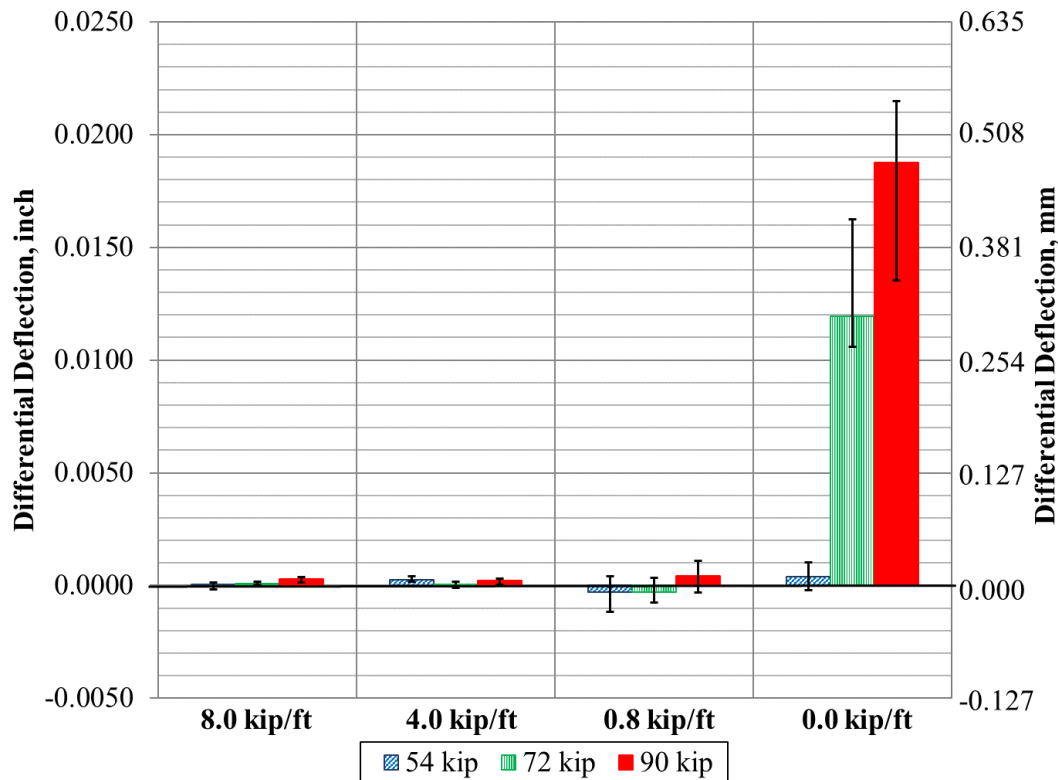
Source: FHWA.
1 inch = 25.4 mm.
1 kip = 4.448 kN.
1 kip/ft = 14.59 kN/m.

Figure 106. Comparison of Δ_δ in beams with partially cracked unstiffened full-depth conventional connections based on the level of PT force.

The *AASHTO LRFD Bridge Design Specifications* recommends installation of transverse PT to develop a minimum of 0.25 ksi (1.7 MPa) compression at connection.[6] The *Precast Prestressed Concrete Bridge Design Manual* recommends PT forces ranging from 6 to 16 kip/ft (88 to 233 kN/m).[3] In general practice, the transverse PT force is commonly applied at the beam ends and at diaphragm locations. This limits the benefits of the PT effects to only the areas immediately surrounding these locations. Because of the discrete PT application points, the transverse PT force is not uniform along the connections, reducing its ability to mitigate tensile deformations in the connections and thus allowing cracks to initiate and propagate. If the transverse PT force can be more evenly distributed along the span, the system performance could improve from the increase in keyway shear strength due to the confinement force spread along the bridge length.[40] The induced compression can also compensate for some of the transverse tensile strain from structural loading, shrinkage, and thermal effects. In this study, the transverse PT force was applied at the beam ends and at the two in-span diaphragms along the 48-ft (14.6-m) span. (Refer to figure 22 for overall testing configuration.) High-strength PT bars were used at each PT location, reacting against 7- by 7- by 2-inch (178- by 178- by 51-mm) bearing plates. The bar was located mid-height in the shear key, about 9 inches (229 mm) from the top surface.

97

The transverse compression strain on the top surface of the shear key at 0, 4, and 10 ft (0, 1.2, and 3.0 m) away from the PT locations was measured before and after PT. It was found that the compression force dissipated quickly from the PT point. Figure 107 shows the distribution of compressive strains near the two middle PT points. When the bars had a PT of 100 kip (445 kN), the strain gauges located above the PT bar showed compressive strain readings between 150 and 250 με. Under the same PT, the strain gauges 4 and 10 ft (1.2 and 3.0 m) away from the PT bar recorded compressive strain readings of only 80 and 25 με, respectively. This strain corresponds to a compressive stress in the connection of about 800 psi (5.52 MPa) at the PT location. This is less than half of the 2,050-psi (14.1-MPa) compressive stress calculated to be present under the bearing plates of the PT rods. The stress decreased to only 300 psi (2.07 MPa) within 4 ft (1.2 m) of the PT location and only 100 psi (0.69 MPa) 10 ft away. This means that the PT force was not as effective at locations away from the application points. Similar results were observed by others for the full-depth conventional grout connections. A finite element model was developed by Sharpe to investigate the distribution of the transverse PT force.[44] The model indicated that PT forces dissipate quickly away from the PT locations. The system performance could be improved if the transverse PT force is well distributed along the span.
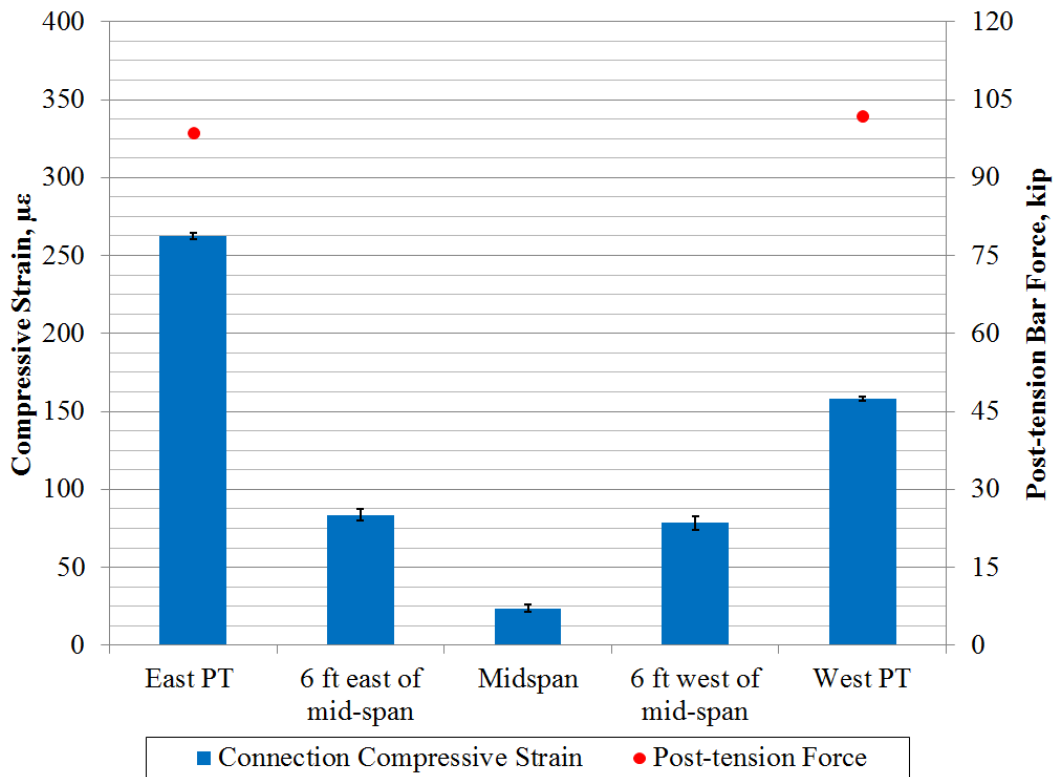
Source: FHWA.
1 kip = 4.448 kN.
1 ft = 0.305 m.

Figure 107. Graph. Connection compressive strain recorded during PT operation.

The level of PT was not found to affect the load carrying or $\varDelta_\delta$ in the beams as long as the connection was intact. For cracked connections with transverse PT applied, the connection could still effectively transfer the load, although $\varDelta_\delta$ increased. When the transverse PT force is

removed, cracked connections can lose their ability to limit $\varDelta_\delta$ and their capacity to effectively transfer the moment. This results in increases in all of the measured factors, especially $\varDelta_\delta$.

UHPC VERSUS CONVENTIONAL GROUT

This section compares the performance of the UHPC connections with the performance of the conventionally grouted connections. The full-depth conventionally grouted connection was included even though the connection could only be tested while the connection was cracked. The conventionally grouted values are taken from the series with 0.8 kip/ft (12 kN/m) of PT force, given that PT is a critical part of the detail.

Figure 108 and figure 109 show a comparison of longitudinal strain in beams with conventional and UHPC connections and partial- and full-depth connections, respectively. The partial-depth connection showed higher strain in both beams when a UHPC connection was used. The behavior of the full-depth connection was different, with the strain in the loaded beams about equal, while the strain in the unloaded UHPC beam was much greater than the strain in the unloaded conventionally grouted beam.
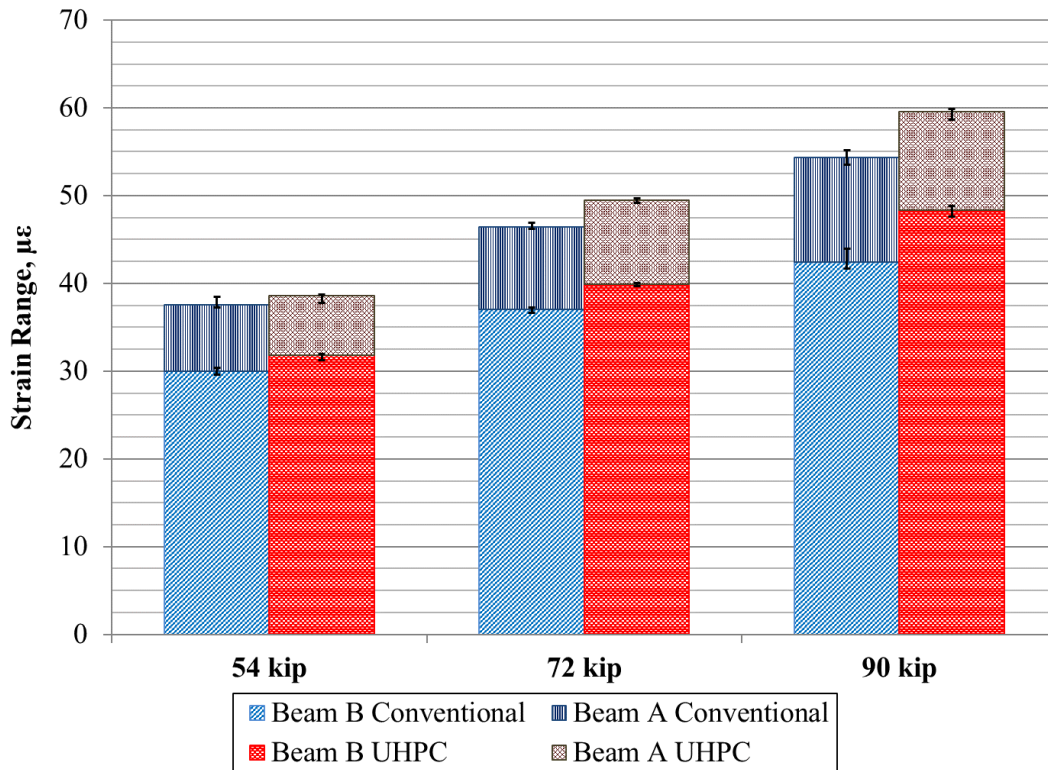
Source: FHWA.
1 kip = 4.448 kN.

Figure 108. Graph. Comparison of the longitudinal strain ranges in the fully stiffened beams with a partial-depth connection.
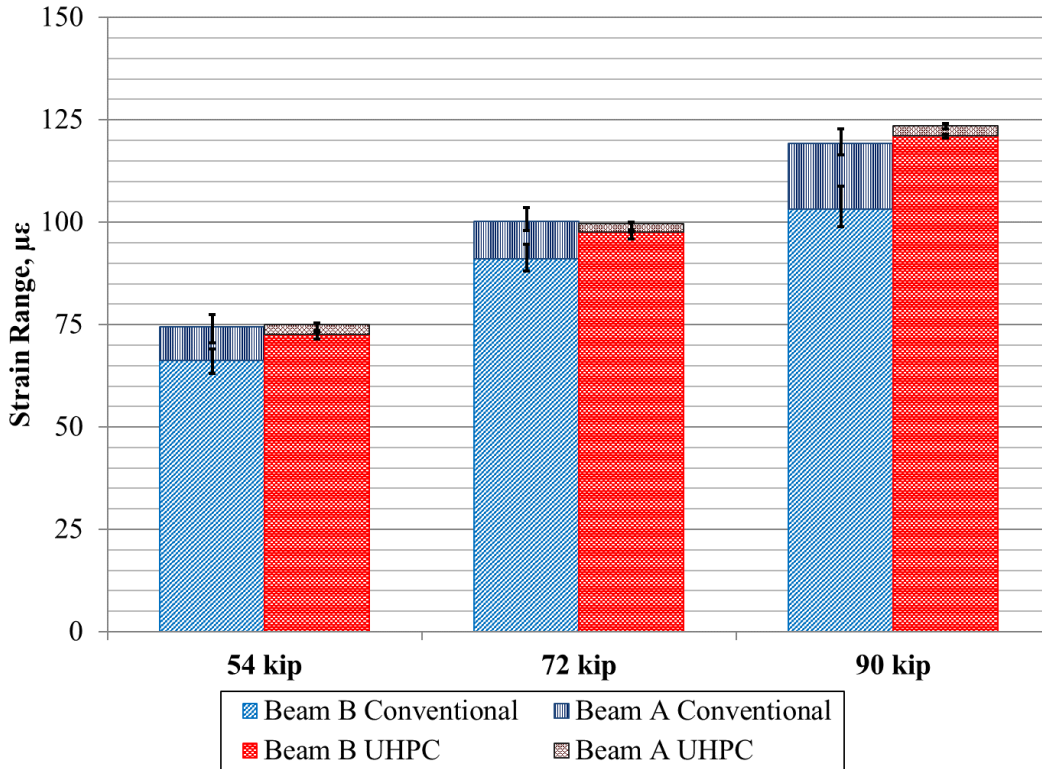
Source: FHWA.
1 kip = 4.448 kN.

Figure 109. Graph. Comparison of the longitudinal strain ranges in the unstiffened beams with a full-depth connection.

This difference in performance in the full-depth connections becomes evident in the proportion of moment carried by the loaded beam as well. Figure 110 shows the proportion of moment in the full-depth unstiffened beams. The proportion of moment based on strain and $\varDelta_\delta$ for the UHPC connection were both about 50.5 percent, while the partially cracked conventionally grouted connection had a proportion of moment of about 53 percent based on strain and 60 percent based on deflection. The larger value for $\varDelta_\delta$ was due to the larger $\varDelta_\delta$ of the cracked connection.
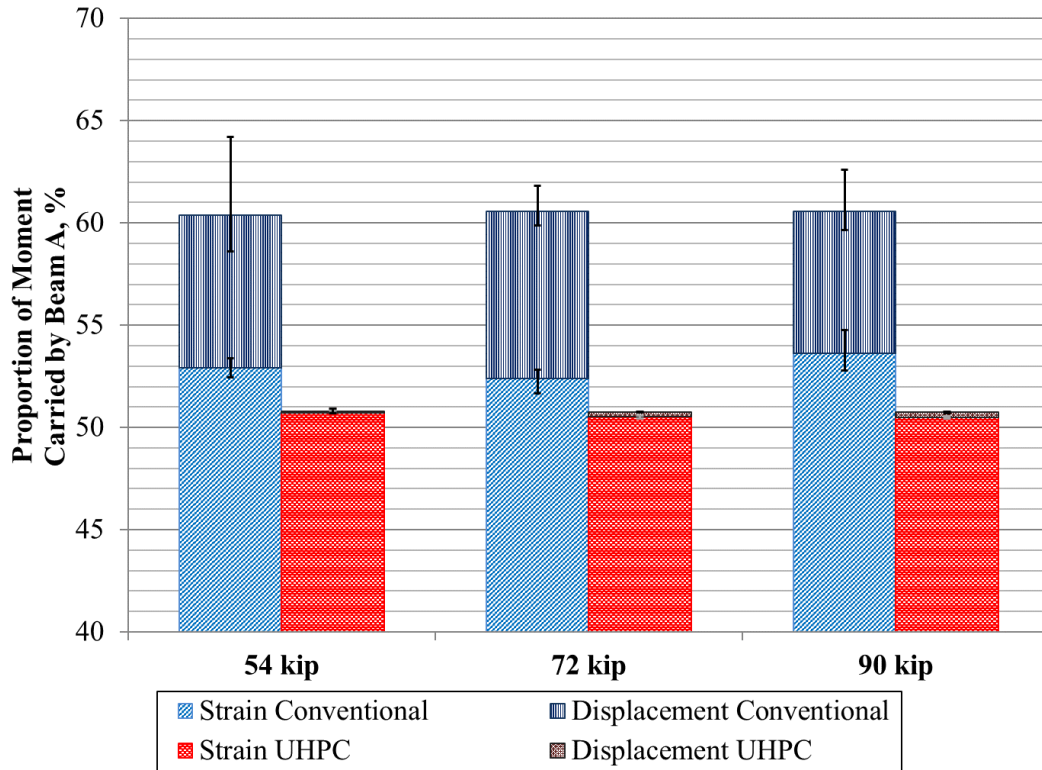
Source: FHWA.
1 kip = 4.448 kN.

Figure 110. Graph. Comparison of the loaded beam proportion of moment in the unstiffened beams with a full-depth connection.

Both the UHPC connections and conventionally grouted connections were able to limit Δ_δ to within 0.004 inch (0.102 mm), as shown in figure 111 for the partial-depth connection and figure 112 for the full-depth connection.
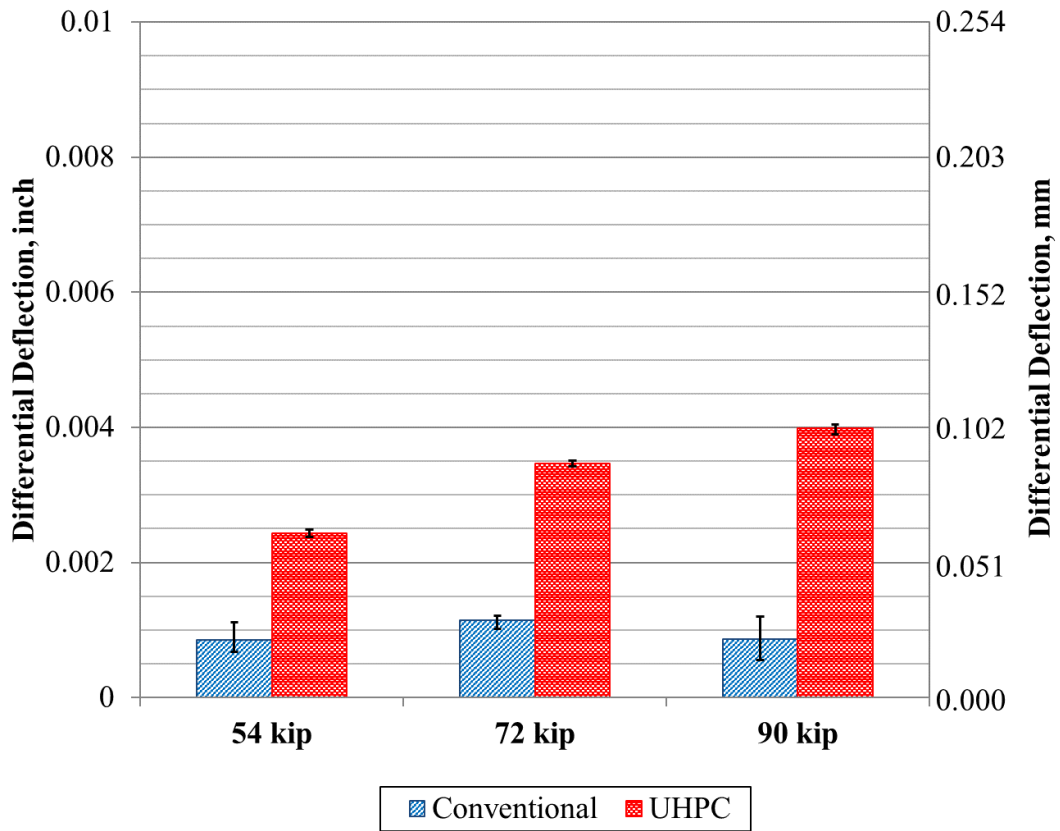
Source: FHWA.
1 inch = 25.4 mm.
1 kip = 4.448 kN.

Figure 111. Graph. Comparison of Δ_δ of the fully stiffened beams with a partial-depth connection.
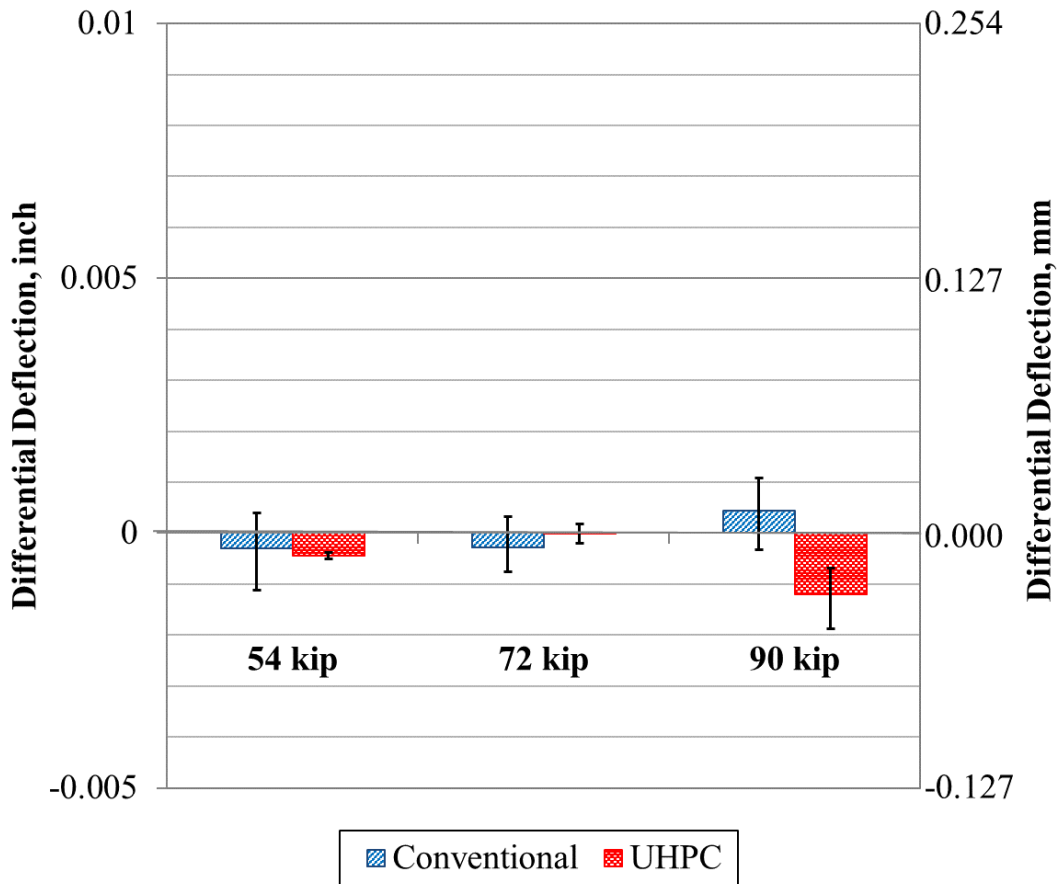
Source: FHWA.
1 inch = 25.4 mm.
1 kip = 4.448 kN.

Figure 112. Graph. Comparison of Δ_δ of the unstiffened beams with a full-depth connection.

The performance of conventionally grouted connections is comparable to the performance of UHPC connections. The UHPC connection was found to be more robust than the conventionally grouted connection, however. The UHPC connection did not use PT; therefore, it did not run the risk of increasing Δ_δ and losing load distribution if the PT force was lost. It also reduced the likelihood of connection cracking, further reducing the possibility of increasing Δ_δ. As was described previously, if the conventional connection is cracked and PT forces are lost, the ability for the connection to limit Δ_δ and effectively transfer the load can be compromised.

103

CHAPTER 6. SUMMARY AND CONCLUSIONS

Full-scale testing on adjacent box beam connection methods was conducted as part of this study. Four shear key connection designs were evaluated. The first two designs utilized both partial- and full-depth conventional grouted connections with various levels of transverse PT. The other two designs utilized partial- and full-depth UHPC connections with non-contact lap-spliced reinforcement. Transverse PT was not used in the UHPC connections. The beams were subjected to 10 cycles of thermal loading and millions of cycles of structural loading.

SUMMARY

The main findings are summarized as follows:

- The thermal loading generated in the study produced a temperature gradient between the top and bottom flanges of approximately 50 °F (28 °C) and resulted in an upward deflection of approximately 0.47 inch (11 mm). The applied thermal loading cycles did not initiate any significant cracks in the connections.

- The cyclic structural loading applied in this study was severe. The most extreme case in this study utilized a maximum loading range of 90 kip (400 kN) with a 5-kip (22-kN) minimum load. Within the most restrained test setup, this created an $M_{equivalent}$ of 498 kip-ft (673 kN-m) transferred through the connection.

- When a connection was uncracked, cyclic structural loading was not seen to initiate cracking. This was true regardless of level of PT in conventionally grouted connections.

- The calculated shear forces transferred through the connection were small. Maximum shear stress in the partial-depth beams was calculated to be 23 psi (161 kPa).

- When there were preexisting cracks in conventionally grouted connections, cyclic structural loading was observed to propagate the cracks independent of the level of transverse PT force applied. Cracks propagated more quickly under lower levels of PT.

- With higher levels of transverse PT force, the cracked connection could still effectively transfer the load, though Δ_δ increased slightly. When the transverse PT force was removed, the cracked connection could quickly lose its ability to limit Δ_δ. This could reduce its capability to effectively transfer the applied loads between adjacent beams.

- If the transverse PT force was applied before casting the grout, the loss of the PT force after casting may cause transverse tensile forces to develop in the connection. This could lead to cracking if the beams exhibited a large enough amount of relative sweep in their as-fabricated shape.

- When the connection was uncracked, beams with conventional grout connections had similar load distribution performance as beams with UHPC connections. However, the interface between the conventional grout and box beam concrete was the weak link of the system and could crack if a sufficient load or deformation occurs.

105

- The behavior of the adjacent box beam bridges with UHPC connections could be expected to be comparable with an equivalent structural system with no field-cast connections. The mechanical capacity of the UHPC connection was observed to enhance connection capacity so that, under the application of large transverse tensile stresses, tensile rupture occurred in the precast concrete box beams.

- Full-depth connections showed slight improvements in load distribution between beams. This is likely due to the increased depth of the connection, which significantly increased the transverse flexural and shear stiffnesses of the connection. However, increasing the depth of the connection increases construction costs and possibly construction complexity.

- A partial-depth UHPC connection appears to be sufficient to achieve the performance requirements.

CONCLUSIONS AND RECOMMENDATIONS

Conclusions and recommendations related to adjacent box beam connection design and performance evaluation include the following:

- The performance and efficiency of the shear key can be evaluated for load transfer by determining the proportion of moment carried by the loaded beam.

- Δ_δ between adjacent beams can be a good indicator of the serviceability performance of a connection. Based on the tests in this study, Δ_δ for in-tact connections were below 0.005 inch (0.127 mm), while the *Precast Prestressed Concrete Bridge Design Manual* seeks to limit Δ_δ between adjacent box beams to 0.02 inch (0.51 mm) for spans up to 100 ft (30.5 m).[3]

- $M_{equivalent}$, which calculates the moment transferred through the connection from a loaded beam to adjacent beams, can be used to compare the test results from this study with other bridge designs that have different geometries and loading conditions.

- Transverse PT can limit differential movement between beams, compensate for some transverse tensile strains across the connections, and assist with load transfer between beams after connection cracking. Increased transverse PT force distribution along the length of the connections could enhance system performance as the keyway shear strength increases with more confinement force. However, as commonly deployed today, transverse PT only effectively confines a small area near the PT locations. This transverse PT would likely be most valuable after connection degradation has already begun, thus serving to limit large Δ_δ between adjacent beams.

- Based on the concurrent research by De la Varga et al., a minimum interface bond strength of 150 psi (1.0 MPa) is recommended when selecting a grout material.[17] This helps to avoid interface cracking due to eccentrically placed external loads and may assist with the mitigation of transverse tensile forces and deformations due to thermal loads and material shrinkage.

APPENDIX. BOX BEAM DESIGN DETAILS

Drawings associated with the fabrication of the box beams are found in this appendix.
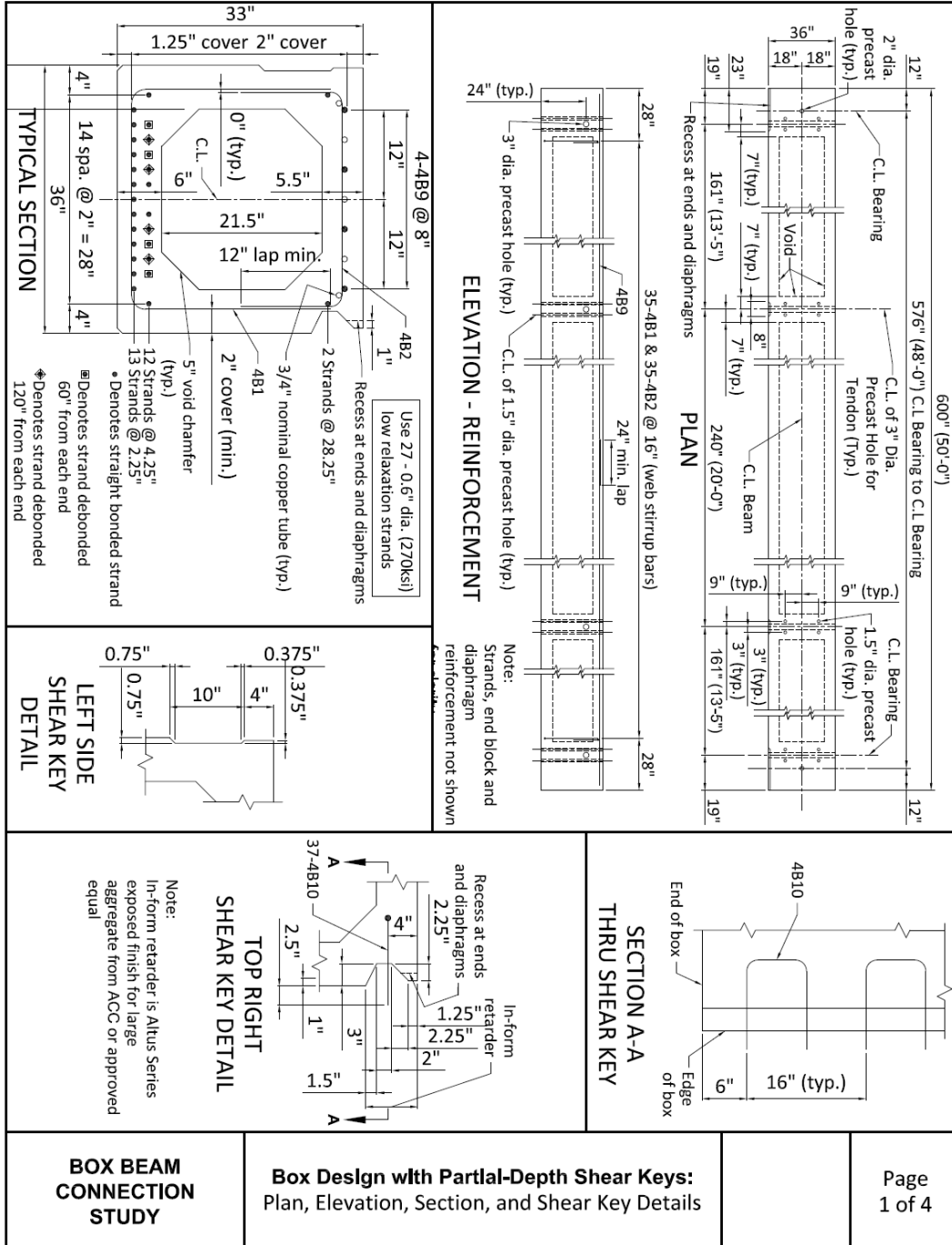
Source: FHWA.
1 inch = 25.4 mm.

Figure 113. Drawing. Box design with partial-depth shear keys showing plan, elevation, section, and shear key details.

Source: FHWA.
1 inch = 25.4 mm.

Figure 114. Drawing. Box design with partial-depth shear keys showing notes, details, and reinforcement schedule.

TYPICAL SECTION

33"
1.25" cover 2" cover
4"
14 spa. @ 2" = 28"
36"
4"
0" (typ.)
C.L.
6" 5.5"
21.5"
12" lap min.
4-4B9 @ 8"
12" 12"

Use 27 - 0.6" dia. (270ksi) low relaxation strands

5" void chamfer (typ.)
12 Strands @ 4.25"
13 Strands @ 2.25"
1,3/4" nominal copper tube
2" cover (min.)
4B1
1 (typ.)
4B2
1"
2 Strands @ 28.25"
Recess at ends and diaphragms
Recess at ends and diaphragms

◨ Denotes strand debonded 60" from each end
◈ Denotes strand debonded 120" from each end
● Denotes straight bonded strand

ELEVATION - REINFORCEMENT

16.5" (typ.)
3" dia. precast hole (typ.)
C.L. of 1.5" dia. precast hole (typ.)
35-4B1 & 35-4B2 @ 16" (web stirrup bars)
24" min. lap
4B9
28"
28"

Note:
In-form retarder is Altus Series exposed finish for large aggregate from ACC or approved equal

Note:
Strands, end block and diaphragm reinforcement not shown

PLAN

600" (50'-0")
576" (48'-0") C.L Bearing to C.L Bearing
36"
18" 18"
23"
19"
12"
2" dia. precast hole (typ.)
7" (typ.)
7" (typ.)
7" (typ.)
8"
Void
C.L. Bearing
C.L. of 3" Dia. Precast Hole for Tendon (Typ.)
161" (13'-5")
240" (20'-0")
C.L. Beam
C.L. Bearing
Recess at ends and diaphragms
9" (typ.) 9" (typ.)
3" (typ.)
3" (typ.)
161" (13'-5")
1.5" dia. precast hole (typ.)
C.L. Bearing
28"
19"
12"

LEFT SIDE SHEAR KEY DETAIL
0.75" 0.375"
4" 4"
0.75" 0.375"

TOP RIGHT SHEAR KEY DETAIL
37-4B10
2.625"
2.625"
2.875"
4"
Recess at ends and diaphragms
2.25"
1.25"
2.25"
In-form retarder
2"
1.313"

BOTTOM RIGHT SHEAR KEY DETAIL
37-4B10
5"
3"
2.5"
2.5"
1.5"
2"
Recess at ends and diaphragms
1"
In-form retarder
2.625"
A
A

SECTION A-A THRU SHEAR KEY
End of box
4B10
Edge of box
6" 16" (typ.)

| BOX BEAM CONNECTION STUDY | Box Design with Full-Depth Shear Keys: Plan, Elevation, Section, and Shear Key Details | | Page 3 of 4 |

Source: FHWA.
1 inch = 25.4 mm.

Figure 115. Drawing. Box design with full-depth shear keys showing plan, elevation, section, and shear key details.

Notes: (typical all pages)
1) Prestressing strand shall be 0.6 in. diameter with a guaranteed ultimate strength of 270 ksi
2) Strand jacking force = 44 kips per strand
3) Concrete shall have a minimum compressive strength of 4 ksi at transfer and 6 ksi at 28 days
4) All bar reinforcement shall be ASTM A615 Grade 60
5) All exposed corners except the top shall be chamfered to 0.75", unless otherwise dimensioned
6) Bar spacing may be slightly adjusted to avoid interference with the precast holes
7) Copper tubing shall extend 12" beyond both ends of beams and shall be watertight under 40 psig
8) Strand shall extend 36" beyond both ends of beams, unbent and with wires still wrapped around king

PLAN - END BLOCK REINFORCEMENT

36"
18" 18"
3" 3"
3"
2"
2"
7"
2"

3-4B5 @ 4.5"
2-4B4
4B6
1-4B3
4B1 & 4B2
Void
3B8
C.L. Bearing
C.L. of 3" Dia. Precast Hole for Tendon (Typ.)
3" 3"
3-4B7 @ 4.5"

ELEVATION - END BLOCK REINFORCEMENT

Note:
Strands and 4B9 bars not shown for clarity

0" (typ.)
2" cover
4B5
4B5
4B4
4B3
4B7
C.L. Bearing
3" dia. precast hole
4B1 & 4B2
1-4B8
7.5"
4-4B6 @ 6"

PLAN - DIAPHRAGM REINFORCEMENT

1" cover
6" 6"
1-4B7
1-4B7
4B8
C.L. of 3" Dia. Precast Hole for Tendon (Typ.)

ELEVATION - DIAPHRAGM REINFORCEMENT

Note:
Strands and 4B9 bars not shown for clarity

1" cover
12" 9"
4B7
3" dia. precast hole
1-4B7
4B7
1-4B8
1-4B8

ELEVATION - BEAM LIFTER DETAIL

6" 27" 8"
15" +/-
2 lifting loops @ each end
4 - 1/2" dia. strands/loop min.
(typ. both ends)

Notes:
1) All dimensions are out-to-out dimensions
2) Bars shown on the shedule are for one beam only

Type 1
A B C D

Type 2
B C D

Type 3
E F E F

REINFORCEMENT SCHEDULE

Mark	No.	Type	Size	A	B	C	D	E	F
4B1	35	2	4	28"	29.5"	28"			
4B2	35	4	4	14"	29.5"	14"			
4B3	4	3	4						
4B4	8	3	4						
4B5	12	2	4	24"	29"	0"			
4B6	8	2	4	48"	28.5"	48"			
4B7	20	1	4	12"	29"	0"			
4B8	12	1	4	31"					
4B9	4	2	4	595"				29"	29.5"
4B10	74	2	4	12"	8.5"	12"		21"	29.5"

Source: FHWA.
1 inch = 25.4 mm.

BOX BEAM CONNECTION STUDY

Box Design with Full-Depth Shear Keys:
Notes, Details, and Reinforcement Schedule

Page 4 of 4

Figure 116. Drawing. Box design with full-depth shear keys showing notes, details, and reinforcement schedule.

ACKNOWLEDGEMENTS

REFERENCES

1. Graybeal, B. (2017). *Adjacent Box Beam Connections: Performance and Optimization*, Report No. FHWA-HRT-17-094, Federal Highway Administration, Washington, DC.

2. Russell, H.G. (2011). "Adjacent Precast Concrete Box-Beam Bridges: State of the Practice," *PCI Journal*, *56*(1), pp. 75–91, Precast/Prestressed Concrete Institute, Chicago, IL.

3. PCI Bridge Design Manual Steering Committee. (2011). *Precast Prestressed Concrete Bridge Design Manual*, Third Edition, Precast/Prestressed Concrete Institute, Chicago, IL.

4. Huckelbridge, A.A., El-Esnawi, H., and Moses, F. (1995). "Shear Key Performance in Multibeam Box Girder Bridges," *Journal of Performance of Constructed Facilities*, *9*(4), pp. 271–285, American Society of Civil Engineers, Reston, VA.

5. Association of State Highway and Transportation Officials. (2002). *Standard Specifications for Highway Bridges*, 17th Edition, American Association of State Highway and Transportation Officials, Washington, DC.

6. Association of State Highway and Transportation Officials. (2013). *AASHTO LRFD Bridge Design Specifications*, Sixth Edition, American Association of State Highway and Transportation Officials, Washington, DC.

7. Association of State Highway and Transportation Officials. (2010). *AASHTO LRFD Bridge Construction Specifications*, Third Edition, American Association of State Highway and Transportation Officials, Washington, DC.

8. El-Remaily, A., Tadros, M.K., Yamane, T., and Krause, G. (1996). "Transverse Design and Adjacent Precast Prestressed Concrete Box Girder Bridge," *PCI Journal*, *41*(4), pp. 96–113, Precast/Prestressed Concrete Institute, Chicago, IL.

9. Hanna, K.E., Morcous, G., and Tadros, M.K. (2007). "Transverse Design and Detailing of Adjacent Box Beam Bridges," *Proceedings of the 2007 PCI National Concrete Bridge Conference*, Phoenix, AZ.

10. Canadian Standards Association. (2000). *Design of Highway Bridges*, CSA S6-00, Canadian Standards Association, Rexdale, Ontario, Canada.

11. Miller, R.A., Hlavacs, G.M., Long, T., and Greuel, A. (1999). "Full-Scale Testing of Shear Keys for Adjacent Box Girder Bridges," *PCI Journal*, *44*(6), pp. 81–90, Precast/Prestressed Concrete Institute, Chicago, IL.

12. Graybeal, B. (2012). *Construction of Field-Cast Ultra-High Performance Concrete Connections*, Report No. FHWA-HRT-12-038, Federal Highway Administration, Washington, DC.

13. French, C.E., Shield, C.K., Klaseus, D., Smith, M., Eriksson, W., Ma, Z.J., Zhu, P., Lewis, S., and Chapman, C.E. (2011). *Cast-in-Place Concrete Connections for Precast Deck Systems*, NCHRP Report 173, National Cooperative Highway Research Program, Washington, DC.

14. Yuan, J. and Graybeal, B. (2016). "Full-Scale Testing of Shear Key Details for Precast Concrete Box-Beam Bridges," *Journal of Bridge Engineering*, *21*(9), p. 14, American Society of Civil Engineers, Reston, VA.

15. Graybeal, B. (2011). *Design and Construction of Field-Cast UHPC Connections*, Report No. FHWA-HRT-14-084, Federal Highway Administration, Washington, DC.

16. Graybeal, B. (2011). "Fatigue Response in Bridge Deck Connection Composed of Field-Cast Ultra-High Performance Concrete," *Transportation Research Record*, *2251*, pp. 93–100, Transportation Research Board, Washington, DC.

17. De la Varga, I., Haber, Z.B., and Graybeal, B.A. (2016). "Performance of Grouted Connections for Prefabricated Bridge Elements-Part I: Material-Level Investigation on Shrinkage and Bond," *Proceedings of the PCI National Bridge Conference*, Precast/ Prestressed Concrete Institute, Chicago, IL.

18. Yuan, J. and Graybeal, B. (2014). B*ond Behavior of Reinforcing Steel in Ultra-High Performance Concrete*, Report No. FHWA-HRT-14-089, Federal Highway Administration, Washington, DC.

19. Yuan, J. and Graybeal, B. (2015). "Bond of Reinforcement in Ultra-High Performance Concrete (UHPC)," *ACI Structural Journal*, *112*(6), pp. 851–860, American Concrete Institute, Farmington Hills, MI.

20. De la Varga, I. and Graybeal, B. (2016). *Dimensional Stability of Grout-Type Materials Used as Connections for Prefabricated Bridge Elements*, Report No. FHWA-HRT-16-008, Federal Highway Administration, Washington, DC.

21. Swenty, K.S. and Graybeal, B. (2013). *Material Characterization of Field-Cast Connection Grouts*, Report No. FHWA-HRT-13-041, Federal Highway Administration, Washington, DC.

22. Graybeal, B. (2011). *Ultra-High Performance Concrete*, Report No. FHWA-HRT-11-038, Federal Highway Administration, Washington, DC.

23. Graybeal, B. (2006). *Material Property Characterization of Ultra-High Performance Concrete*, Report No. FHWA-HRT-06-103, Federal Highway Administration, Washington, DC.

24. ASTM C39/C39 M-17b. (1994). "Standard Test Method for Compressive Strength of Cylindrical Concrete Specimens," *Book of Standards Volume 04.02*, ASTM International, West Conshohoken, PA.

25. ASTM C469/C469M-94. (1994). "Standard Test Method for Static Modulus of Elasticity and Poisson's Ratio of Concrete in Compression," *ASTM Book of Standards Volume 04.02*, ASTM International, West Conshohocken, PA.

26. ASTM C496/C496M-90. (1990). "Standard Test Method for Splitting Tensile Strength of Cylindrical Concrete Specimens," *ASTM Book of Standards Volume 04.02*, ASTM International, West Conshohocken, PA.

27. ASTM C1018-97. (1997). "Standard Test Method for Flexural Toughness and First-Crack Strength of Fiber-Reinforced Concrete (Using Beam With Third-Point Loading)," *ASTM Book of Standards Volume 04.02*, ASTM International, West Conshohocken, PA.

28. AASHTO T132. (2000). *Standard Method of Test for Tensile Strength of Hydraulic Cement Mortars*, American Association of State Highway and Transportation Officials, Washington, DC.

29. ASTM C512/C512M-87. (1987). "Standard Test Method for Creep of Concrete in Compression," *ASTM Book of Standards Volume 04.02*, ASTM International, West Conshohocken, PA.

30. ASTM C157/C157M-93. (1993). "Standard Test Method for Length Change of Hardened Hydraulic-Cement Mortar and Concrete," *ASTM Book of Standards Volume 04.02*, ASTM International, West Conshohocken, PA.

31. AASHTO TP60. (2000). *Coefficient of Thermal Expansion of Hydraulic Cement Concrete*, American Association of State Highway and Transportation Officials, Washington, DC.

32. ASTM C1202-97. (1997). "Standard Test Method for Electrical Indication of Concrete's Ability to Resist Chloride Ion Penetration," *ASTM Book of Standards Volume 04.02*, ASTM International, West Conshohocken, PA.

33. AASHTO T259. (2000). *Standard Method of Test for Resistance of Concrete to Chloride Ion Penetration*, American Association of State Highway and Transportation Officials, Washington, DC.

34. ASTM C672/C672M-92. (1992). "Standard Test Method for Scaling Resistance of Concrete Surfaces Exposed to Deicing Chemicals," *ASTM Book of Standards Volume 04.02*, ASTM International, West Conshohocken, PA.

35. ASTM C944/C944M-95. (1995). "Standard Test Method for Abrasion Resistance of Concrete or Mortar Surfaces by the Rotating Cutter Method," *ASTM Book of Standards Volume 04.02*, ASTM International, West Conshohocken, PA.

36. ASTM C666/C666M-97. (1997). "Standard Test Method for Resistance of Concrete to Rapid Freezing and Thawing," *ASTM Book of Standards Volume 04.02*, ASTM International, West Conshohocken, PA.

37. ASTM C1260-94. (1994). "Standard Test Method for Potential Alkali Reactivity of Aggregates (Mortar-Bar Method)," *ASTM Book of Standards Volume 04.02*, ASTM International, West Conshohocken, PA.

38. Annamali, G. and Brown, R.C. (1990). "Shear Transfer Behavior of Post-Tensioned Grouted Shear Key Connections in Precast Concrete-Framed Structures," *ACI Structural Journal*, *87*(1), pp. 53–60, American Concrete Institute, Farmington Hills, MI.

39. Bakht, B., Jaeger, L.G., and Cheung, M.S. (1983). "Transverse Shear in Multibeam Bridge," *Journal of Structural Engineering*, *109*(4), pp. 936–949, American Society of Civil Engineers, Reston, VA.

40. Buyukozturk, O., Bakhoum, M.M., and Beattie, M. (1990). "Shear Behavior of Joints in Precast Concrete Segmental Bridges," *Journal of Structural Engineering*, *116*(12), pp. 3,380–3,401, American Society of Civil Engineers, Reston, VA.

41. Gulyas, R.J., Wirthlin, G.J., and Champa, J.T. (1995). "Evaluation of Keyway Grout Test Methods for Precast Concrete Bridges," *PCI Journal*, *40*(1), pp. 44–57, Precast/Prestressed Concrete Institute, Chicago, IL.

42. Issa, M.A., Ribeiro, C.L., Abdalla, H.A., Islam, S., and Issa, M.A. (2003). "Performance of Transverse Joint Grout Materials in Full-Depth Precast Concrete Bridge Deck Systems," *PCI Journal*, *48*(4), pp. 92–103, Precast/Prestressed Concrete Institute, Chicago, IL.

43. ASTM C882/C882M-13a. (2013). "Standard Test Method for Bond Strength of Epoxy-Resin Systems Used With Concrete by Slant Shear," *ASTM Book of Standards Volume 04.02*, ASTM International, West Conshohocken, PA.

44. Sharpe, G.P. (2007). *Effect of Cracking of Shear Keys in Multi-Beam Bridges*, Master Thesis, Texas A&M University, College Station, TX.